Evolution of cooperation in bacterial biofilms

A stochastic model for the growth and sinking of bacterial mats

Johannes Knebel

München 2011

Evolution of cooperation in bacterial biofilms

A stochastic model for the growth and sinking of bacterial mats

Johannes Knebel

Masterarbeit
an der Fakultät für Physik
der Ludwig–Maximilians–Universität
München

vorgelegt von
Johannes Knebel
aus Rostock

München, den 27. September 2011

Gutachter: Prof. Frey
Zweitgutachter: Prof. Braun

Abstract

Cooperation phenomena are ubiquitous in nature. Although stunning to explain within the framework of evolution, a fundamental question is why individuals living together in a colony act altruistically since free-riders may receive the same benefit without paying any cost, and hence have an evolutionary advantage over cooperators.
We study the experimental investigation of cooperation by Rainey & Rainey [1] in which the bacteria strain *Pseudomonas fluorescens* rapidly diversifies in a spatially heterogeneous environment through genetic mutation. Cooperative groups are established by the overproduction of an adhesive polymer. The mutual attachment after cell division enables the cooperators to form a mat at the liquid-air interface of the broth pot. This evolutionary advantage of cooperation, mediated by the access to oxygen, is, however, subverted by a defecting trait which causes the sinking of the mat on a faster time scale than in absence of these free-riders.

In this thesis, we investigate the interplay between the biologically relevant timescales influencing the dynamics of cooperation in the mat experiment. We define a stochastic model for the growth and sinking of bacterial mats. A mat is characterized by the number of cooperating and defecting cells, by the effective mat volume, and by the mat density. The number of cooperators and defectors follows a stochastic update [2]. Microscopically, defectors are always better off, but cooperative groups can grow larger in size. Within an effective coarse-grained description, the growth of the mat volume is abstracted in a deterministic, non-spatial picture. In this averaged view, we assume that the mat only grows at its surface. Hereby, we effectively introduce a scaling hypothesis for the dynamics of the mat volume: the growth rate of the mat volume is proportional to its square root. Moreover, the mat expansion is mediated by the presence of cooperating cells. Without cooperators, the mat would not grow in size.
The mat density is then computed via the microscopic occupation of the mat volume. Thereby, cooperators contribute with a smaller weight to the mat density than defectors since they overproduce the sticky polymer. The mat starts to sink, when its density reaches the density of water.

This mat model combines population dynamics with its internal evolution for mat populations. Regarding an ensemble of mats, the average percentage of cooperators reveals a transient increase of cooperation after some time due to demographic fluctuations in the beginning of the growth dynamics. The lower the initial size of the mat, the higher is the impact of stochastic fluctuations on the mat dynamics including the maximal population

size and the sinking time of the mat. Cooperative groups grow larger in size and sink later in time, and thus have a higher probability to survive in a structured environment. The sinking time increases if the selection pressure is lowered or if the mat expansion is accelerated.
By applying repeated population bottlenecks, this stochastic effect may pave the way for the maintenance of cooperation in structured populations. More generally, our work provides conceptual insights into the requirements and mechanisms for the evolution of cooperation, and the transition from single cells to multicellularity.

Zusammenfassung

Kooperationsphänomene sind in der Natur allgegenwärtig. Obwohl sich Kooperation im Rahmen der Evolutionstheorie eindrucksvoll erklären lässt, ist es immer noch ein Rätsel, warum Individuen alruistisches Verhalten zeigen, insbesondere wenn man bedenkt, dass Trittbrettfahrer eine kooperierende Gemeinschaft unterwandern können, indem sie von der Kooperation der anderen profitieren, ohne selbst zur Kooperation beizutragen und damit Kosten sparen. Folglich haben Trittbrettfahrer aus evolutionärer Sicht immer einen Vorteil.

In dieser Masterarbeit wird ein Experiment von Rainey & Rainey [1] studiert, in dem Kooperation auf bakterieller Ebene untersucht wurde. Wenn man den Bakterienstamm *Pseudomonas fluorescens* in einer räumlich strukturierten Umgebung aussetzt, kann man beobachten, dass sich diese Bakterien vergleichsweise schnell durch genetische Mutation an die Umgebung anpassen. Im Fall, dass man diese Bakterien in einer ungestörten Nährlösung in einem Glasgefäß wachsen lässt, können sich kooperative Gruppen dadurch bilden, dass die Bakterien ein bestimmtes klebriges Polymer zu viel produzieren. Die Überproduktion dieses Polymers hat zur Folge, dass zwei Bakterien nach der Zellteilung aneinander kleben bleiben. Dadurch können die Bakterien eine Art Matte formen, die an der Wasseroberfläche schwimmt, was den Vorteil mit sich bringt, dass die Bakterien jetzt besseren Zugang zu Sauerstoff haben.
Dieser evolutionäre Vorteil, der durch Kooperation zustande kommt, wird von Bakterien unterwandert, die in der Matte sitzen können, ohne dabei einen Beitrag zur Mattenstruktur zu leisten. Aus spieltheoretischer Sicht sind sie klassische Trittbrettfahrer. Diese werden auch Defektoren genannt, um sie von den Kooperatoren zu unterscheiden. Defektoren nutzen den Vorteil der kooperierenden Individuen aus, ohne selbst einen Beitrag zur Kooperation zu leisten. Als Folge dessen sinkt die Matte auf einer deutlich kürzeren Zeitskala, als wenn die Defektoren abwesend wären. Damit wird die Lebensfähigkeit der Matte durch die Anwesenheit der Defektoren aufs Spiel gesetzt.

In dieser Arbeit wird das Zusammenspiel der biologisch relevanten Zeitskalen untersucht, die die Dynamik der Kooperation in dem Mattenexperiment bestimmen. Dazu wird ein stochastisches Modell aufgestellt, dass das Wachstum und das Sinken einer Matte beschreibt. Eine Matte wird als ein Objekt betrachtet, dass durch die Anzahl der Kooperatoren, die Anzahl der Defektoren, und durch das effektive Mattenvolumen sowie der Mattendichte charakterisiert ist.
Dabei folgt die Anzahl der Kooperatoren und Defektoren einer stochastischen Dynamik [2]. Auf der einen Seite haben Defektoren immer einen evolutionären Vorteil gegenüber Koop-

eratoren, denn sie haben keine Kosten für die Kooperation, auf der anderen Seite können kooperative Gruppen schneller wachsen und größer werden. Das Wachstum des Mattenvolumens wird auf einer vergröberten Skala deterministisch und nicht-räumlich beschrieben. In dieser gemittelten Sichtweise wird angenommen, dass die Matte nur an ihrer Oberfläche wächst. Damit wird effektiv ein Skalenverhalten eingeführt: Die Wachstumsrate des Mattenvolumens ist proportional zur Wurzel des Volumens. Darüber hinaus ist die Anwesenheit der Kooperatoren essentiell für die Ausbreitung der Matte. Ohne Kooperatoren wäre die Matte nicht in der Lage, zu wachsen. Die Dichte der Matte wird dann als die mikroskopische Besetzung des effektiven Mattenvolumens berechnet. Dabei wird dem Fakt Rechnung getragen, dass Kooperatoren einen kleineren Beitrag zur Dichte als Defektoren leisten, weil sie das klebrige Polymer zu viel produzieren. Die Matte beginnt dann zu sinken, wenn ihre Dichte den Wert der des Wassers erreicht hat.
Dieses Mattenmodell vereint Wachstumsdynamik und interne Evolution für Mattenpopulationen. Bei der Betrachtung eines Ensembles von Matten stellt man fest, dass der Anteil der Kooperatoren über alle Matten gemittelt nach einer gewissen Zeit des Abfalls wieder steigt und das Anfangsniveau übersteigt. Der Grund dafür liegt in demografischen Fluktuationen zu Beginn der Mattendynamik. Je kleiner zu Beginn die Populationsgröße ist, umso größer ist der Einfluss von stochastischen Fluktuationen auf die Dynamik der Matten, was zum Beispiel die Maximalgröße der Matte und die Zeit des Sinkens einschließt. Kooperativere Gruppen können größer wachsen und sinken später und haben damit eine höhere Überlebenwahrscheinlichkeit in strukturierten Umgebungen. Der Zeitpunkt des Sinkens der Matte wird erhöht, wenn man den Selektionsdruck verringert oder den Einfluss der Mattenausbreitung erhöht.

Dieser stochastische Effekt könnte den Weg zur Aufrechterhaltung von Kooperation in strukturierten Populationen bereiten, wenn man Populationsengpässe betrachtet. Allgemeiner liefert diese Arbeit einen Beitrag zum Verständnis der Voraussetzungen und Mechanismen der Evolution von Kooperation und des Übergangs von Einzelzellern zu multizellulären Organismen.

Contents

1 Multicellularity and the dilemma of cooperation

1.1 Evolution of life forms

Nature presents us with a stunning diversity of complex life forms. The origin of life [3, 4, 5], biodiversity [6, 7, 8], and the development of different organizational levels of life [9, 10] are some distinguished phenomena challenging biologists and – increasingly so – physicists alike.
To illustrate the latter issue, consider the example of the human body [11]. All the different cell types such as blood, skin, or liver cells work together in the human body. These cells depend on each other, and some are physically attached to one another. Individual cells cannot just split off in vivo, leave the body, and live as single-celled entities. Instead, one observes cooperation phenomena at different organizational levels. Single cells form tissues, single tissues and single cells together form organs and all entities at different levels are well-organized in the human body. Only the collective as a whole is able to survive, and it also has to survive for the lower-level entities to live. Furthermore, the human organism reproduces as a whole, but only specialized cells, namely gametes, can form offspring organisms. How and why did all other individual cells in the human body give away their ability to reproduce as individuals in the course of evolution?
Taking the other organizational direction into account, many human beings consciously or unconsciously organize in groups in which they collaborate and cooperate with each other to achieve a common goal; they live together in a family, they work together in a company, and exhibit social commitment.
Interestingly, all these transitions from one organizational level to another [12, 9] involve the change from many objects interacting on a lower scale to a unified, bigger object consisting of all smaller entities, and operating as a whole on a larger scale.

In modern biology, the development of organisms is interpreted within the framework of evolutionary theory. The fundamental principles of the theory of evolution refer to Charles Darwin and his groundbreaking work "The origin of species" from 1859 [3] in which he reveals the fundamental driving forces of evolution. Variation, selection, and heredity have proven to be an adequate approach to explain evolutionary dynamics and provide powerful tools to account for the evolution of species, speciation, and biodiversity – just to name a few examples [3, 13]. From today's point of view, with the knowledge of modern genetics,

evolutionary dynamics can be based upon a few principles including variation, natural selection, and heredity [14, 15, 16], which are summarized as follows.

- Phenotypic variation: Individuals show different phenotypic expressions in a population. In other words, they can differ in their morphological, behavioral, or any other observable property.

- Differential reproduction: Some phenotypes are slightly "better" adapted to environmental factors than others in the population. Hence, the individuals' growth, reproduction and survival rates will vary depending upon their phenotypic adaption to the environment which may change in time. In that sense, their contributions to later generations will also vary. The individuals which are "better" adapted to the environment will have a higher number of offspring, which we will refer to as the individual's fitness. This process is called selection and is often referred to as the survival of the fittest.

- Heredity: The genotype of an offspring, or in other words its genetic code, is highly correlated to the genotype of its parents. The genetic code, however, is also subject to variation in many ways. Sexual reproduction, for example, combines the genetic information of the parental organisms. Furthermore, spontaneous and induced mutations can alter the genotype.
  The genotype of an organism determines its phenotype to a large extent. The exact genotype-phenotype map, however, is highly complex and is subject to numerous influences such as random description errors and environmental factors. For instance, the gene expression, which is an essential part of this genotype-phenotype map, is not yet fully understood and is still subject of ongoing research [17, 18].

For a detailed review of these evolutionary principles, see [16, 15].

1.2 From single cells to multicellularity

One of the major challenges is to explain the transition from single cells to multicellularity [19, 20, 21] from a Darwinian point of view, that is by means of the described principles of evolutionary dynamics.
What are the advantages of a multi-cellular organism over single-celled entities? First of all, multicellular organisms are simply bigger in size than a single cell. If one thinks of the multicellular organism as a big ball consisting of single cells, the ratio between surface and volume decreases as the number of constituting cells rises. As a consequence, a multi-celled entity is protected more easily from predators, environmental factors, or other threats than singled-cells are. Moreover, the depletion of resources can be carried out more effectively, and by division of labor, the metabolism of the whole organism can work more efficiently. Because of its higher complexity, some cells may be able to specialize to specific tasks as a

preliminary stage towards differentiation. The development of a germ line, accounting for sexual reproduction, is a specific characteristics of this organizational level [22, 23]. The multicellular organism may occupy new niches and adapt to new environmental situations, which it has not been able to at the single-celled stage.

In order to gain deeper insight into the transition from singular cells towards a multicellular organism, one would have to understand why individual cells cooperate with each other in the first place and how mechanisms for the stabilization of cooperation could work in the framework of Darwinian evolution. The problem of the transition, at its core, lies in the following questions [24],

1. How does a group of cells form? Why do single cells form a cooperative group?

2. How can disruptive effects of cheaters in the group be minimized? How can cooperation be maintained in the long run?

3. How might the cooperative group reproduce as a whole?

1.2.1 The dilemma of cooperation

The first question involves the antagonistic nature of cooperative behavior, which is often referred to as the dilemma of cooperation. On the one hand, the whole population profits from the existence of individuals enhancing the fitness of all members of the group. These cooperating individuals are called cooperators. For example, cooperators could provide a public good from which all members of the population benefit. On the other hand, free-riders, that are organisms not contributing to the cooperation, do not have to bear the costs of cooperation, but still receive the full benefit of the cooperators. Therefore, free-riders, which we will also refer to as defectors, can reproduce faster than cooperators. They have an evolutionary advantage over the cooperators and will ultimately outperform the cooperating individuals. In this way, the viability of cooperators is always at risk although it would be optimal for all individuals to cooperate.

Even though cooperation is threatened by evolutionary dynamics, many examples for cooperative behavior are known in nature, for instance, public good producing bacteria such as *Pseudomonas aeruginosa* [25, 26, 27] and *Pseudomonas fluorescens* [28, 1]. In the next chapter, we will discuss one specific experiment with *Pseudomonas fluorescens* showing how cooperative behavior can occur in nature at the level of microbes. More generally, the formation of biofilms is often investigated in this context in order to study social bacteria including the occurrence of cooperation and multicellularity.
Other examples for stable cooperation of higher developed life forms include bee colonies, where eusocial behaviour can be observed [29, 30]. Ant colonies are a striking example of cooperative social behaviour as well [31, 32, 33].

1.2.2 Maintenance of cooperation

We have seen that the dilemma of cooperation limits the success of cooperative behaviour in the course of evolution and thus hampers the evolutionary transition from single cells to multicellular organisms. Since, nevertheless, many examples of stable cooperative behavior can be observed in nature, we will discuss the second question from section 1.2 in the following: how can cooperation be maintained in the long run?
In nature, there are many mechanisms of how disruptive effects of free-riders can be minimized and of how cooperative behavior can be retained in the long run. These mechanisms can be structured depending upon the cooperator's ability to recognize and memorize other cooperators, and the individual's ability to actively adjust its appearance and behavior. Means relying on the memory and the active adjustment of the behavior are referred to as reciprocity measures [34, 35, 36]. It includes the application of strategies for repeated interactions, as the famous tit for tat strategy for the repeated prisoner's dilemma [37], or the application of cultural strategies, as kinds of "legal policies", punishment, and other means of regulating social behaviour, to give some examples [38, 39].
If individuals are not able to actively distinguish between cooperators and defectors, and to customize their behavior, the notion of relatedness gains significance. These mechanisms, which are especially important to "lower level" species such as microbes, go under the name of assortment means. Due to structural and environmental factors, cooperators will interact with other cooperators with a higher probability than with defectors.

One often distinguishes between two assortment principles promoting the maintenance of cooperation: kin selection and group selection [40]. It is again emphasized that we only deal with passive forms of assortment in this context and no active choice of the interaction partner is carried out by the individuals. The distinction between kin selection and group selection and its importance for the maintenance of cooperation is controversially discussed in the scientific community and is still subject of an ongoing debate (see for example [35]). Historically, kin selection describes the idea that cooperation can be maintained if the indirect or inclusive fitness surmounts the direct or individual fitness disadvantage of cooperators. Direct fitness affects the individuals at the individual level, that is defectors are microscopically better off than cooperators. Indirect fitness, however, refers to the benefit from related individuals. Simply speaking, individuals will cooperate if the benefit for the organism's relatives is greater than the individual cost of cooperation. Hamilton's rule, $b \cdot r > c$ [41, 42], states that the less closer the relatedness, $0 \leq r \leq 1$, to the interacting individuals is, the higher the benefit of cooperation, b, has to be in order to surmount the costs, c. In this context, Haldane's famous quotation, "I would lay down my life for two brothers or eight cousins"[43], illustrates this point of view.

Nevertheless, both principles, kin selection and group selection, can be regarded as just being two sides of the same coin and we will discuss it in this way [44, 45]. For an outline of some aspects of the historical debate, the reader is referred to the relevant literature which can be found, for example, in [46, 47, 48].

Crucial for the maintenance of cooperation at the stage of individuals living in one population is that cooperators preferentially interact with other cooperators. In the simplest case, this preferential interaction could be mediated by an additional structure that allows for the division of the whole population into sub-populations, see figure 1.1 for an illustration.

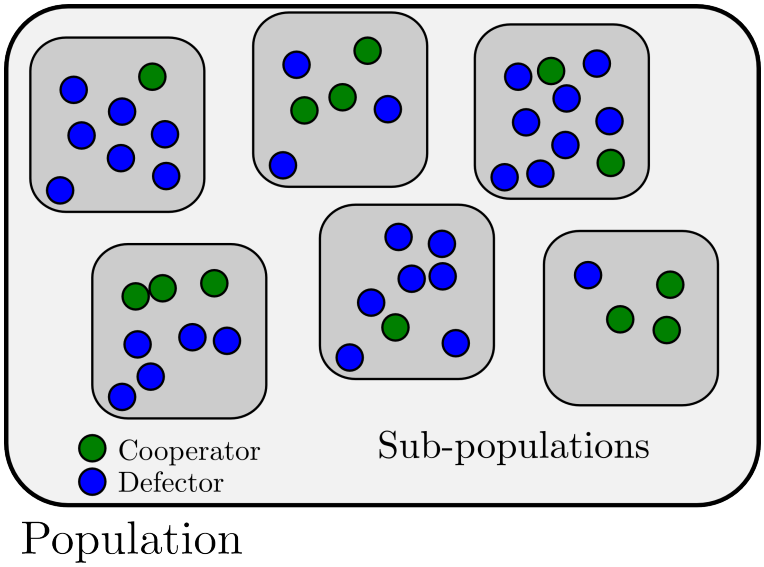

Figure 1.1: Division of the whole population into sub-populations. Crucial for the maintenance of cooperation is that cooperators preferentially interact with other cooperators. In the simplest case, this preferential interaction could be mediated by the division of the whole population into sub-populations. Within each sub-population, selection pressure acts on the individuals such that defectors are always better off than cooperators (intra-group selection). Selection pressure could also act on different sub-populations. Here, cooperative groups are favored over non-cooperative groups (inter-group selection). The evolutionary outcome depends on the relation between intra- and inter-group evolution, that is the relation between the two levels of selection (multi-level selection).

We will give two examples for this to happen later on. If one is able to distinguish between these two levels, selection can act on both levels. The corresponding theory is referred to as multi-level selection. On the one hand, selection acts on individuals within one sub-population (intra-group selection). Here, defectors are always better off than cooperators. On the other hand, selection may also act between the different sub-populations, such that more cooperative groups are favored than less cooperative groups in the course of evolution (inter-group selection). The evolutionary outcome depends on the relation between intra- and inter-group evolution, that is the relation between the two levels of selection [10]. For cooperation to be maintained, the advantage of cooperative sub-populations on the group level has to be big enough to dominate the selection disadvantage of cooperators on the lower level, that is within one sub-group [49]. If one refers only to the selection acting on

the different sub-populations, the term "group selection" is commonly used.
The assortment into sub-populations could be passively driven by environmental factors, for example by diffusion-limited dispersal of the common good promoted by cooperators [42], such that cooperation is acting only locally within a sub-population. If this assortment is actively driven by relatedness to other individuals in some sense, one speaks of kin discrimination. We will understand this term in the "weak sense" [44], where the group discrimination refers to the recognition of other cooperators, in contrast to kin selection in the "strict sense", where one emphasizes the degree of relatedness of the whole genome as described above.
Price and Hamilton could show, however, that only the division of a big population, consisting of cooperators and defectors, into sub-populations is necessary to formulate a condition for the maintenance of cooperation in mathematical terms [49]. In this understanding, the "weak" interpretation of kin selection as given above is sufficient.
As already indicated earlier in this chapter, it remains to be revealed, how the transition between the different levels of selection could occur in nature. We have argued that if selection acted on several levels, it could lead to the maintenance of cooperation. Nevertheless, we have to understand, how natural selection, acting only on single individuals, can imply a fitness measure on the group level. This shift has to involve additional structural elements on the population level, leading to sub-populations, such that cooperative groups have an evolutionary advantage over non-cooperative groups.

Experimental results to this shift are rarely known, but we will introduce a microbial experiment of Rainey & Rainey in the next chapter which shows the emergence and the dilemma of cooperation, and which could serve as a guiding example for future investigations of this transition. The mathematical framework in which evolutionary dynamics is conveniently formulated will be introduced in chapter 3. In chapter 4, we will then develop a stochastic mat model that describes and explains the occurrence of cooperation effects in microbial biofilm colonies. The analysis will be motivated by and based upon the spirit and the outcome of the Rainey & Rainey experiment. We will analyze the developed mat model and compare the outcome of numerical simulations to the experimental observations in chapter 5. Finally, chapter 6 is devoted to the proposal of repeated population bottlenecks that might pave the way to stable cooperation scenarios.

2 Cooperation experiment of Rainey & Rainey

In this chapter, we describe an experiment which was carried out by Rainey & Rainey in 2003 [1], and which is often cited in the context of the evolution of cooperation in microbial systems. The experiment will serve as an illustration of many problems we have already encountered in the discussion of cooperative phenomena, namely the question of how cooperation could arise in the course of evolution in the first place and how it could be maintained thereafter.

2.1 Experimental setup and growth of mat

The experiment of Rainey & Rainey involves the investigation of the growth dynamics of the well-studied bacteria strain *Pseudomonas fluorescens*, which is sketched in figure 2.1.

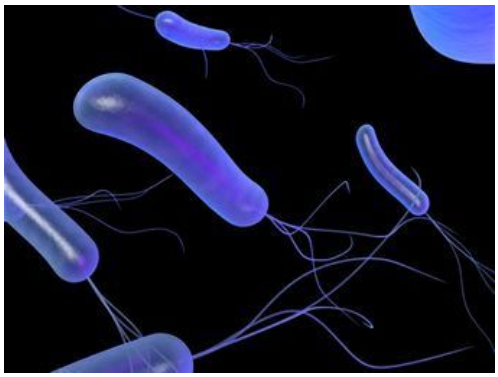

Figure 2.1: Sketch of *Pseudomonas fluorescens*, adapted from [50]. *P. fluorescens* is a rod shaped, obligate aerobic bacterium which rapidly adapts to new environmental conditions due to genetic mutation. In this way, *P. fluorescens* is a good example to test evolutionary theory, especially the evolution of cooperation [1].

P. fluorescens is a rod shaped, obligate aerobic bacterium that is able to live under different environmental conditions, e.g. in soil, water, and plants. The need for oxygen is an important characteristics of its metabolism and is critical to its viability. Without oxygen,

the gain of energy due to the splitting of sugars is inhibited and the bacteria cannot grow or might even die [51].

In the Rainey & Rainey experiment, the so-called ancestral smooth (SM) *P. fluorescens* strain is used as the initial genotype from which all other populations were founded. The name SM refers to the smooth appearance of its colony morphology as shown in figure 2.2 after agar-plating. The bacteria are cultured in a static glass vial containing a mixture of water and a nutrient, which we will refer to as broth in the following.
Another important feature of the setup is the introduction of a spatially structured environment for the bacteria growth, which is induced by an unmoved broth pot. By not shaking and not stirring the broth pot, a gradient of oxygen concentration builds up with high concentration of oxygen close to the liquid-air interface and very low oxygen concentration at the bottom of the vessel [52, 53]. Regarding the metabolism of the bacteria, a high oxygen concentration is much more preferred as mentioned above. Bacteria, whose metabolism works more efficiently and faster due to the presence of higher oxygen concentration, will have a higher doubling rate compared to bacteria having only access to a low concentration of oxygen. Thus, bacteria with access to a high concentration of oxygen will be favored in the course of evolution.
To summarize, the effect of spatial heterogeneity within the broth pot is that bacteria that are able to live close to the liquid-air interface grow faster and, thus, have an evolutionary advantage over the bacteria which are farther away from the surface.

A key attribute of *P. fluorescens* is the rapid adaption of its phenotype to new environmental situations [28], which plays a crucial role in the experiment. *P. fluorescens* is, metaphorically speaking, a real adjustment artist. When the SM strain is cultured in the broth phase, it will rapidly diversify in this spatially structured environment. The diversification process is mainly driven by simple genetic mutations leading to different phenotypic expressions [54, 55, 56, 57, 58].
Two of the most prominent representatives of these niche specialists are the wrinkly spreader (WS) and the fuzzy spreader (FS), again named after their morphological appearance, which can be seen in figure 2.2 after agar-plating.

2.2 Emergence and dilemma of cooperation

The experiment of Rainey & Rainey focuses on the wrinkly spreader which is derived directly in the broth pot from the SM ancestral strain via a single genetic mutation [55]. This mutation causes the change of the cell cycle regulation, namely the change of the gene expression of a cellulose-like polymer (CLP). As a result, the CLP is overproduced outside the bacteria cell and acts like glue between the polymer-producing bacteria. It can be assumed that the phenotypic state of the wrinkly spreader in which this CLP is overproduced can be reached by many possible simple mutations from the SM genotype

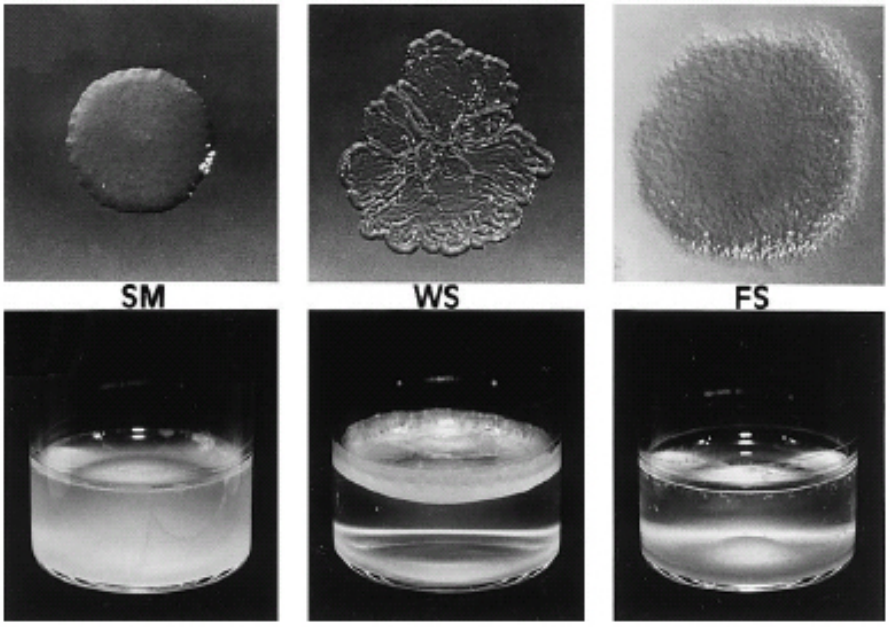

Figure 2.2: One distinguishes three different phenotypes of *P. fluorescens*, each named after its appearance after agar-plating (upper lane) [28]. The left panel shows the ancestral smooth (SM) strain, the middle panel depicts the wrinkly spreader (WS), and the right panel shows the fuzzy spreader (FS). WS and FS strain are derived from the SM genotype by genetic mutation. The WS phenotype arises after only approximately 20 generations if the broth pot is not stirred and not shaken. FS bacteria grow at the floor of the vial (lower lane), whereas WS cells colonize the liquid-air interface of the solution. Due to an overproduction of a cellulose-like polymer that acts like a glue between the WS cells, they are able to form a mat. The WS trait only survives transiently in a heterogeneous environment in which an oxygen gradient can build up. In a homogeneous solution, the WS phenotype is rapidly outperformed by the smooth strain.

[55]. This adaption explains the rapid diversification of the SM ancestral strain. It takes roughly 20 generations in a spatially structured environment to observe the WS phenotype in a broth phase in which only SM bacteria have been cultured in the beginning [59].
After cell division, the two WS daughter cells will stay connected to one another. If this mutation occurs close to the liquid-air interface, the WS cells can attach to the edge of the glass vial. Growing from this supporting point, the bacteria will spread rapidly and form a fine biofilm at the liquid-air interface. It is also observed, however, that some WS cells can form little rafts swimming at the surface of the solution before attaching to the edge of the glass pot [60]. As the population of WS cells in this self-supporting mat grows, the whole broth surface will be colonized. Its structure also changes from a fine biofilm to a clearly visible and robust mat, which will ultimately suffer under its own prosperity: the mat becomes too dense and will sink as shown in figure 2.3.

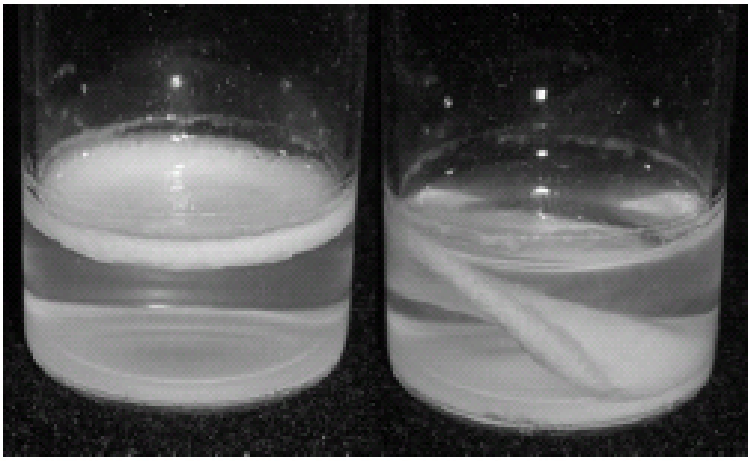

Figure 2.3: Growth and sinking of the mat as an example for the occurrence and the dilemma of cooperation; pictures adapted from [54]. The wrinkly spreader (WS) overproduces a glue-like polymer such that two WS daughter cells remain stuck together after cell division. The WS cells can attach to the edge of the glass vial and colonize the liquid-air interface of the solution. The biofilm grows rapidly in size and thickness (left picture). A mat is build up that will suffer under its own prosperity and ultimately sink since the biomass of the bacteria in the mat surmounts the stabilizing forces of the mat structure (right picture). More interestingly, the growth of the mat is further limited by the occurrence of mutations from a WS cell to an ancestral SM cell in the mat which causes the sinking process on a significantly shorter timescale. This observation is an example for the dilemma of cooperation. Defecting genotypes penetrate the mat like cancer cells threaten a healthy tissue since the fitness of the defectors in the mat is even higher than the fitness of the WS cells. The defectors gain the same benefit of the mat formation but have no cost for the production of the sticky polymer in contrast to the cooperating WS cells. The optimum for the whole microbial colony would be attained if only cooperating cells were present in the mat.

In the last chapter, we have presented the dilemma of cooperation stating that cooperators are threatened by defectors which save the cost, but still benefit from the cooperation. Ultimately, defectors will outperform the cooperators although cooperation would be optimal for the whole population. This configuration is also observed in the mat experiment.
The success of the mat growth is actually limited by the emergence of mutants that arise *de novo* from the WS genotypes by genetic mutation [1]. These mutants from the CLP expressing cells have the property of not overproducing the glue-like substance and resembling the ancestral strain of SM cells in many attributes. They live in the mat close to the liquid-air interface, and hence gain the same rewards of high oxygen concentration. In contrast to the cooperating WS cells which are fixed in the mat frame, these mutants are motile and do not support the skeleton of the mat. In this way, they do not contribute to the mat structure. These cells will be called defectors in contrast to the WS, which will be referred to as cooperators in order to signify their contribution to the mat structure.

Ancestral SM cells and defecting cells show a similar smooth morphology, and the same fitness in an unstructured environment can be assumed [55]. Fitness is always measured in terms of the doubling rate during the exponential growth phase, and the fitness of the ancestral SM strain is defined to be 1 [1].

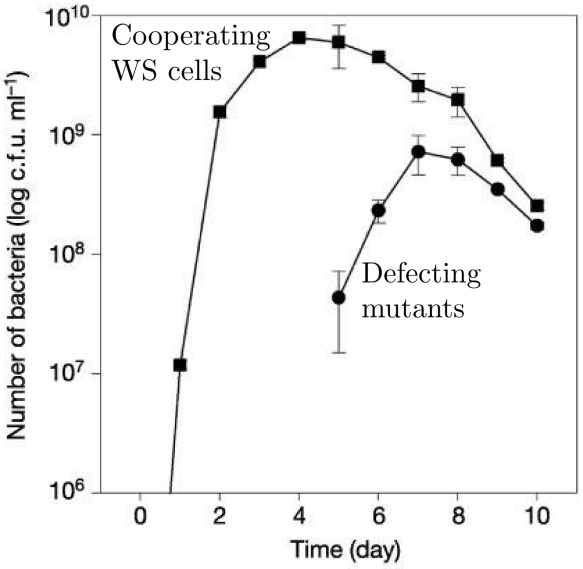

Figure 2.4: Emergence of defecting cells in the mat [1]. The number of cooperating WS cells (squares) and the number of defecting mutants (circles) in the mat are counted at different points in time in colony-forming units (c.f.u.) per ml. The number of cooperating WS cells increases rapidly until day 3 because of the access to oxygen mediated by the mat formation. The mat is, however, threatened by defecting mutants which arise *de novo* from the WS genotypes by genetic mutation. These mutants do not contribute to the mat structure since they do not overexpress the sticky polymer. They have an evolutionary advantage over the cooperating WS cells which leads to a dilemma of cooperation. As a consequence, the number of defecting cells in the mat increases rapidly until day 7. The number of cooperating WS cells is already decreasing from day 4 on due to the sinking of the mat.

The WS cells have a significantly lower fitness of $0.33-0.80$ compared to the SM phenotype in an unstructured environment [55, 1, 61]. The cooperating cells overproduce the cellulose-like polymer which is highly energy-costly to the metabolism of the WS cells compared to its ancestral SM cells, and results in a reduced doubling rate. Namely, the carbon metabolism of the WS cells shows catabolic defects causing the lowered relative fitness (for metabolic details see [62]). In a homogeneous broth with sufficient oxygen supply, for example realized by a permanently stirred environment, the WS cells would be outperformed by cells not having the costs for the production of the sticky CLP. When the population of WS cells grows in a spatially structured environment, however, the overproduction of CLP turns into

a transient evolutionary advantage for the WS cells. The fitness of the WS cells increases dramatically to 1.6 compared to the SM strain, because of the mat formation and the induced vicinity to oxygen resulting in a reduced doubling time [55]. Moreover, the mat also acts like an additional oxygen blocker to all other cells in the broth phase not living in the mat. Experiments show that this blocking effect of a fully grown mat corresponds to an oil layer of 2 mm in thickness at the surface of the broth applied to the cells in the liquid [1].
The effect of the cooperation of the WS cells and the emergence of defecting cells are quantitatively shown in figure 2.4, which depicts the number of cooperators and defectors in time after the solution has been prepared with the ancestral SM strain. The profit of cooperation on the population level is bigger than the costs at individual level for the WS cells. Therefore, the number of WS bacteria in the mat grows rapidly between day 0 (the first occurrence of a WS cell) and day 2.
The mat growth enhances the fitness of the WS trait, but at the same time the population of WS will be vulnerable to the evolutionary emergence of defectors [1]. Because of the microscopic selective advantage of the defecting phenotype over the cooperating cells, the number of defecting cells in the mat increases rapidly until day 7. The number of cooperating WS cells is already decreasing from day 4 on due to the sinking of the mat. During the sinking process of the mat, the fraction of cooperators in the mat decreases as can be inferred from the two curves in figure 2.4.

In figure 2.5, the consequence of the invasion of the mat by defecting cell types is depicted. The dotted line shows the number of cooperating WS cells in absence of defectors. By scoring the different bacteria phenotypes on agar plates, it is possible to identify mats without defectors. The number of WS in the purely cooperative mat is increasing rapidly in the beginning (growth phase). As already indicated, the mat sinks after day 4 which is caused by an increase of the mat density. The sinking process is reflected by the gradual decrease in the number of cells in the mat.
In presence of defectors, the growth of the WS cells in the mat stays unaffected in the beginning. The invasion of the mat by defectors, however, has a negative impact on its structure. Since the defectors do not produce the sticky polymer that is necessary for the stabilization of the mat, the mat structure is weakened by the defectors. Whereas in the case of absence of defectors in the mat, the sinking process takes approximately the same time as the growth process, the whole mat sinks abruptly after having reached the threshold mat density at day 4 when defecting cells are present in the mat. The instability of the mat gives rise to its sinking, which takes place on a much shorter time scale than in case without defectors.
This effect was also quantified in [1]: A mat infiltrated with 24% defecting cells at day 3 collapses under the weight of 79 mg of glass beads, whereas a mat comprised solely of WS cells collapses only under 432 mg, which is more than the fivefold weight, at day 3. This clearly emphasizes the negative impact of the defectors on the mat structure.

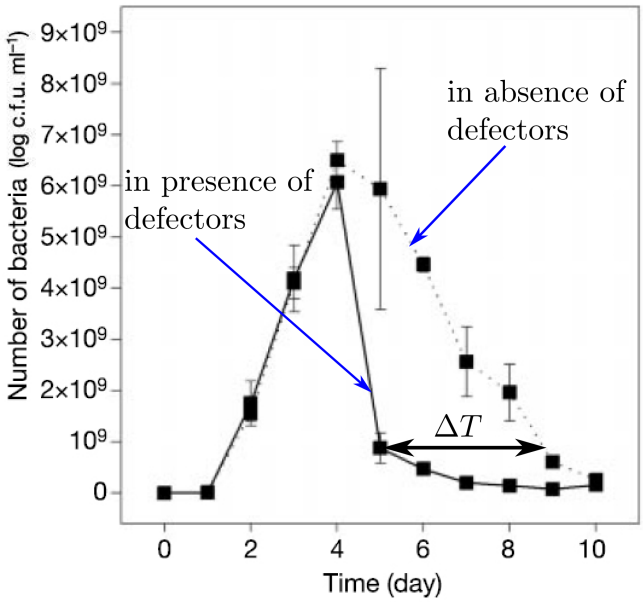

Figure 2.5: Number of cooperating WS cells in the mat with (solid line) and without (dashed line) defecting mutants [1]. The number of bacteria cells is counted on agar plates in colony-forming units (c.f.u.) per ml. The case with no defecting cells is identified afterwards. The sinking of the mat changes qualitatively if defecting cells are present or absent in the mat. In presence of defectors, the mat sinks abruptly and on a much shorter timescale than in absence of defectors since defecting cells do not contribute to the mat skeleton that stabilizes the mat (time difference ΔT). In this way, the viability of the whole population is at risk when defecting cells are present.

2.3 Summary of the experiment

The Rainey & Rainey experiment [1] shows cooperation which emerges due to a single mutation in a spatially heterogeneous environment. Whereas cooperation is costly on the level of single cells, the benefits stemming from the cooperation at group level surmount the costs and result in a transient evolutionary advantage of the cooperating trait over the ancestral one. The spatial heterogeneity is a crucial property of the experiment. This additional structural element is directly related to the competition for nutrients, in this case oxygen, leading to the increased fitness of the cooperators.
The evolutionary transition is, however, put at risk due to the dilemma of cooperation. Cells which are able to reap the profit from the cooperating cells without contributing to the cooperation at group level will have an evolutionary advantage over the cooperators since they do not have to bear the costs for cooperation. The defectors outperform the cooperators. Thus, the viability of the whole population is threatened by these free-riders.

Turning back to chapter 1, where we discussed the transition from single cells to a multicellular organism and formulated the obstacles of this transition in three steps, we recognize

that the Rainey & Rainey experiment addresses the first question, namely how single cells form a cooperative group. In a recent paper [54], Rainey discusses the other two issues, the maintenance of cooperation and the reproduction of the group as a whole, by using the example of the mat formation of *P. fluorescens*. Let us discuss this proposal as a theoretical outlook to the experiment.

2.4 Proposal of Rainey & Kerr: cheaters as the germ line

The third question from section 1.2 (How might the cooperative group reproduce as a whole?) addresses the so-called trade-off between fertility and viability [63]. On the one hand, single-celled organisms can reproduce much more quickly, on the other hand, a multicellular organism might live longer and receives the advantages to its viability as mentioned above. Single cells have to trade-off fertility, that is give away their ability to reproduce independently on their own, in order to reproduce as part of the group, in which they might not be part of the germ line. Only few cells of the multicellular organism will found offspring organisms; all other cells will sacrifice themselves for the whole group. How can this altruistic behaviour be explained in terms of natural selection? How can a germ line emerge in the course of evolution? We assume that bacteria, as indicated earlier, do not have a conscious idea of the bigger picture, and are not aware of the advantages of forming a multicellular organism a priori.

Turning to the experiment of Rainey & Rainey, this transition would mean that mats have to participate in the process of evolution by natural selection as objects on their own. Therefore, one needs variation of the mats on the group level. Moreover, the mats have to be capable of reproducing own copies, and offspring mats have to resemble the parental mats [54]. The key problem is to find a way such that mats can leave offspring groups. In the experiment described in chapter 2, mats are short-lived and an evolutionary dead-end since selection only acts at the level of individual cells, where defectors are always better off than cooperators. As a consequence, the mat collapses at some point in time [54].

The proposal of Rainey and Kerr to resolve this problem involves a consideration out of the ordinary. They regard the defecting bacteria not only as a threat for the maintenance of cooperation, but also as a way out of the dilemma of cooperation. We have seen that cheaters arise as readily by mutation from the cooperating trait as cooperators do from the ancestral SM strain. Since defectors and ancestral SM bacteria show the same phenotypic expression [1], one could imagine that cheaters might mutate back to the WS cooperators. The point is that the cooperating bacteria are stuck in the mat skeleton and cannot leave the mat. In contrast, the defector cells are highly motile and can free themselves of the mat when it sinks since they are not part of the mat frame. In principle they can swim back to the liquid-air interface, mutate back to a cooperating cell and the mat growth process could start all over again as depicted in figure 2.6. In this way, a life cycle could build up with

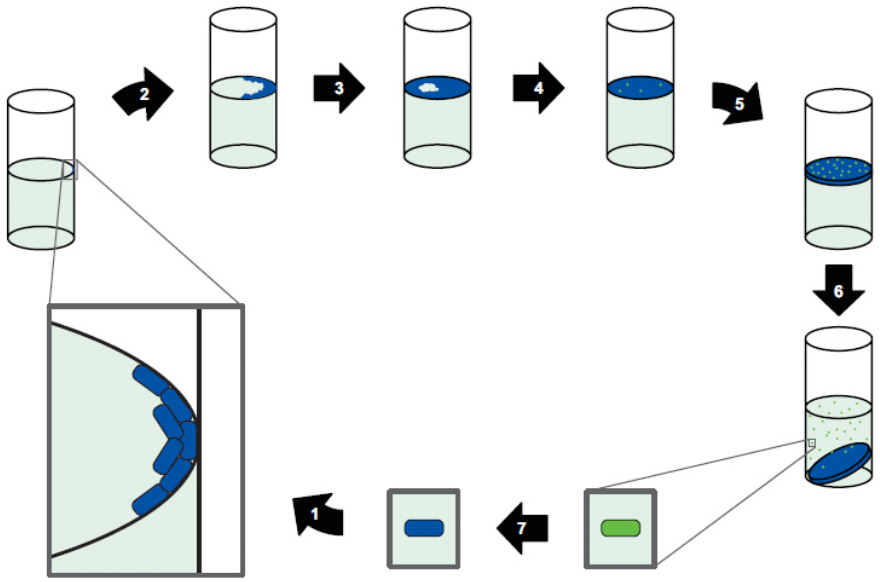

Figure 2.6: Proposal of Rainey & Kerr: cheaters as the germ line [54]. In order to describe the transition from single-celled entities to a multicellular organism, Rainey uses the example of the *P. fluorescens* strain. By proposing a life cycle in which cooperators and defectors regularly mutate to one another, the maintenance of cooperation can be assured and a multi-level selection setup is established. The defectors can be regarded as the germ-line of the cooperating mat which reflects the soma-line. Experimental evidence of this proposal is subject of current research. See text for details.

the cooperative collective, the WS mat, as the soma and the cheaters as the germ-line [54]. Each defector carries the genetic DNA allowing for cooperation after one simple mutation. The innovative idea is that cheating is not only the problem of cooperation, that has to be overcome, but it is also absolutely essential for the maintenance of cooperation. Cheating is part of the solution [24].
In summary, this proposed life cycle describes the transition from single cells to multicellularity by introducing a soma- and a germ-line, whereas cheaters function as the germ cells. Therewith, the maintenance of cooperation can be assured and the multi-level selection setup is established.
One can also change the point of view and regard the cooperating microbes as the germs for the defecting bacteria. The defector cells are like stem cells that can mutate to WS cells. This cooperative phenotype is a helping or scouting cell by building up the mat and sacrificing its life for the germ line, that is the ancestral defecting bacteria [54]. Here, only one mutational direction is needed, namely the mutation from a non-cooperating cell to a cooperating cell.

From a biological point of view, this proposal, however, seems unrealistic at first. The life cycle heavily relies on the occurrence of the right mutation at the right time. Therefore,

the life cycle is unregulated, and rather underlies stochastic fluctuations.
Nevertheless, also the other approaches to a multi-level selection rely on stochastic events. This will become clearer in chapter 6. What seems more challenging is the determination of how a new mat was founded. Rainey proposes that a cheater mutates to a cooperator cell which builds up the new mat. But how could such a way be distinguished from a scenario in which a part of a sinking mat breaks away and these cooperative cells from the collapsed mat form the new mat? From a experimentalist's point of view, it should be only possible to observe whether a new mat has formed or not. The way in which this formation has happened, indirectly via a mutation from a cheater to a cooperator or directly via a cooperator, is hard to infer since the observed outcome should be the same. Moreover, bet hedging bacteria of the *P. fluorescens* strain have been observed recently [64]. These bacteria are able to rapidly switch their phenotype stochastically. If such a bacterium founded a new mat, it would again be challenging to identify its origin. Clearly, some experimental effort has to be carried out in order to verify Rainey's proposal. It will be exciting to see, how these experimental obstacles can be overcome.
In this thesis, we will not follow this "indirect" life cycle of Rainey, but rather concentrate on the aforementioned maintenance of cooperation through the "direct reproduction" of mats in a simplified and artificial setup. We will come back to this discussion at the end of this thesis in chapter 6.

3 Evolutionary Game Theory in Growing Populations

In this chapter we present a brief introduction into the mathematical description of evolutionary dynamics that is used throughout this thesis. The interplay between the principle of natural selection, that is Darwinian evolution, and population growth, is formulated in the most convenient way in terms of evolutionary game theory and population dynamics. Both approaches can be merged into a combined view which was formulated in a recent paper by Melbinger, Cremer & Frey in [2]. This concept enables us to treat the described dilemma of cooperation in growing populations. It will be shown that this stochastic model reveals a transient increase of cooperation caused by demographic fluctuations. For a didactic introduction into this model, the reader is referred to the thesis of Lechner [65]. In chapter 4, these ideas will be applied and extended to a model for the growth and sinking of the mat in the Rainey & Rainey experiment.

3.1 Evolutionary dynamics

Speaking in general terms, evolutionary dynamics focuses on the temporal evolution of a specific trait, strategy, or any other observable characteristics in a population under selection pressure; see [66] for a recent overview. Let us investigate a common approach to this evolutionary dynamics, namely the replicator equation in which the population size is assumed to be constant.

3.1.1 Replicator equation

Consider a well-mixed population with individuals of L different traits. We are interested in the evolution of the state vector $\mathbf{x} = (x_1, \dots, x_L)$, whereas x_S is defined as the fraction of trait S in the total population. We assume that the characteristics labeled by the index $S \in \{1, \dots L\}$ only changes due to its fitness $\Phi_S \in \mathbb{R}$ compared to the average fitness $\Phi_\sim(\mathbf{x}) := \sum_S \Phi_S x_S$ in the whole population. The fitness Φ_S of trait S determines the relative abundances of this trait in the next generation and thereby quantifies its adaption to environmental and other factors. A microscopic derivation is obtained, for example,

from evolutionary game theory which will be described in the next section. One important case is the frequency-dependent fitness. Here, the fitness of a given trait depends on its fraction within the population, that is in general $\Phi_S = \Phi_S(\mathbf{x})$. The higher the fitness Φ_S of trait S is compared to the average fitness $\Phi_\sim$ of the population, the higher will be the percentage of trait S in the next generation [34].
The standard approach to describe the evolution of the relative abundances $\mathbf{x}$ is then given by the so-called replicator equation in which the principle of frequency-dependent selection becomes mathematically manifest [67, 68],

$$\partial_t x_S = (\Phi_S(\mathbf{x}) - \Phi_\sim(\mathbf{x})) \cdot x_S, \quad \text{for } S \in \{1, \dots L\} \ . \tag{3.1}$$

If the interest lies on the relative fitness advantage of a specific trait S over the average fitness of the population, and not on the absolute fitness advantage as above, one introduces the relative fitness,

$$f_S = f_S(\mathbf{x}) := \frac{\Phi_S(\mathbf{x})}{\Phi_\sim(\mathbf{x})} \ . \tag{3.2}$$

The replicator equation in its adjusted form then reads as,

$$\begin{aligned} \partial_t x_S &= \frac{\Phi_S(\mathbf{x}) - \Phi_\sim(\mathbf{x})}{\Phi_\sim(\mathbf{x})} \cdot x_S \ , \\ &= (f_S(\mathbf{x}) - f_\sim(\mathbf{x})) \cdot x_S, \quad \text{for } S \in \{1, \dots L\} \ . \end{aligned} \tag{3.3}$$

By normalizing the fitness as in eq. (3.3), the timescale on which the state vector $\mathbf{x}$ changes is altered. The result of the evolutionary dynamics, however, remains unaffected.
The replicator equation can be induced from the well-studied Price equation, which reveals a deeper understanding of the interplay between the growth factor for species abundances and its trait's characteristics. At its core it states that a specific trait will increase in size if the trait's characteristics is well adapted (positively correlated) to the growth factor. However, since the Price equation can be understood as a consistency relation, it does not reveal more insight into the evolutionary dynamics, we are interested in. Therefore, we will not deepen the discussion at this point, see [44, 45] for further details.
Furthermore, the replicator equation is a deterministic approach to the dynamics of evolution. If we consider a finite population, demographic fluctuations can play a crucial role for the evolutionary outcome of the dynamics. The replicator approach neglects the stochasticity of birth and death events and reflects a mean-field approach which is only valid for $N \to \infty$, if N labels the size of the population. We will highlight this feature in due course, but before let us discuss one possible way to motivate the fitness functions Φ_S from a more microscopic point of view.

3.1.2 Evolutionary game theory

One possible concept to describe and understand how different traits, strategies, or other characteristics compete with each other within one population is evolutionary game theory

[66, 12, 69]. In this framework, each individual of the population is assumed to have one of the L fixed strategies. The goal is to describe the fitness functions Φ_S for $S \in \{1, \dots L\}$, and to find out how successful a certain strategy is over the competing strategies.

Let us exemplify the game-theoretical approach for two different traits characterized by their strategy, namely a cooperating (C) and a defecting (D) strategy. We introduce the so-called payoff matrix $P \in \mathbb{R}^{2\times 2}$ defining the payoff of the specific strategies and prescribing the success of one strategy over another. In classical game theory, the entry $P_{i,j}$ of the payoff matrix is understood as the payoff a player receives when playing strategy i against strategy j played by a different agent. In the context of evolutionary game theory, $P_{i,j}$ describes the payoff of an individual of trait i interacting with a different individual of trait j. The best rational decision is then to play the strategy which maximizes the payoff against all other strategies.
The fitness function will then be computed as,

$$\Phi_S = 1 + s \cdot (P\mathbf{x})_S, \quad \text{for } S \in \{C, D\} \ . \tag{3.4}$$

The parameter s labels the selection strength and relates the influence of the played strategy and the obtained payoff to the background fitness 1. In this way, we can tune the selection pressure and the timescale at which selection acts. In this formulation, the fitness function depends only linearly on the relative abundances $\mathbf{x}$; however there are cases in which a non-linear fitness function is crucial to explain the experimental outcome [70].

Let us elucidate the concept of game theory with the prominent example of the prisoner's dilemma. Two men, having committed a severe crime, are caught by the police and are now separately under interrogation. Both suspects have the possibility to either remain silent or to blame the other one for having committed the crime on his own. They do not know about the other's testimony before the interrogation. If one defendant blames his companion and he remains silent, the betrayer will be released immediately and his companion will be send to jail for ten years. If both criminals blame each other, they will be imprisoned for five years each. Since there are not enough evidences, both defendants can only be condemned for a minor crime if they cooperate and both remain silent. Then each of them is send to prison for one year.
This game can be represented by the payoff matrix as follows,

	C	D
C	-1	-10
D	0	-5

Let us analyze the game from a suspect's point of view. If my companion is a defector, that is he blames me for having committed the crime, I will be send to jail for ten years if I say nothing, or I will be imprisoned for five years if I also defect and blame him for having committed the crime. Hence, if the other criminal defects, I shall also better defect

in order to reduce my time in prison ($-10 < -5$).
On the other hand, if my companion cooperates and remains silent, I will be sentenced to one year; but if I blame him, I will be free. Again, the optimal strategy from my perspective would be to defect ($-1 < 0$).
In mathematical terms, the payoff for a player from an individual's point of view is always maximized if he choses the defecting strategy. This conclusion holds true for all players. Moreover, all players cannot increase their payoff by solely changing their strategy. This situation is referred to as a Nash equilibrium [71].
From an egoistic point of view, both players would then choose to defect, that is both defendants will be send to prison for five years each, although they have the possibility to cooperate and, thus, to reduce the time in prison to one year for each. This social dilemma is caused by the risk of being exploited by defectors, and reflects the dilemma of cooperation we have already encountered in the experiment of Rainey & Rainey. Defectors are always better off although it would be beneficial for all players to cooperate.

For a general two player game and social dilemmas, the payoff matrix is written as [72, 32],

$$\mathrm{P} = \begin{pmatrix} \mathcal{R} & \mathcal{S} \\ \mathcal{T} & \mathcal{P} \end{pmatrix}.$$

The two players are rewarded with the payoff $\mathcal{R}$ if both of them cooperate; however, both players are tempted to defect due to the payoff $\mathcal{T}$. $\mathcal{P}$ is the punishment if both players are defecting and $\mathcal{S}$ quantifies the sucker's payoff. A game leads to a social dilemma if the reward exceeds the punishment $\mathcal{R} > \mathcal{P}$, and at the same time the temptation to defect is larger than the sucker's payoff, $\mathcal{T} > \mathcal{S}$, and the punishment, $\mathcal{T} > \mathcal{P}$.

Let us now turn to the scenario in which the fitness of an individual is given by the expected payoff $\Phi(\mathbf{x})$ of a two player game. We will give a motivation for this situation below. Depending on the entries of the payoff matrix, one can distinguish between four different regimes for the stability of the two strategies within an evolutionary setup and a whole population [66].

- Prisoner's dilemma: $\mathcal{T} > \mathcal{R}$ and $\mathcal{P} > \mathcal{S}$; leads to stable defection, that is cooperators die out.
- Snowdrift game: $\mathcal{T} > \mathcal{R}$ and $\mathcal{P} < \mathcal{S}$; leads to stable coexistence of cooperation and defection.
- Coordination game: $\mathcal{T} < \mathcal{R}$ and $\mathcal{P} > \mathcal{S}$; leads to unstable coexistence of cooperation and defection.
- Mutualism: $\mathcal{T} < \mathcal{R}$ and $\mathcal{P} < \mathcal{S}$; leads to stable cooperation, that is defectors die out.

In summary, the most difficult way to obtain stable cooperation is a setup which is characterized by the properties of the prisoner's dilemma. Therefore, we will take the prisoner's

dilemma as the basis for the microscopic definition of the trait-dependent fitness functions $\Phi_S, S \in \{C, D\}$, but interpret the prisoner's dilemma as a public goods game in the following way,

$$\mathrm{P} = \begin{pmatrix} b-c & -c \\ b & 0 \end{pmatrix} \quad , \; b > c \; .$$

A cooperating individual provides a public good b to the individual with which the interaction takes place. To provide the public good, the cooperator has to invest the cost c. If a cooperator interacts with another cooperator, the payoff will be $b - c$. The cooperator will not receive the benefit if he interacts with a defector, but the defector will be rewarded with the full benefit of the cooperator without paying any costs.
The fitness functions for a cooperating (C) and a defecting trait (D) then read as follows (cf. (3.4)),

$$\begin{aligned} \Phi_C(x) &= 1 + s(bx - c) \; , \\ \Phi_D(x) &= 1 + sbx \; , \\ \Phi_C(x) - \Phi_D(x) &= -sc \; , \\ \Phi_\sim(x) &= x \cdot \Phi_C(x) + (1-x)\Phi_D(x) = 1 + sx(b-c) \; . \end{aligned}$$

The relative trait-dependent fitness functions can be computed accordingly as,

$$\begin{aligned} f_C(x) &= \frac{1 + s(bx-c)}{1 + sx(b-c)} = 1 - sc(1-x) + \mathcal{O}(s^2x^2) = 1 - sc + \mathcal{O}(sx) \simeq 1 - sc \; , \\ f_D(x) &= \frac{1 + sbx}{1 + sx(b-c)} = 1 + scx + \mathcal{O}(s^2x^2) = 1 + \mathcal{O}(sx) \simeq 1 \; , \\ f_C(x) - f_D(x) &= \frac{-sc}{1 + sx(b-c)} = -sc + \mathcal{O}(s^2x) \simeq -sc \; , \\ f_\sim(x) &= x \cdot f_C(x) + (1-x) f_D(x) = 1 \; . \end{aligned} \tag{3.5}$$

We have expanded the denominator in the equations for the relative fitness functions in powers of the selection strength, s, and the fraction of cooperators, x. This expansion is valid since $0 \leq x \leq 1$ always holds, and for our purposes $0 < s \lesssim 0.15$ (weak selection) can be assumed for most cases. The cost c will be set to 1 throughout this thesis.
The important point to notice is that $f_C - f_D \simeq -s$. This relation reflects the property that defectors are microscopically always better off than cooperators. We can quantify the microscopic advantage of defectors by the strength of selection s. Equation (3.3) then quantifies the temporal evolution of each trait. Note that the x-averaged fitness $f_\sim$ is simply 1 for the case of relative fitness functions.

3.2 Population dynamics

Population dynamics describes the temporal evolution of the number of individuals N living in a population. In other words, we are interested in the change of the number of individuals, in contrast to evolutionary dynamics which focused on the temporal evolution of different traits within one population of fixed size.
Especially, population dynamics studies the internal and external influences on the growth of a population. External factors involve, for example, environmental conditions such as the access to nutrients and the existence of toxics, the interaction with preys and predators, or geometric restrictions. The feedback of individuals on the growth of the population can be used as an example for an internal factor. In the following, let us briefly review some of the basic growth laws.

The growth law of Malthus

This growth law assumes that each individual reproduces with a constant per capita growth rate r [73],

$$\partial_t N(t) = r \cdot N(t) \ ,$$

which leads to the exponential growth law, $N(t) = N_0 \cdot e^{rt}$, whereas N_0 prescribes the initial population size. This growth law holds true, for example, if nutrients are abundant in a bacterial colony [74].

The growth law of Verhulst

The growth of a population, however, is often limited due to finite resources or confined space. In order to account for this situation, Verhulst introduced a negative term to the differential equation from above [75],

$$\partial_t N(t) = r \cdot N(t) - \frac{N(t)^2}{K} \ , \tag{3.6}$$

with K as the carrying capacity. In this picture, the population can only grow to the value of $r \cdot K$ in size in a sigmoid way (see figure 3.1) which can, again, be often observed in bacterial and microbial colonies [76, 74]. The solution to this differential equation is given by,

$$N(t) = \frac{rKN_0e^{rt}}{rK - N_0 + N_0e^{rt}} = \frac{rK}{(rK/N_0 - 1)e^{-rt} + 1} \ . \tag{3.7}$$

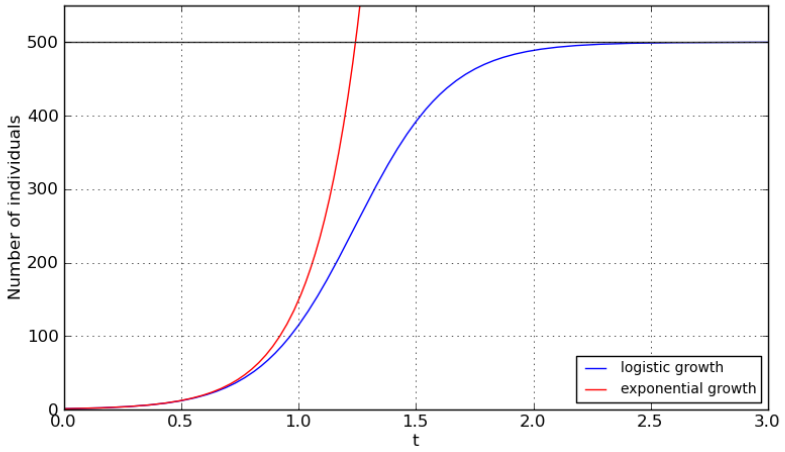

Figure 3.1: Comparison of exponential and logistic growth. In both cases, we have set $r = 5$; for the logistic growth, we have $K = 100$ (cf. eq. (3.6)). The logistic growth levels off in a sigmoid way at the value $r \cdot K$ in contrast to the exponential growth which grows unbounded. Note, however, that the initial dynamics, that is the dynamics at a small individual number, is similar for both growth laws.

General growth laws

In general, the growth of a population can be described in mathematical terms by the following ordinary differential equation,

$$\partial_t N(t) = F(N(t), t) \ ,$$

with F as a non-linear function in N. The growth might be explicitly time-dependent, for example, if the supply with nutrients varies in time or if any other seasonal effects play a role.
In most cases, the growth of a microbial colony can be divided into four phases [74]. In the beginning, bacteria are founded in a medium and will grow only in size before reproduction processes start. During this lag period, the number of bacteria remains approximately constant. Thenceforth, the bacteria start to divide and an exponential growth phase can be observed until the number of bacteria levels off due to geometric restrictions, for example. This time period in which the growth rate of individuals in the population is balanced with the death rate such that the total number of bacteria remains constant is referred to as the stationary phase. Subsequently, the number of bacteria can decline at some point in time if the microbial colony is not supplied with additional nutrients.

Population growth of more than one species

The standard approach to the growth of a population constituted of more than one species is the Lotka-Volterra model [77, 78]. This model describes the dynamics of two species, one prey species A and one predator species B, with a system of two coupled ordinary differential equations of first order in time,

$$\partial_t N_A(t) = N_A \cdot (r_1 - r_2 N_B) \ ,$$
$$\partial_t N_B(t) = -N_B \cdot (r_3 - r_4 N_B) \ ,$$

The first equation reflects the constant growth of the prey with rate r_1. Species B preys species A. As a consequence, the number of prey N_A decreases with rate r_2, and the number of predators N_B increases with rate r_4. The survival of the predators is under threat since food supply is only assumed to be given by the presence of species A. Hence, N_B constantly decreases with rate r_3.

3.3 Stochastic formulation of growth processes

In our description of evolutionary and population dynamics, we have only applied a deterministic approach, so far. We treated the number of individuals as continuous and did not include demographic fluctuations in our description. In nature, however, evolutionary and population dynamics are governed by per capita birth and death events. Hence, these processes are intrinsically stochastic. Sometimes, it is important to include demographic fluctuations and correlations into the analysis since they can alter the qualitative behaviour of the outcome of a model [2, 79]. By applying a mean-field approach, which neglects these fluctuations and correlations in the system, it could happen that not all features of the experimental observation are captured. Some effects might be entirely stochastic.

One suitable approach to include stochastic fluctuations into the description of growth processes is the formulation of Markov processes which are a particular class of stochastic processes [80, 81]. Stochastic processes focus on the probability to find a specific set of random variables (a state), for example the number of individuals of different traits, at a specific point in time. In contrast, a deterministic mean-field approach asks only for the average number of individuals and neglects all correlations. This will become clearer when we introduce the stochastic process for the logistic growth later on. A Markov process is characterized by the property that the conditional probability distribution of a future state only depends on the state the system governs at the present time. All past states do not determine the future state directly. In this sense, Markov processes are said to be memoryless. The time evolution of the probability distribution is determined by the master equation which is a first-order differential equation in time. This equation entirely bases upon the Markov property of the stochastic process.

Let us elucidate the presented approach for an example, we have already encountered in the discussion of growth laws, namely the logistic growth. In this example, the qualitative outcome will not be changed by including stochastic fluctuations in our analysis, however quantitative results change. Nevertheless, the discussion of the logistic growth is still worthwhile in order to introduce some of the key concepts which will also be used later on. Another prominent stochastic model is, for example, the Fisher-Wright model [79, 82] which focuses on the relation between different traits in a population of fixed size.

3.3.1 Stochastic description of the logistic growth

In the logistic growth, we consider the dynamics of the number of individuals of one trait S. The number of individuals is called N and is treated as a stochastic variable. We are interested in the probability density $P(N,t)$ quantifying the probability to find N individuals at time t.
For birth and death processes, we further assume that the total number of individuals is increased or decreased by only one individual at each birth and death event. For these so-called one-step processes, the master equation which constitutes the temporal evolution of the probability distribution $P(N,t)$, reads as follows [80, 81],

$$\begin{aligned}\partial_t P(N,t) &= \Gamma_{S\to 2S}(N-1,t)\cdot P(N-1,t) + \Gamma_{S\to\emptyset}(N+1,t)\cdot P(N+1,t) - \\ &\quad - \Gamma_{S\to 2S}(N,t)\cdot P(N,t) - \Gamma_{S\to\emptyset}(N,t)\cdot P(N,t)\ , \\ &= \left((\mathbb{E}^- - 1)\Gamma_{S\to 2S}(N,t) + (\mathbb{E}^+ - 1)\Gamma_{S\to\emptyset}(N,t)\right) P(N,t)\ ,\end{aligned}$$

where $\Gamma_{S\to 2S}$ and $\Gamma_{S\to\emptyset}$ denote the birth and death rates, respectively. Note that the temporal evolution of the probability distribution $P(N,t)$ is determined by the balance between gain and loss terms. The probability to reach state N at time t is increased if at time t either $N-1$ individuals live in the population and an additional individual is born, or the colony consists of $N+1$ individuals and one individual dies. The probability to observe N individuals at time t decreases if N individuals are present and one individual is reproduced or dies at time t.
In the last line, the notion of the step operator $\mathbb{E}^{\pm}$ was introduced. This operator increases or decreases formally the number of individuals by one. For a general population with L different traits, the vector of the number of individuals for each trait is given by $\mathbf{N} = (N_1,\ldots,N_L)$ and we define the step operator by,

$$\mathbb{E}_i^{\pm} f(\mathbf{N},t) := f(N_1,\ldots,N_i \pm 1,\ldots,N_L)\ .$$

The logistic growth model is specified by the following growth and death rates ($n=1$),

$$\begin{aligned}\Gamma_{S\to 2S} &= g(N)\cdot N\ ,\ \text{with } g(N) = r,\ r>0\ , \\ \Gamma_{S\to\emptyset} &= d(N)\cdot N\ ,\ \text{with } d(N) = \frac{N}{K},\ K>0\ .\end{aligned}$$

Individuals reproduce constantly with rate r and die with rate N/K.
From the master equation we can infer the temporal evolution equation of the k-th moment ($k \geq 1$) of N,

$$\partial_t \left\langle N^k \right\rangle = \partial_t \sum_{N=0}^{\infty} N^k P(N,t) = \sum_{N=0}^{\infty} N^k \ \partial_t P(N,t) \ . \tag{3.8}$$

Upon inserting the master equation into eq. (3.8), one obtains for the moment equations,

$$\begin{aligned}
\partial_t \left\langle N^k \right\rangle &= \sum_{N=0}^{\infty} N^k \ \partial_t P(N,t) \ , k \geq 1 \ , \\
&= \sum_{N=0}^{\infty} N^k \ \left((\mathbb{E}^- - 1) g(N) + (\mathbb{E}^+ - 1) d(N) \right) N P(N,t) \ , \\
&= \left\langle \Gamma_{S \to 2S} \cdot ((N+1)^k - N^k) - \Gamma_{S \to \emptyset} \cdot (N^k - (N-1)^k) \right\rangle \ , \\
&= \left\langle \sum_{i=1}^{k} \binom{k}{i} N^i \left(g(N) - d(N)(-1)^{k-i} \right) \right\rangle \ , k \geq 1 \ .
\end{aligned} \tag{3.9}$$

Hence, the first two moments of the stochastic variable N can be computed via the following differential equations,

$$\begin{aligned}
\partial_t \langle N \rangle &= \langle N(g(N) - d(N)) \rangle \ , \\
&= r \langle N \rangle - \frac{1}{K} \left\langle N^2 \right\rangle \ ,
\end{aligned} \tag{3.10}$$

$$\begin{aligned}
\partial_t \left\langle N^2 \right\rangle &= \langle N(g(N + d(N)) \rangle + 2 \left\langle N^2 \cdot (g(N) - d(N)) \right\rangle \ , \\
&= r \langle N \rangle + \frac{1}{K} \left\langle N^2 \right\rangle + 2r \left\langle N^2 \right\rangle - \frac{2}{K} \left\langle N^3 \right\rangle \ .
\end{aligned} \tag{3.11}$$

The crucial point to note here is that the dynamics of the k-th moment depends on the value of the $(k+1)$-th moment which gives rise to an infinite cascade of moment equations.

We can neglect, however, all correlations in the system by applying the mean-field approximation,

$$\langle \phi(N) \rangle = \phi(\langle N \rangle) \ ,$$

for an arbitrary function ϕ. In other words, all higher moments of the stochastic variable N are neglected. For this reason, the obtained solutions of the moment equations are called deterministic in this context. The mean-field equation for $\langle N \rangle$ reads in this approximation,

$$\partial_t \langle N \rangle \simeq \langle N \rangle \left(r - \frac{\langle N \rangle}{K} \right) \ , \tag{3.12}$$

which coincides with the rate equation of the logistic growth (3.6). In the mean-field approximation, we obtain for the stationary case, which is characterized by $\partial_t \langle N \rangle_{\mathrm{st}} = 0$,

$$r - \frac{\langle N \rangle_{\mathrm{st}}}{K} = 0 \Rightarrow \langle N \rangle_{\mathrm{st}} = rK \ , \tag{3.13}$$

which is reached by the mean-field solution (3.7) for $t \to \infty$ as mentioned earlier; in other words $\langle N \rangle_{\mathrm{mf}} \to \langle N \rangle_{\mathrm{st}} = rK$ for $t \to \infty$. This mean-field result, however, does not reflect the stationary case of the stochastic system properly. Stochastic simulations reveal a different outcome. One can show that the actual mean of the number of individuals is $\langle N \rangle \approx rK - 1$. In this specific example of the logistic growth, the differences between the deterministic approach and the stochastic solution are only of quantitative nature, but sometimes the inclusion of stochastic fluctuations can alter the qualitative behaviour of the system dramatically. We will highlight this important feature in the upcoming discussion of two different growth models in section 3.4 and chapter 4.

3.3.2 Analytical treatment of stochastic fluctuations

A convenient method to incorporate stochastic fluctuations into the analysis, is the so-called van Kampen system size expansion [81]. This method systematically includes demographic fluctuations around the mean-field solution. The basic idea is to rewrite the stochastic variable N as follows,

$$N = \Omega \cdot n(t) + \sqrt{\Omega} \cdot \xi \ , \tag{3.14}$$

whereas Ω is the system size parameter, $n(t) = \langle N \rangle_{\mathrm{mf}} / \Omega$ denotes the deterministic solution, and ξ defines the stochastic variable accounting for the fluctuations in N. The stochastic noise term is weighted with $\sqrt{\Omega}$. This ansatz accounts for the scaling relation of Gaussian fluctuations which scale with the square root of the system size. Other scaling exponents, however, could also make sense depending on the particular problem [83].
The van Kampen ansatz is inserted into the master equation which is then expanded in powers of the system size Ω. This procedure results in a Fokker-Planck-type equation for the probability distribution of the fluctuations, and one can infer first-order differential equations for the first and higher moments of the fluctuation ξ. By solving the ODEs for the first moment $\langle \xi \rangle$, one obtains a solution for the mean individual number,

$$\langle N \rangle = \Omega \cdot n(t) + \sqrt{\Omega} \cdot \langle \xi \rangle \ ,$$

representing an improved mean-field result by including the effect of stochastic fluctuations. Further details and a pedagogical introduction to the van Kampen expansion can be found, for example, in the thesis of Stephani [84].

- Start with n groups with $(N_{i,j}, x_{i,j})$ at time t_j with $i \in \{1, \dots n\}$ and j labeling the point in time.
- Compute the rates $\Gamma_{S\to 2S}(x_{i,j}, N_{i,j})$ and $\Gamma_{S\to\emptyset}(x_{i,j}, N_{i,j})$ for all $i \in \{1, \dots n\}$, determine the cumulated rate vector $\Gamma_{\text{tot},k} = \sum_i^k \Gamma_i$ and the sum of all rates $\Gamma_{\text{tot}} = \sum_i^n \Gamma_i$.
- Sample random number r_1, and compute the next point in time,

$$t_{j+1} = t_j - \ln r_1/\Gamma_{\text{tot}} \ .$$

- Sample random number r_2, determine group number at which reaction takes place, and execute reaction. Group number and reaction point are both determined by the number m fulfilling,

$$\Gamma_{\text{tot},m} = \sum_{i=1}^{m} \Gamma_i < r_2 \cdot \Gamma_{\text{tot}} \leq \sum_{i=1}^{m+1} \Gamma_i = \Gamma_{\text{tot},m+1} \ .$$

- Update all n groups to $(N_{i,j+1}, x_{i,j+1})$ at time t_{j+1} and iterate.

Figure 3.2: Operation of the Gillespie algorithm for the stochastic cooperator-defector model presented in section 3.4. The Gillespie algorithm falls into the class of kinetic Monte Carlo algorithms. At each loop, the algorithm makes use of two random numbers in order to sample from the probability distribution of which only the temporal evolution is known (via the master equation). The idea is to simulate n groups each of which follows a stochastic trajectory determined by the master equation.

3.3.3 Numerical simulations of stochastic processes: Gillespie algorithm

Analytical calculations are often not feasible for stochastic processes especially when the dynamics of the growth process is more complicated than in the logistic growth. Nevertheless, we would like to gain insight into the behaviour of the stochastic system and compare it to the biological picture and the mean-field solution. This comparison can reveal the influence of stochastic fluctuations on the dynamics of the system. One possibility to obtain a deeper understanding of the stochastic system is to focus on numerical realizations of the stochastic dynamics. Stochastic algorithms are designed in such a way that they mimic the dynamics of the stochastic variables by drawing samples from the probability distribution for the random variables of interest. Most of the times, the probability distribution for the random variables is not known. Its temporal evolution, however, can be determined via the master equation.

A stochastic algorithm simulating the dynamics of a random variable, of which only the

master equation of its probability distribution is known, is the Gillespie algorithm [85]. The Gillespie algorithm falls into the class of kinetic Monte Carlo algorithms. Figure 3.2 illustrates the operation of the algorithm for the stochastic cooperator-defector model presented in the next section. In order to draw conclusions on the average behaviour of the stochastic system, many realizations of single trajectories of the random variables have to be investigated. In other words, the algorithm will only be valuable when executed for an ensemble of the stochastic system.

3.4 Entangled view: Evolutionary game theory in growing populations

In this section, we introduce a coupled approach of evolutionary dynamics and population dynamics and therewith follow closely the model of Melbinger et al. [2]. See also the theses of Cremer [44] and Melbinger [45] for details.
Before we turn to the formulation of the model, let us point out why a coupling of these two fields is reasonable. First of all, both evolutionary and population dynamics rely on birth and death events. Therefore, the total number of individuals in a population will never be constant, and studying evolution within a growing group seems to be the natural setup.
Moreover, the assumption that evolutionary dynamics and population dynamics can be idealized as being independent does not hold in many cases. It is clear that population dynamics depends on its internal structure, for example on how different traits are related to each other. The converse direction is evident as well; the dynamics between defectors and cooperators, for example, affects the growth of the total number of individuals in a population [86]. Of course, the concrete interplay between population dynamics and internal evolution is a matter of timescales. In general, population dynamics will act on a much shorter timescale than internal evolution does. For some biological systems, however, the coupling between both dynamics cannot be neglected. Biofilms are often referred to represent such systems [87, 27, 88, 89].
Furthermore, we have one particular experiment in mind, namely the Rainey & Rainey experiment, which showed the emergence and the dilemma of cooperation. There are two mechanisms, we would like to model. Firstly, groups with a higher fraction of cooperators will grow larger and faster than groups with a lower fraction of cooperators since it is beneficial to have cooperators in the group. Secondly, defectors are microscopically always better off than cooperators. They have an evolutionary advantage over the cooperators since they do not contribute to the cooperation but still benefit from the presence of the cooperators.
We will now present the generic approach of Melbinger et al. to exactly account for the effects one has observed in the experiment. The model couples both, evolutionary and population dynamics, in a stochastic model in order to include demographic fluctuations.

3.4.1 The cooperator-defector model of Melbinger et al.

- The state of the stochastic system is defined by two random variables, which characterize two different traits in a well-mixed population. We distinguish between the cooperating trait, C, and the defecting trait, D, which are described by the number of cooperators, N_C, and by the number of defectors, N_D, respectively. Equivalently, the state can be characterized by the total number of individuals, N, and the fraction of cooperators, x,

$$N = N_C + N_D \ , \qquad x = \frac{N_C}{N} \ .$$

- Our focus lies on the time-dependent probability distribution $P(N_C, N_D, t)$ which quantifies the probability to find the system at time t with N_C cooperators and N_D defectors.

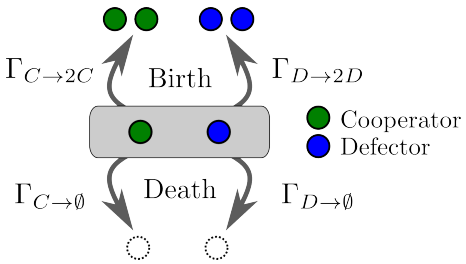

Figure 3.3: Illustration of the stochastic one-step process in the cooperator-defector model, adapted from [2]. At each point in time, the number of individuals can be increased or decreased by one. The rates for the birth and death of an individual depend on its trait (cooperator or defector). The innovative idea of Melbinger et al. is to decompose birth and death rates into a global part, which is trait-independent, and a relative part, which is trait-dependent. In this way, evolutionary dynamics and population dynamics are combined in this model.

The temporal evolution of the number of cooperators and defectors in this stochastic one-step Markov process is determined by the master equation for the probability distribution $P(N_C, N_D, t)$,

$$\begin{aligned}
\partial_t P(N_C, N_D, t) &= \sum_{S=C,D} \left((\mathbb{E}_S^- - 1)\Gamma_{S\to 2S} + (\mathbb{E}_S^+ - 1)\Gamma_{S\to\emptyset} \right) P(N_C, N_D, t) \ , \qquad (3.15) \\
&= \Gamma_{C\to 2C}(N_C - 1, N_D, t) \cdot P(N_C - 1, N_D, t) + \\
&\quad + \Gamma_{C\to\emptyset}(N_C + 1, N_D, t) \cdot P(N_C + 1, N_D, t) + \\
&\quad + \Gamma_{D\to 2D}(N_C, N_D - 1, t) \cdot P(N_C, N_D - 1, t) + \\
&\quad + \Gamma_{D\to\emptyset}(N_C, N_D + 1, t) \cdot P(N_C, N_D + 1, t) - \\
&\quad - (\Gamma_{C\to 2C}(N_C, N_D, t) + \Gamma_{C\to\emptyset}(N_C, N_D, t)) \cdot P(N_C, N_D, t) - \\
&\quad - (\Gamma_{D\to 2D}(N_C, N_D, t) + \Gamma_{D\to\emptyset}(N_C, N_D, t)) \cdot P(N_C, N_D, t) \ .
\end{aligned}$$

In the last line, we explicitly expanded the master equation to elucidate the compact notation in eq. (3.15). For an illustration of the one-step process see figure 3.3.

- This model is specified by growth and death rates for the cooperating and defecting trait, implemented as birth and death events via $\Gamma_{S\to 2S} = G_S \cdot N_S$ and $\Gamma_{S\to\emptyset} = D_S \cdot N_S$ for $S \in \{C, D\}$. G_S and D_S define the per capita birth and death rates. The basic and innovative idea is now to decompose both rates into a global part, which is trait-independent, and a relative part, which is trait-dependent,

$$\begin{aligned}\Gamma_{S\to 2S}(N_C, N_D) &= \Gamma_{S\to 2S}(N, x) = g(x, N) \cdot f_S(x) \cdot N_S \quad , \; S \in \{C, D\} \; , \\ \Gamma_{S\to\emptyset}(N_C, N_D) &= \Gamma_{S\to\emptyset}(N, x) = d(x, N) \cdot \omega_S(x) \cdot N_S \quad , \; S \in \{C, D\} \; .\end{aligned}$$

The global fitness $g(x, N)$ and the global weakness $d(x, N)$ affect the dynamics of the population as a whole. The relative fitness $f_S(x)$ and relative weakness $\omega_S(x)$ represent the relative advantage or disadvantage of one trait over another. They explicitly depend on the trait.
In this way, evolutionary dynamics and population dynamics are merged in this model. Both approaches can be recovered from this combined view by setting the respective other fitness to 1.
The global fitness rates are specified as follows,

$$\begin{aligned}g(x, N) &= 1 + px, \; p > 0 \; , \\ d(x, N) &= \frac{N}{K}, \; K > 0 \; .\end{aligned}$$

The definition of $g(x, N)$ accounts for the effect that cooperative groups grow larger than non-cooperative groups. The higher the fraction of cooperators is in the group, the larger the group will grow in size. Hence, the global fitness is assumed to increase with x. As the most direct approach, a linear increase of g with x is assumed. The parameter p quantifies the advantage of cooperative groups.
The global death rate is motivated by the logistic growth and is characterized by the carrying capacity K.
The trait-dependent part is specified as follows,

$$\begin{aligned}\omega_S(x) &= 1 \quad , \; S \in \{C, D\} \; , \\ f_S(x) &= \frac{\Phi_S(x)}{\Phi_\sim(x)} \quad , \; S \in \{C, D\} \; .\end{aligned}$$

The relative weakness is set to 1 for both traits since we assume that the chances of survival are equal for cooperators and defectors. The relative fitness, however, should reflect the fact that defectors are always better off than cooperators. Hence, we choose the relative fitness functions from eqs. (3.5) in order to model the microscopic interaction as a prisoner's dilemma setup. We have already highlighted that this setup

can be interpreted as a public good game in which cooperators have an evolutionary disadvantage over the defectors (see section 3.1). Therefore, we apply,

$$\begin{aligned}\Phi_C(x) &= 1 + s(bx - c) \ , \\ \Phi_D(x) &= 1 + sbx \ , \\ \Phi_\sim(x) &= x \cdot \Phi_C(x) + (1-x)\Phi_D(x) = 1 + sx(b-c) \ ,\end{aligned}$$

with $b = 3$ and $c = 1$, and s as the selection strength which is a free parameter in this model. As already mentioned earlier, the crucial point is that $f_C < f_D$. It was shown that the important information about the selective advantage of defectors over cooperators is already contained in the following equations which can be regarded as independent of game theoretic considerations,

$$\begin{aligned}f_C(x) &= 1 - s \ , \\ f_D(x) &= 1 \ .\end{aligned}$$

The greater the selection pressure s, the higher is the advantage of defectors in the course of evolution.

By having specified the rates in the described way, we have set up a stochastic model that combines frequency dependent selection with population growth dynamics. In order to analyze the influence of intrinsic demographic fluctuations, we have to analyze the mean-field solutions first.

3.4.2 Moment equations of the cooperator-defector model

We derive the moment equations for $\langle N \rangle$ and $\langle x \rangle$ from the master equation (3.15) in the same way as it was already carried out in eq. (3.9) for the logistic growth. For the first moment of N_C and N_D, one obtains in general,

$$\begin{aligned}\partial_t \langle N_S \rangle &= \langle \Gamma_{S\to 2S}(N_C, N_D, t) - \Gamma_{S\to\emptyset}(N_C, N_D, t) \rangle \ , \\ &= \langle N_S \cdot (g(x,N) f_S(x) - d(x,N)\omega_S(x)) \rangle \ ,\end{aligned}$$

for $S \in \{C, D\}$. In terms of the variables x and N, these equations read as,

$$\begin{aligned}\partial_t \langle N_C \rangle &= \partial_t \langle x \cdot N \rangle \ , \\ &= \langle x \cdot N \cdot (g(x,N) f_C(x) - d(x,N)\omega_C(x)) \rangle \ , \\ \partial_t \langle N_D \rangle &= \partial_t \langle (1-x) \cdot N \rangle \ , \\ &= \langle (1-x) \cdot N \cdot (g(x,N) f_D(x) - d(x,N)\omega_D(x)) \rangle \ .\end{aligned}$$

Adding both equations leads to,

$$\begin{aligned}\partial_t \langle N \rangle &= \partial_t \langle N_C + N_D \rangle \ , \\ &= \langle N \cdot (g(x,N) f_\sim(x) - d(x,N)\omega_\sim(x)) \rangle \ , \\ &= \langle N \cdot (g(x,N) - d(x,N)) \rangle \ .\end{aligned}$$

In the last step, the definition of $f_\sim(x)$ was applied. As mentioned earlier, this definition has the property,

$$f_\sim(x) = x \cdot f_C(x) + (1-x) \cdot f_D(x) = x \cdot \frac{\Phi_C(x)}{\Phi_\sim(x)} + (1-x) \cdot \frac{\Phi_D(x)}{\Phi_\sim(x)} = 1 \ ,$$

and the same holds true for $\omega_\sim(x) = 1$. In summary, we arrive at the following two moment equations which will be the starting point of our further analysis,

$$\partial_t \langle N \rangle = \langle N \cdot (g(x,N) - d(x,N)) \rangle \tag{3.16}$$
$$\partial_t \langle x \cdot N \rangle = \langle x \cdot N \cdot (g(x,N) f_C(x) - d(x,N) \omega_C(x)) \rangle \tag{3.17}$$

3.4.3 The population average of the fraction of cooperators

Before we proceed with the mean-field analysis, let us study one particular interesting observable, namely the population fraction of cooperators. Consider a population consisting of n groups as depicted in figure 3.4.

Each of the n groups is comprised of $N_{C,i}$ cooperators and $N_{D,i}$ defectors for all $i \in \{1, \dots n\}$. All n groups follow the same stochastic dynamics as described above. By decomposing the whole population into n groups, we have effectively introduced a structure on the population. We have mentioned in chapter 1 that such a population structure could pave the way for the maintenance of cooperation. For the moment, we are not interested in how such a division of the whole population into sub-populations might have arisen in nature. The significance of the population structure will be discussed later on in chapter 6.

It is of interest, however, how the overall fraction of cooperators, $\langle x \rangle_{\text{pop}}$, evolves in time. We will refer to this quantity as the population average of the fraction of cooperators since it focuses on the percentage of cooperators in the whole population of n groups. From the meaning of $\langle x \rangle_{\text{pop}}$, its mathematical definition is evident,

$$\langle x \rangle_{\text{pop}} := \frac{\sum_{i=1}^n N_{C,i}}{\sum_{i=1}^n N_i} \ . \tag{3.18}$$

By rewriting this fraction, we can identify the observable of interest $\langle x \rangle_{\text{pop}}$ with the ensemble average of the number of individuals,

$$\langle x \rangle_{\text{pop}} = \frac{\sum_{i=1}^n N_{C,i}}{\sum_{i=1}^n N_i} = \frac{\frac{1}{n}\sum_{i=1}^n N_{C,i}}{\frac{1}{n}\sum_{i=1}^n N_i} = \frac{\langle N_C \rangle}{\langle N \rangle} \ .$$

Note that this observable is in general different from the ensemble average of x,

$$\langle x \rangle = \left\langle \frac{N_C}{N} \right\rangle \neq \frac{\langle N_C \rangle}{\langle N \rangle} = \langle x \rangle_{\text{pop}} \ .$$

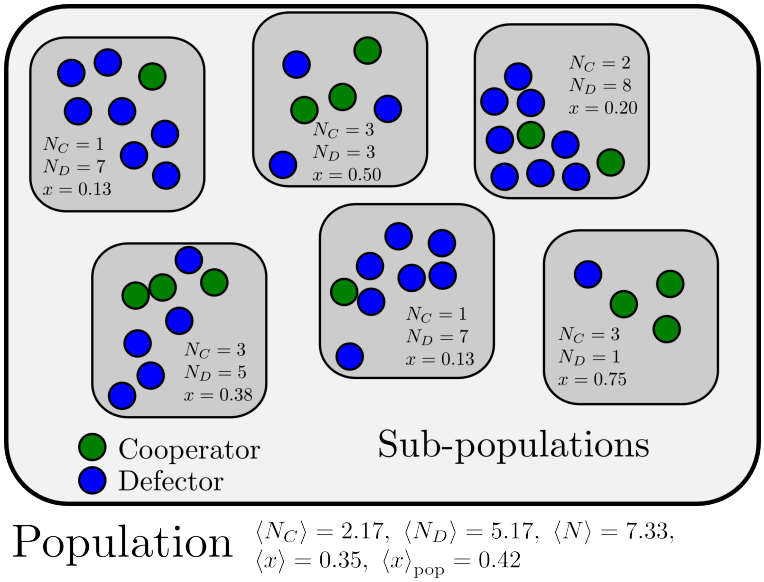

Figure 3.4: Illustration of the population average of the percentage of cooperators. Consider a population consisting of 6 groups at time $t > 0$. Due to demographic fluctuations, the number of defectors and cooperators varies within each sub-population. Within each group $i \in \{1, \dots 6\}$, the fraction of cooperators is computed via $x_i = N_{C,i}/N_i$, and the average percentage of a group is then given as $\langle x \rangle = 1/6 \sum_i^6 x_i = 0.35$. The main observable of interest, however, is the average fraction of cooperators $\langle x \rangle_{\text{pop}}$ over the whole population. In this simple structured population, it is actually the crucial observable in order to understand how cooperation can be maintained. Here, we compute $\langle x \rangle_{\text{pop}} = \langle N_C \rangle / \langle N \rangle = 0.42$, which is higher than the ensemble mean $\langle x \rangle$.

It is also noteworthy that the notion of $\langle x \rangle_{\text{pop}}$ does not make sense if one interprets the population average for one group only. In contrast, $\langle x \rangle$ can be interpreted as the mean fraction of cooperators of one group only. In the picture of an ensemble of groups in one population, however, the definition of $\langle x \rangle_{\text{pop}}$ does make sense. It is actually a crucial observable in order to understand how cooperation can be maintained in structured populations. Hence, we will focus our attention on the dynamics of $\langle x \rangle_{\text{pop}}$ in the following.

3.4.4 Mean-field analysis of the cooperator-defector model

In this section, we will analyze the cooperator-defector model of Melbinger et al. [2] in the mean-field approximation, that is we neglect all correlations and fluctuations in the system. In particular, we are interested in the mean individual number, $\langle N \rangle$, the mean percentage of cooperators in the population, $\langle x \rangle$, and the introduced population x-average $\langle x \rangle_{\text{pop}}$.
Up to now, we have formulated all derivations towards eqs. (3.16), (3.17) in full generality.

Now, we specify the rates accordingly to the model of Melbinger et al.. Furthermore, we neglect all correlations and fluctuations in the system, and apply the mean-field approximation, $\langle\phi(N)\rangle = \phi(\langle N\rangle)$ for an arbitrary function ϕ. For the mean individual number $\langle N\rangle$, one obtains from eq. (3.16) in the mean-field picture,

$$\partial_t \langle N\rangle \overset{\text{MF}}{\simeq} \langle N\rangle \left(1 + p\langle x\rangle - \frac{\langle N\rangle}{K}\right) , \tag{3.19}$$

Comparing this result to eq. (3.13), we recognize that the mean-field equation reduces to the logistic growth equation if we set $p = 0$. In this sense, the model of Melbinger et al. can be regarded as a natural extension of the logistic growth involving evolutionary dynamics. The growth of the mean number of individuals is basically a logistic growth with the x-dependent carrying capacity $(1 + px)K$.
For the population average of x, we obtain,

$$\langle x\rangle = \left\langle \frac{N_C}{N}\right\rangle \overset{\text{MF}}{\simeq} \frac{\langle N_C\rangle}{\langle N\rangle} = \langle x\rangle_{\text{pop}} .$$

In other words, both x-averages coincide in the mean-field picture. By applying eq. (3.17), the temporal evolution of $\langle x\rangle_{\text{pop}}$ in the mean-field can be computed as follows,

$$\begin{aligned}
\partial_t \langle x\rangle_{\text{pop}} = \partial_t \left(\frac{\langle N_C\rangle}{\langle N\rangle}\right) &= \frac{\partial_t\langle N_C\rangle}{\langle N\rangle} - \frac{\langle N_C\rangle}{\langle N\rangle^2}\partial_t\langle N\rangle , \\
&\overset{\text{MF}}{\simeq} \langle x\rangle \left((1 + p\langle x\rangle) f_C(\langle x\rangle) - \frac{\langle N\rangle}{K}\right) - \langle x\rangle_{\text{pop}} \left(1 + p\langle x\rangle - \frac{\langle N\rangle}{K}\right) , \\
&\overset{\text{MF}}{\simeq} -s\langle x\rangle(1 - \langle x\rangle)(1 + p\langle x\rangle) \simeq \partial_t\langle x\rangle .
\end{aligned} \tag{3.20}$$

We would like to highlight two important observations at this point. The time at which the fraction of cooperators changes on average is $\tau_x \propto 1/s$ since $s \simeq 0.05 \ll 1$ (weak selection) and $p \simeq 10$, thus $g = (1+px)$ lies in the order of 1. The mean individual number $\langle N\rangle$, however, changes on a timescale $\tau_N \propto 1$. Hence, the population growth is much more rapidly than the timescale at which selection acts. As a consequence, the individual number can grow nearly towards the carrying capacity $1 + px_0$ in the beginning since the fraction of cooperators changes only slowly during this initial period (see figure 3.5). More importantly, the population average of the fraction of cooperators decreases for all times since $s > 0$ meaning that cooperators will ultimately die out.

3.4.5 Stochastic analysis of the cooperator-defector model

Let us now investigate how the mean-field behaviour changes due to the inclusion of stochastic fluctuations. Figure 3.5 shows the outcome of a simulation which involves the dynamics of 10000 groups. As one can see from the left plot, the stochastic result for the

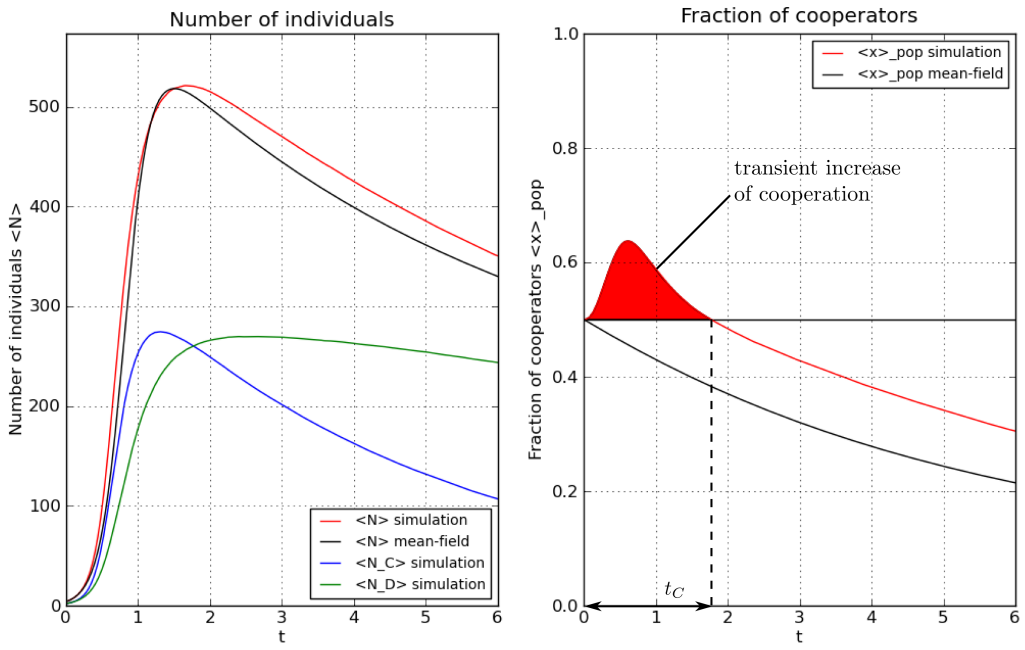

Figure 3.5: Results of the stochastic simulation of the dynamics of 10000 groups versus mean-field solution for $\langle N \rangle$ and $\langle x \rangle_{\text{pop}}$ in the cooperator-defector model. The left subplot shows also the average number of cooperators and defectors as obtained from the simulation. The mean-field solution for the total number of individuals represents the stochastic curve in good accordance. The behaviour of the population average of the fraction of cooperators, however, reflects a striking change when we include stochastic fluctuations into our analysis. Whereas the mean-field solution for $\langle x \rangle_{\text{pop}}$ declines strictly monotonically for all times, the stochastic simulation reveals an overshoot, that is a transient increase of cooperation. This effect is purely due to demographic fluctuations and can be characterized by the time t_C in which $\langle x \rangle_{\text{pop}}$ exceeds its initial value x_0. The population average of the percentage of cooperators is the main observable of interest since it describes the change of the fraction of cooperators in a structured population.
Chosen parameters: $s = 0.05, p = 10, K = 100, b = 3, c = 1$.
Initial values: $N_0 = 4, x_0 = 0.5$.

average total number of individuals is in good accordance with the mean-field solution. The behaviour of the population average of the fraction of cooperators, however, reflects a striking change when we include stochastic fluctuations into our analysis. Whereas the mean-field solution for $\langle x \rangle_{\text{pop}}$ declines strictly monotonically for all times, the stochastic simulation reveals an overshoot, that is a transient increase of cooperation at the beginning of the evolutionary dynamics. Hence, the transient increase of cooperation is a purely stochastic effect which is due to demographic fluctuations. The typical size of demographic fluctuations scales as $1/\sqrt{N}$. In other words, stochastic fluctuations will have a higher im-

pact on the dynamics if the number of individuals is relatively low, that is in the beginning of the evolution. In Figure 3.5, we have started the dynamics with all groups containing two cooperators and two defectors. Since tiny fluctuations in the number of individuals have a high impact on the fraction of cooperators in that group, the peaked distribution in x over the whole ensemble of groups broadens immediately after the dynamics is started. The population growth, as we have seen, dominates the influence of the selection pressure in the beginning. Since we introduced a global growth rate that favors cooperative groups ($g = 1 + px$), groups with a higher fraction of cooperators will grow larger than groups with a lower percentage of cooperators. In this way, demographic fluctuations are asymmetrically amplified towards an increasing fraction of cooperators for the initial dynamics. Therefore, the population average $\langle x \rangle_{\text{pop}}$ will increase because cooperative groups have a larger weight in the average due to their larger size. For larger times, however, selection pressure drives the system ultimately towards a state in which only defectors survive. Only purely cooperative groups can remain stable in the long run.
The transient increase of cooperation can be characterized by the time t_C in which $\langle x \rangle_{\text{pop}}$ exceeds its initial value x_0. Melbinger et al. show numerically and analytically in [2] that t_C decreases with a higher selection strength s. The higher the selection pressure is, the shorter is the time period in which cooperation can increase. Moreover, the transient increase of cooperation is more pronounced the smaller the individual group size N_0 is. The less individuals are present in the beginning of the dynamics, the higher is the impact of demographic fluctuations scaling as $\propto 1/\sqrt{N_0}$. The asymmetric amplification of fluctuations is also promoted by a lower initial percentage of cooperators x_0 with the result that the maximal fraction of cooperators increases with a dropping value of x_0.

3.5 Summary

In this chapter we have introduced both the concept of evolutionary dynamics and population dynamics. By combining the two approaches in a stochastic setup, Melbinger et al. established a model to study evolutionary game theory in growing populations. This model is designed in such a way that it reflects the two basic properties we have already encountered in chapter 1. Firstly, cooperative groups will grow larger and faster than non-cooperative groups (mediated by parameter p) since it is beneficial to have cooperators in the group. Secondly, defectors have an evolutionary advantage over the cooperators (mediated by parameter s) since they do not contribute to the cooperation but still benefit from the presence of the cooperators.
By analyzing the population mean of the percentage of cooperators, one observes an overshoot in this observable. The transient increase in $\langle x \rangle_{\text{pop}} = \langle N_C \rangle / \langle N \rangle$ is a purely stochastic effect driven by demographic fluctuations. The model, however, cannot explain the maintenance of cooperation for longer times. Ultimately, cooperation will cease.
Nevertheless, Melbinger et al. could show that cooperation can be maintained by means of repetitive fragmentation of populations into smaller sub-populations [90]. We will discuss

this approach in chapter 6 later on.

4 Mat Model

In this chapter, we want to take the experiment of Rainey & Rainey [1] as basis for a stochastic model that accounts for the main effects that were observed in the experiment and that have been described in chapter 2. The focus will be put on modeling the emergence of cooperation in this biological experiment, the dilemma of cooperation and on a proposal to maintain cooperation in the long run later on. Thereby, the spirit of the generic cooperator-defector model of Melbinger et al. will be applied to the specific situation in the mat experiment.

First of all, we explain why the naive application of the introduced cooperator-defector model of Melbinger et al. to the mat experiment of Rainey & Rainey is not possible in a direct way (section 4.1). By discussing the phenomenology of the growth and sinking process of the mat, we will identify the effective mat density as an additional structural element to the model of Melbinger et al. (section 4.2). The cuboid model of the mat will be introduced in section 4.3 and the concept of the effective mat density will be introduced. We derive the dynamics of the mat expansion and the mat density from a phenomenological approach (section 4.4), and define the coupling of the mat structure to population dynamics. The final stochastic mat model is formulated in section 4.6 and summarized in figure 4.8 which illustrates the central ideas and results of this chapter. As an aside and consistency check of the mat model, the temporal evolution of the mat density is derived in section 4.8.

4.1 Scope and limitations of the mat model

Let us set the scope of the mat model. First, it will be helpful to identify the features that are *not* goal of the description within this mat model. The experiment of Rainey & Rainey mainly points out the qualitative effects of the evolution of cooperation in these mat populations. In this way, the available data mostly contains only a few experimental realizations. See for example figure 2.5, where each data point represents the average over three measurements of the number of cooperators. Stochastic fluctuations and measurement uncertainties will limit the scope of quantitative conclusions. Hence, we should not aim at fitting the data with the mat model or try to extract quantitative results.
Moreover, the mat experiment depends on many parameters, for example the exact extension of the glass pot and the density contribution of a cooperating and a defecting

bacterium. Furthermore, biological details play a crucial role for the mat growth process and the dilemma of cooperation. How does the mat grow at its front? How often do mutations occur from a cooperating genotype to a defecting genotype and how is this change in genotype translated into phenotypic expression? The answers to these questions are not known to smallest detail and limit the scope of application of the mat model.
We can model, however, the main effects from a somewhat coarse-grained point of view by not including all microscopic details. Still, we can gain a qualitatively accurate description of the experiment. We will take the qualitative results as motivation and decide on an abstract model in an averaged view that should be robust under changes of parameters and specific functional dependencies. The model should express the observational fact that defectors are always better off than cooperators on a microscopic level, but mats with a higher fraction of cooperators can grow larger and will ultimately survive longer.
In chapter 3, we have already introduced a stochastic model coupling both evolutionary dynamics with population growth. In addition to this model, the Rainey & Rainey experiment has a structural element that limits its direct application, namely the spatial heterogeneity of the experimental setup. It results in the development of a mat, whose structure couples back to population dynamics. All in all, we want to introduce an extension of the aforementioned stochastic model that describes the emergence and the dilemma of cooperation in a growing mat population by reproducing the experimental results of Rainey & Rainey qualitatively. We shall evaluate the mat model on how it meets these demands. Later on, we will also investigate the possibility of regrouping steps of these mat populations to propose a possible way to maintain cooperation.

4.1.1 Setting up the null model

Let us point out why a direct approach as presented in chapter 3.4 cannot be sufficient to describe the effect of the evolution of cooperation and conflict in the experimental bacterial populations [1].
If we consider the evolution of one species only, which we will refer to as the null model in the following, in the framework of the model of Melbinger et al., the dynamics reduces to a logistic growth. This aspect can be seen from the master equation (3.15) for the coupled model in the case where $x = 1$ (only cooperating trait present) or $x = 0$ (only defecting trait present).
In this way, the model of Melbinger et al. can be regarded as an extension of the logistic growth to a population with two traits, one cooperating and one defecting, as desired. It was shown in section 3.3 that for the logistic growth, the average number of individuals only increases and levels off at around the value of the imposed carrying capacity K.

In the Rainey & Rainey experiment, however, we have seen that the number of cooperators decreases after some time and converges to zero due to the sinking of the mat (cf. figure 4.1). In other words, the null model of Melbinger et al. is not sufficient to describe the qualitative outcome of the experiment adequately. This point also becomes clear from a mathematical

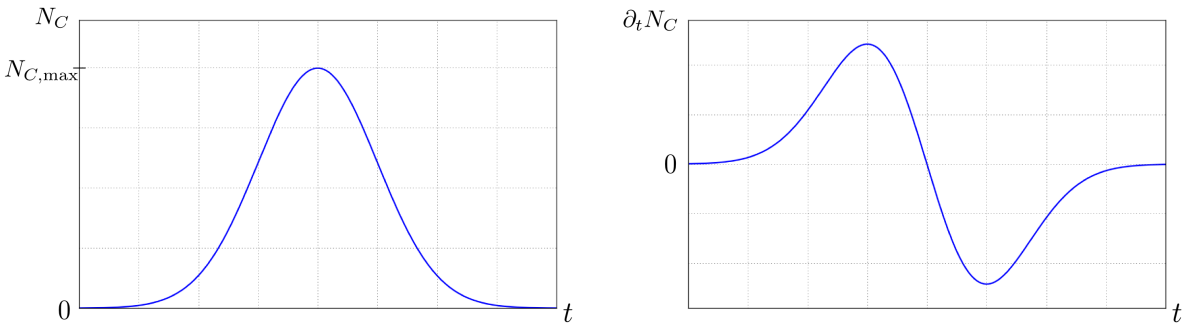

Figure 4.1: Qualitative sketch of the number of cooperators (left) and its derivative (right) over time from the experiment. The number of cooperators increases in the beginning due to the mat growth. After having passed the maximal individual number $N_{C,\max}$, the mat sinks and the population number decreases in time.

point of view. If we look at the mean-field equations from chapter 3.4 for the null model, that is for only one cooperating trait present in the experiment, we obtain

$$\partial_t N_C \overset{\text{one trait}}{=} \partial_t N = h(N) \ . \tag{4.1}$$

This equation is a first order ordinary differential equation (ODE) that has the property to be autonomous since it does not explicitly depend on time. The point is that this autonomous ODE cannot reproduce a qualitative behaviour, observed in the experiment (cf. figure 4.2), where we have an increase and a decrease of the individual number for every value of $N_C < N_{C,\max}$. The derivative $\partial_t N_C$ would have to take two different values for one value of N_C which is not possible in a mathematical frame. In other words, $\partial_t N_C(N_C)$ would not be well-defined.

To resolve this mathematical problem, we have two obvious generalizations of eq. (4.1) at hand.

- We could introduce an explicit time dependence of the function $h(N) \to h(N,t)$. For example, the ODE for a Gaussian solution would fit in this picture. The problem of this approach lies in the physical interpretation of the explicit time dependence. What is the mechanism that determines the time scale of the function $h(N,t)$? Actually we are interested in such a time scale from a physical point of view and do not want to introduce this scale by hand. The timescale defined on which $\partial_t N$ changes should come out of a reasonable physical model. Thus, the physics of the population dynamical problem limits the application of this approach.

- We could introduce a new variable ρ, independently defined of N, and formulate the time development of that variable. Clearly, the dynamics of ρ has to be coupled to the dynamics of N in order to account for the decrease of N after having passed its

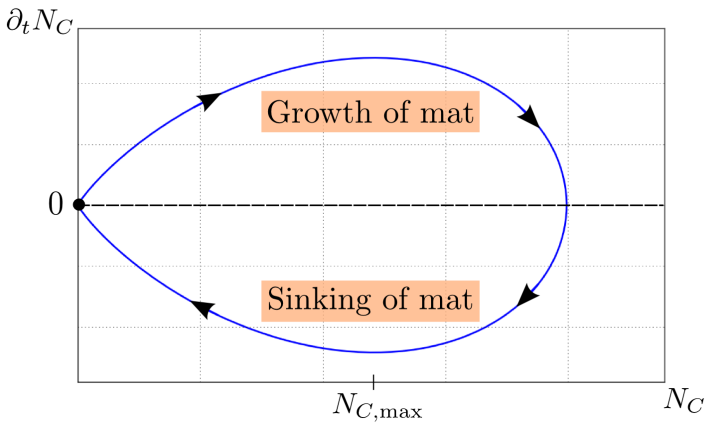

Figure 4.2: Plot of $\partial_t N_C$ versus N_C derived from the plots in figure 4.1. The curve shows that the derivative of the individual number $\partial_t N_C$ cannot be a function of one variable N_C only, even in absence of defectors. For one value of N_C, two according values of the derivative exist, one during the phase of the mat growth ($\partial_t N_C > 0$), and one during the sinking of the mat ($\partial_t N_C < 0$). The function $\partial_t N_C(N_C)$ would be not be well-defined. To resolve this mathematical problem, we will introduce a new variable ρ and identify it as effective mat density. The dynamics of ρ will be coupled to the dynamics of the number of individuals and account for the drop in N_C.

maximum (cf. figure 4.2),

$$\partial_t N = h_1(N, \rho) \ ,$$
$$\partial_t \rho = h_2(N, \rho) \ .$$

By introducing the new variable ρ, the problem with an explicit definition of a timescale does not arise. Moreover, it seems promising from the physics point of view to identify the new variable ρ with a structural element of the mat growth, namely the effective density of the mat. The sinking of the mat is actually caused by an increased mat density, and results in a decrease of the bacteria number in the mat as described in chapter 2.

We will investigate the physics of the evolution of the structure and the density of the mat in more detail in the next section since this picture will be the basis of the proposed stochastic model for the bacteria growth.

4.2 Phenomenology of the growth and sinking of the mat

Let us briefly examine the physics of the mat and the phenomenology of the mat density in order to motivate the second option of the proposed solutions to resolve the difficulty with the null model from last section.

An extended object will sink in a basin filled with water if the buoyancy force F_B the object experiences in water is lower than its gravitational force F_G (see figure 4.3 for an illustration). The buoyancy force is the gravitational force of the water the object displaces. Hence, the process of sinking starts if $F_B \geq F_G$, or equivalently $\rho_{\text{mat}} \geq \rho_{\text{H}_2\text{O}}$. That is, if the average density of the mat exceeds the density of water, the mat will sink.

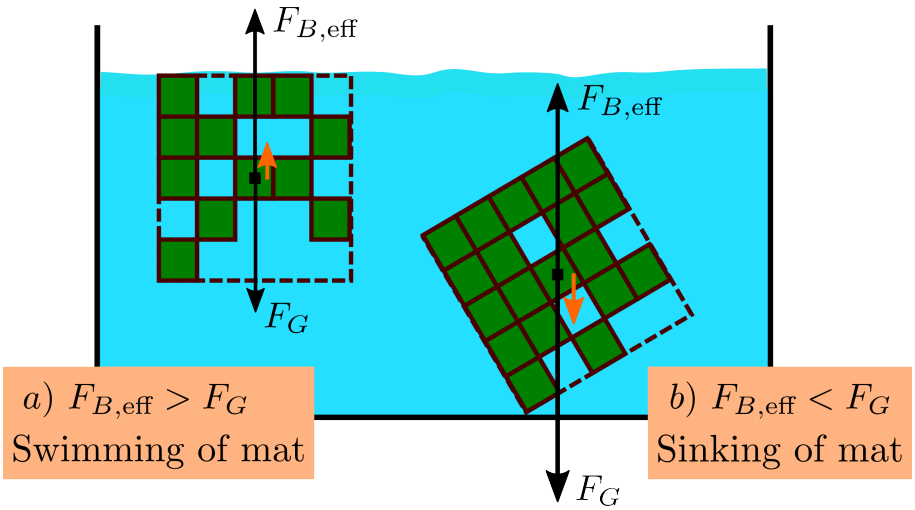

Figure 4.3: Swimming (a) and sinking (b) of the mat. The behavior of the mat is determined by the effective buoyancy force and the gravitational force acting on the mat. The effective buoyancy force combines the actual buoyancy force, that is the gravitational force of the water the mat displaces, the attachment forces between the bacteria expressing the extracellular polymer and the glass vial, and the surface tension of the mat. Later on, we will introduce the effective mat volume (dashed contour) and the effective density to account for these effects (see section 4.3). The mat will sink if the effective buoyancy force is less than the gravitational force of the mat (b). When the mat expands (a), the effective buoyancy force exceeds the gravitational force such that the mat swims.

In this picture, we assume that only the buoyancy force of the mat is responsible for the swimming and sinking of the mat. The experiment (cf. chapter 2) shows, however, that the wrinkly spreader cells also attach firmly to the glass vial [55]. This attachment cannot be neglected when discussing the forces that lead to the formation of the mat. Moreover, surface tension might contribute as a force acting against gravitation. Due to our ignorance of these forces and other microscopic details, we shall nevertheless regard the buoyancy force as a net force accounting for the microscopic details and giving rise to the swimming and sinking of the mat (see figure 4.3). This averaged view is mediated by the notion of an effective mat density which will be defined and explained carefully in section 4.3. For now, we want to introduce the phenomenological picture of the growth and sinking of the mat and its relation to the mat density.

In figure 4.4 the mat density is plotted versus time and the sinking process of the mat is

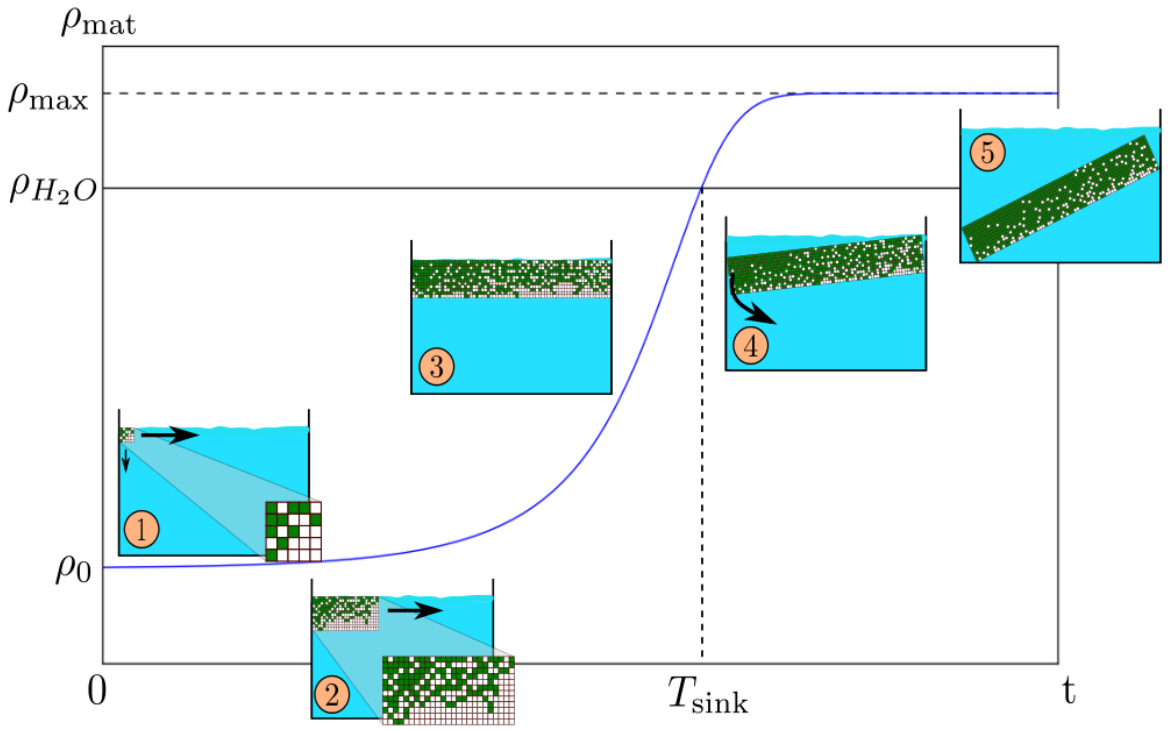

Figure 4.4: Phenomenology of the growth and the sinking of the mat. The effective mat density is plotted versus time and the sinking process of the mat is depicted as a result of the increase of the effective mat density. The effective density does not only account for the density contribution of the bacteria, but also for their attachment to the glass vial. The actual bacteria mat is depicted by the green filled cells. Here, we do not distinguish between cooperating and cheating cells. The white cells are places which are not occupied by the mat. They will be involved in the mat model later on, where the effective mat volume is defined as the smallest cuboid containing the bacteria mat. Note that there is no time scale given for the sinking process (it could be linear, logarithmic, etc.). This qualitative picture has to be justified by a microscopic model for the mat density, which will be subject of the following sections. For a detailed description, see text.

depicted as a result of the density increase. The phenomenological picture of the sinking process is the same for both solely cooperative mats and mats with cooperators and defectors. We will discuss the influence of defecting bacteria on the dynamics of the mat later on. In the beginning, a few cooperating bacteria attach to the edge of the pot at the liquid-air interface through the overproduction of the extracellular glue-like polymer. The bacteria cluster as close as possible to the water surface since the high concentration of oxygen is advantageous to their metabolism and gives rise to an evolutionary advantage

over the ancestral cells in the broth. The cluster will expand in the following in all possible spatial directions (cf. figure 4.4 (1)). However, the oxygen concentration decreases rapidly with distance to the liquid-air interface [52]. As the presence of oxygen is the main driver for the effective growth rate of the bacteria cells (cf. chapter 2), the horizontal growth is faster than the growth towards the bottom of the pot. Effectively, the vertical growth will be highly dominated by the horizontal growth (cf. figure 4.4 (2)).
The first expanding bacteria at the front of the mat build up the skeleton of the mat from which the space between the skeleton frames will be filled up with more bacteria (cf. figure 4.4 (3)). The latter process will be referred to as aggregation or interior growth, whereas the horizontal and vertical expansion of the mat will be called front growth from now on.
Because of the finite extension of the broth pot, the horizontal growth will cease at some point in time and hence the total front growth rate converges to zero. Thenceforth, the interior growth dominates the front growth and results in a sharp increase of the mat density. The average mat density ultimately reaches the density of the broth phase which is approximately the density of water which causes the sinking of the mat (cf. figure 4.4 (4)). During the sinking process, the density could slightly increase further on since there may be some parts of the mat that are still close to the liquid-air interface, where oxygen is present in high concentration. Finally, the value of the mat density levels off at the maximal value $\rho_{\max}$ (cf. figure 4.4 (5)).
If the experimentalists used a pot with a large extension (or imagine an infinitely extended glass vial), the mat would also sink ultimately. Since the vertical growth is limited by the supply of oxygen in the water, which rapidly decreases with distance to the liquid-air interface, the interior growth will always dominate locally after some time and lead to an local increase of the density towards the density of water although the averaged density of the whole mat could lie below the value of the density of water. Therefore, the whole mat will also kink for an infinitely extended pot, but more slowly than for a finite pot. In summary, the extension of the pot has an impact on the total number of bacteria in the mat and the time scale at which the sinking of the mat takes place.

In presence of defecting bacteria, that is bacteria not overproducing the sticky polymer, the sinking process of the mat will be accelerated. Defecting bacteria are not conducive to the mat expansion since other bacteria cannot attach to a defecting cell. Hence, only cooperators strengthen the structure of the mat by expansion. Moreover, if the network of cooperating bacteria is dense enough, defectors can get stuck in this network. Since defectors do not overproduce the glue-like polymer, a defecting bacterium in the mat contributes to the mat density with an effective density much greater than a cooperator does. They can be regarded as an additional weight pushing the effective mat's density ρ_{mat} faster to the critical value $\rho_{\text{H}_2\text{O}}$ at which the mat starts to sink.
If we have two mats with the same total number of individuals, one with cooperators only and one with both cooperators and defectors, the latter will sink faster than the solely cooperative one since the spatial density distribution in the cooperative mat will be more homogeneous than in the mat with cooperators and defectors. Thus, the swimming of

the cooperative mat is much more stable than for the mixed mat. This difference in the structure of the two mats leads to a gradual sinking of the mat if only cooperators are present and an abrupt drop of the mat if defectors are present in the mat.

4.3 Notion of the effective mat density

Up to now, we have gained an intuitive picture of the phenomenology of the growth and sinking of the mat, as well as the dynamics of the mat density. In order to translate the presented influences and dependencies into mathematical language, we will now define a model for the mat and its density. We will describe the sinking of the mat later on by taking care of the structural element, namely the effective mat density.

4.3.1 Cuboid model of the mat

At each point in time, the mat will be idealized by a cuboid with M sites, whereas each cell has a length of size a. The cuboid with M sites is the smallest cuboid containing the mat volume and can be viewed as the cuboid-like convex hull of the mat; see figure 4.5 for an illustration. M is then the effective mat volume. The notion of an effective mat volume is necessary for the definition of a mat density on a macroscopic level which will be presented shortly. The fictive M sites of the mat can be free or occupied by the N bacteria cells in the mat. The effective volume M is determined by the way in which the mat grows. The more crinkly the mat grows, the bigger will be the difference between the effective volume M and the actual number of occupied sites N. For a compactly growing mat, N will only be slightly less than M. A further discussion of the growth of the mat volume will be presented in due course. Note that M is a discrete stochastic variable due to the stochasticity of the mat growth process. Nevertheless, M will be treated as a continuous deterministic variable because of our ignorance of microscopic details of the mat growth process. This abstraction will be pointed out later on. We will measure all lengths in the microscopic length unit a, and, as a consequence, the volume of the mat is simply $V_{\text{tot}} = M$. The microscopic length scale a corresponds to the effective extension of a bacterium cell such that a^3 models the effective volume of a bacterium. The extension of *Ps. fluorescens* lies in the order of 10^{-7} m [52] and similarly does a.

4.3.2 Model for the effective mat density

As already mentioned, the mat will sink if its effective density, ρ_{mat}, exceeds the density of water, ρ_{H_2O}. We have argued that we will understand the buoyancy force in a generalized

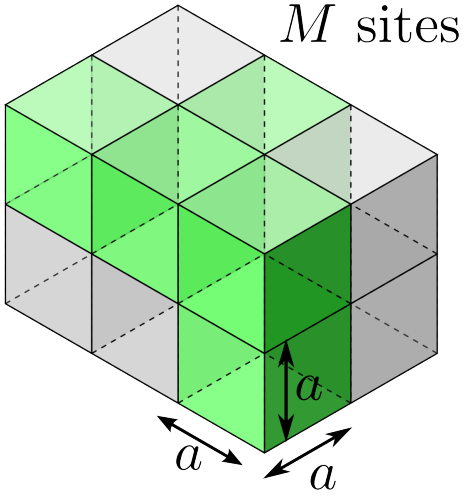

Figure 4.5: Cuboid model of the mat. We consider the mat as a cuboid with an effective volume V_{tot}. The cuboid can be thought of as being composed of M cubic cells, each of which having an extension of length a. The length a refers to the spacial extension of a bacterium. The cuboid with M sites is the smallest cuboid containing the mat volume and can be viewed as the cuboid-like convex hull of the mat. Each cell of this cuboid is then empty or occupied by a bacterium (indicated by a green cell). If we measure lengths in units of a, the total volume of the mat is given by $V_{\text{tot}} = M$. In the depicted example, the mat consists of 5 bacteria (green cells, $N = 5$) occupying an effective mat volume of $M = 12$ sites. The normalized mat density would then be $\gamma = 5/12 \cdot z_{\sim}(x)$ (see text for detailed explanation).

sense such that it also includes the surface tension of the mat and the forces responsible for the attachment of the glass vial. In this picture, the effective density of the mat includes these effects as well.

As a first approach, we will define the effective mat density microscopically as the occupation density of the effective mat volume, that is proportional to N/M. The density contribution of a bacteria cell has to be greater than the density of water to account for the sinking of the mat at some point. For that reason, we assign the density contribution $\rho = z \cdot \rho_{\text{H}_2\text{O}}$, with $z > 1$, to each occupied cell in the effective mat volume. If cooperators and defectors had the same contribution to the mat density, this relation would lead to,

$$\rho_{\text{mat}} = \frac{N}{M} \cdot z \cdot \rho_{\text{H}_2\text{O}} \ .$$

The density contributions of a cooperating cell and a defecting cell, however, are different. As described above, only cooperators overproduce the sticky polymer. Therefore, we distinguish both traits by their structure factor z_C and z_D. With the density contributions $\rho_C = z_C \cdot \rho_{\text{H}_2\text{O}}$ for a cooperator, and $\rho_D = z_D \cdot \rho_{\text{H}_2\text{O}}$ for a defector, this notion translates into a different contribution to the mat density. We impose $1 < z_C < z_D$ for the structure factors such that $\rho_{\text{H}_2\text{O}} < \rho_C < \rho_D$. With these different density contributions, we have to

weight the contributions according to the number of bacteria present in the mat:

$$\rho_{\text{mat}} = \frac{1}{M} \cdot (N_C \cdot \rho_C + N_D \cdot \rho_D) = \frac{\rho_{\text{H}_2\text{O}}}{M} \cdot (N_C \cdot z_C + N_D \cdot z_D) \ .$$

In order to couple the mat density to population dynamics later on, it will be useful to define the normalized mat density γ as follows,

$$\gamma := \frac{\rho_{\text{mat}}}{\rho_{\text{H}_2\text{O}}} \ . \tag{4.2}$$

The normalized mat density, γ, varies in a range $0 < \gamma \leq \rho_{\max}/\rho_{\text{H}_2\text{O}} =: \gamma_{\max}$ with $\gamma_{\max} > 1$. The mat sinks when $\gamma = 1$ is reached. For our purpose, we can assume that $\gamma_{\max} \simeq 1$ since the sinking process of the mat itself can be simplified as being density-independent once the mat has arrived at the critical density $\gamma = 1$.

In the picture of the cuboid model of the mat, one obtains for the normalized density,

$$\gamma = \frac{\rho_{\text{mat}}}{\rho_{\text{H}_2\text{O}}} = \frac{1}{M} \cdot (N_C \cdot z_C + N_D \cdot z_D) = \frac{N}{M} \cdot (x \cdot z_C + (1-x) \cdot z_D) = \frac{N}{M} \cdot z_\sim(x) \ , \tag{4.3}$$

where the definition of an x-averaged function (cf. section 3.4) was applied in the last step. The function $z_\sim(x)$ interpolates linearly between the two border cases $z_\sim(x \to 1) = z_C$ and $z_\sim(x \to 0) = z_D$ with both z_C and z_D being greater than 1, and hence $z_\sim(x) > 1$.

In general, the normalized density γ can be regarded as the observable that accounts for the structure of the mat. This structural parameter determines the success of the group since the mat sinks when $\gamma = 1$ is reached.
In the following, we will investigate how the structural observable γ, or equivalently the effective mat volume M, evolves in time and how it can be coupled to the stochastic growth dynamics of the mat. Note again that we have $2 + 1$ independent variables, namely x, N, and either γ or M; γ and M are related to each other via eq. (4.3).

4.3.3 Impact of front and interior growth on the effective mat density

Let us now discuss the influence of the front growth and the interior growth on the effective mat volume in order to combine the phenomenological picture, we have obtained in section 4.2, with the definitions from above. Both growth processes are visualized in figure 4.6.

- We have seen that cooperators build up the mat skeleton and hence increase the effective volume of the mat. This front growth of the mat (cf. figure 4.6 (a)) results in a decrease of the mat density since the mat is expanding, and reflects a pressure of the dynamics of the mat density towards $\rho_{\min}$, which is the minimal density the

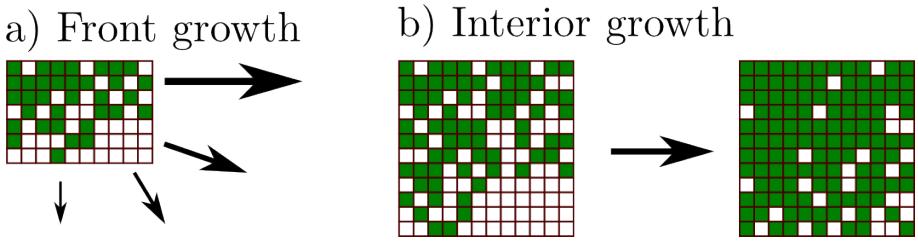

Figure 4.6: Mat growth processes. The lattice represents the effective mat volume composed of M cells. The green cells characterize the cells which are occupied by bacteria.
(a) The front growth involves the expansion of the mat. Only cooperators build up the mat skeleton and hence increase the effective volume of the mat. It results in a decrease of the normalized density of the mat. The growth in the horizontal direction dominates the expansion in the vertical direction since oxygen is abundant only at the liquid-air interface. The expansion of the mat is limited by the finiteness of the broth pot.
(b) The interior growth is an aggregation process resulting in an increase of the mat density. It is idealized to be proportional to the number of free places in the effective mat volume. Later on, we will assume for the interior growth that defectors have a greater growth rate than cooperating cells since they are microscopically better off than cooperators.

mat could have if only the mat skeleton was built up.
Furthermore, the rate of the front growth is monotonically increasing with the fraction of cooperators, x, since only cooperators can build up the mat skeleton. Hence, the front growth rate of the mat should increase with a higher fraction of cooperators. This effect is limited by the geometrical boundary conditions of the experimental setup, e.g., the finiteness of the broth pot. If the front of the mat reaches the boundary of the pot, the expansion at the front comes to a halt.

The growth of the mat is only due to the presence of cooperators – without cooperators, the mat would not grow. Hence, the mat model will only be applicable for $0 < x_0 \leq 1$, with x_0 as the initial percentage of cooperators in the mat.
Actually, the results of Rainey & Rainey suggest that in the beginning of the mat growth only cooperating bacteria are present some of which mutate to a defecting bacterium later on (see chapter 2). Mutation rates in the coding region lie typically in the range of 10^{-7} to 10^{-11} [91]. In other words, one nucleotide per 10^7-10^{11} nucleotides per cell generation changes due to mutation. Furthermore, the error rate of the gene expression, that is the translation of the genetic information into phenotypic expression, is approximately 10^{-9} for microbes [92]. In total, the mutation rate in the sense of the rate corresponding to the change in the phenotype can be assumed to be in the order of 10^{-7}. This order of magnitude is also backed up by the quantitative analysis of figure 2.4, where the numbers of cooperators and defectors in the mat experiment are plotted over time. Defecting cells can be estimated to appear approximately between day 1 and day 2, when 10^6-10^7 cooperating bacteria

are already present in the mat.

For the sake of clarity and simplicity, however, we do not model the mutations from a cooperating WS bacterium to a defector, but start the dynamics with a certain amount of defectors in the mat instead. Nevertheless, for a more realistic model, mutations can be included in this population growth model, too. The reader is referred to [65] for the implementation and the analysis of mutation processes in a stochastic cooperator-defector growth model.
By neglecting these mutations, it follows that the initial fraction of cooperators x_0 should be slightly less than 1 to account for an adequate description of the experimental situation.

- The interior growth (cf. figure 4.6 (b)) is an aggregation process resulting in an increase of the density. This effect is a driving force for the dynamics of the mat density towards a maximal density, $\rho_{\max}$. The interior growth rate will be modeled to be proportional to the number of free places in the mat. This point will be explained more carefully later on.
  The aggregation process should depend on the mat structure and the total number of bacteria N in the mat. We can also assume that the aggregation process is faster the more defectors are present in the mat since we model defectors to have an evolutionary advantage over cooperators as motivated in chapter 2 and implemented in chapter 3.

4.4 Mathematical formulation of the mat growth process

In the last section, we have defined the effective mat volume M and the related normalized mat density γ, and identified them as the structural quantities characterizing the sinking of the mat. Here, the phenomenological picture, we have gained up to now, will be specified in a mathematical framework to determine the temporal evolution of the effective mat volume. Furthermore, we will determine the growth rate of the mat in terms of the normalized density γ.

4.4.1 Front growth

As mentioned above, the definition of the density makes only sense if we have already cooperators in the mat since only they can form the mat. Thus, the mathematical description which is derived in this section will only be valid for $x_0 > 0$ and $M > 0$.
We want to account for three effects that influence the front growth, that is the dynamics of the temporal evolution of V_{tot}.

- The higher the fraction of cooperators, the faster the growth rate of the total volume V_{tot}. In general, the front growth rate will be a monotonically increasing function of

the fraction of cooperators. For simplicity, we assume,

$$\partial_t V_{\text{tot}}(t) \propto x(t) \ . \tag{4.4}$$

Since only cooperators account for the mat expansion, the fraction of cooperators at the front will always be slightly higher than the percentage of cooperators over the whole mat. In other words, assumption (4.4) reflects a lower bound for the front growth rate of the effective mat volume.

- The growth rate of the total mat volume should be directly linked to the surface of the mat volume A_V. As a first step, we can apply the approximation that the volume of the mat grows proportional to the surface of the cuboid (as in figure 4.7), that is $\partial_t V_{\text{tot}}(t) \propto A_V(t)$.
  Furthermore, we may assume that the front growth of the mat effectively takes place at its lateral surface since the vertical growth rapidly ceases because of the anoxic conditions below the liquid-air interface (cf. section 4.2). In this way, we simplify the initial dynamics of the mat growth, but describe the mat expansion accurately for later times. Again, this simplification underestimates the front growth process, and makes it harder for mats to survive.
  Let us refer to the maximal vertical extension of the mat in the glass vial as l. If we model the top surface of the cuboid to be a square with side length k, the volume of the cuboid will be $V_{\text{tot}} = l \cdot k^2$ and its lateral surface $A_V = 4 \cdot kl$. Note that the vertical extension of the mat l is treated as constant here. Therefore, we obtain the relation,

$$A_V(t) \propto V_{\text{tot}}^{\frac{1}{2}} \ . \tag{4.5}$$

For our further analysis, only this scaling behaviour is of importance since we will introduce a proportionality constant for the dynamics of $\partial_t V_{\text{tot}}$, anyway. The same result can also be inferred from modeling the mat as a cylinder with height l and radius k.

If the mat grew along all directions, the exponent in eq. (4.5) would change to 2/3. The different scaling relation with exponent 1/2 is caused by the abstraction of the mat growth taking effectively place in two dimensions instead of three. The proportionality between the change of the volume of the mat and the closure of its surface is valid for compact growth scenarios, which can be assumed if nutrients are abundant in the broth phase [93]. If nutrients are, however, lacking or aggregation is diffusion-limited [94], different scaling exponents will be obtained for the proportionality,

$$A_V(t) \propto V_{\text{tot}}^{\nu} \ ,$$

with ν as the scaling exponent. One example for diffusion-limited aggregation, giving rise to the appearance of fractals and fractal dimensions, is the Eden model [95, 96, 97]. Investigations of this model show (see for example [98]) that one obtains a scaling

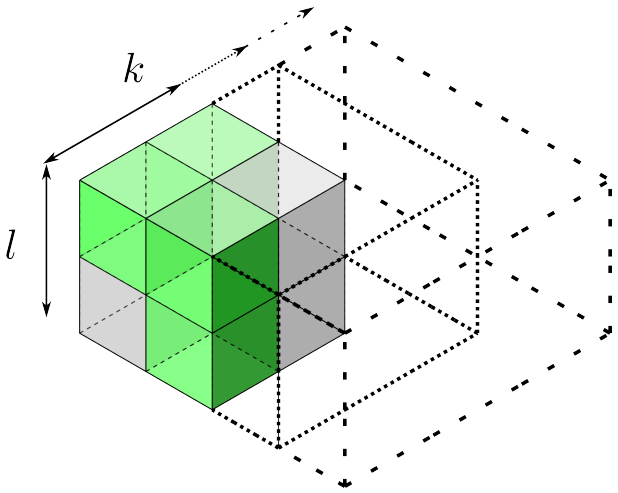

Figure 4.7: Expansion of the effective mat volume. In the mathematical approach, we assume that the growth of the mat only takes place in the horizontal direction. Then, the effective volume of the mat (that is the smallest cuboid comprising the bacteria which are depicted as green cells) only expands at its lateral surface. In other words, we expect $\partial_t V_{\mathrm{tot}}(t) \propto A_V(t) = 4 \cdot l \cdot k(t)$ and because of geometrical reasons ($V_{\mathrm{tot}}(t) = l \cdot k(t)^2$), it follows $A_V(t) \propto V_{\mathrm{tot}}^{1/2}$. The same result is obtained by considering a mat modeled by a cylinder with height l and radius $k(t)$.

exponent $\nu \geq 1/2$ for a growth in two dimensions.
One can understand this relation by imagining a wrinkly surface at which the bacteria can grow. Such a mat, with a volume which is equal to a cuboidal mat, has a much larger surface than the cuboidal one due to its crinkliness. In general, the rougher the surface of a cluster is, the bigger the growth exponent ν will be. In the experiment of Rainey & Rainey, however, nutrients are abundant in the glass vial. Hence, the assumption of $\nu = 1/2$ should be an adequate approximation – at least on a coarse-grained level.
Nevertheless, detailed microscopic growth models for biofilms exist and are well-studied [52, 99, 53, 100]. Many of them model the front growth in an adequate manner by involving many fitting parameters. Here, we keep the growth model as simply as possible in order to account for the main feature we are interested in, that is the interplay between the cooperator-defector dynamics and the structural element of the mat. For this purpose, we have neglected the spatial structure of the mat and introduced an averaged view on the mat, instead.

- In order to account for the finite size of the mat, we can introduce a limiting factor that prevents the mat from further growing if a certain volume is reached. We model this characteristics by introducing a limiting factor of $\partial_t V_{\mathrm{tot}}(t) \propto (1 - \frac{V_{\mathrm{tot}}}{V_{\mathrm{max}}})$ as known from the logistic growth. V_{max} is the carrying capacity of the front growth process and corresponds to the maximal volume the mat can reach. In case of a broth pot without a closed boundary – imagine for example a lake in which the bacteria can

attach to the shore at one side and form a mat that grows into the lake – we would let $V_{\max}$ diverge, $V_{\max} \to \infty$.

Putting all three effects together, we end up with,

$$\begin{aligned} \partial_t V_{\text{tot}}(t) &\propto x(t) \cdot A_V(t) \cdot \left(1 - \frac{V_{\text{tot}}(t)}{V_{\max}}\right) , \\ &\propto x(t) \cdot V_{\text{tot}}^{\frac{1}{2}} \cdot \left(1 - \frac{V_{\text{tot}}(t)}{V_{\max}}\right) , \\ \Rightarrow\ \partial_t M &= c_1 \cdot x(t) \cdot M(t)^{\frac{1}{2}} \cdot \left(1 - \frac{M(t)}{K}\right) =: m(x, M) , \end{aligned} \tag{4.6}$$

with K as the maximal number of possible sites of the mat that can be occupied, and c_1 as the proportionality constant, which basically influences the time scale of the front growth. The function $m(x, M)$ was introduced for short-hand notation. Note that at first sight, the dynamics of the effective mat volume M only depends directly on the values of x and M, but not on N, the numbers of bacteria in the mat. In the full stochastic model, however, the dynamics of x is coupled to N (see section 4.6), and hence the mat growth also depends on the number of bacteria in the mat.

The important step towards the ODE (4.6) lies in the assumption that the volume of the mat grows at its surface with $A_V \propto V_{\text{tot}}^{1/2}$. Although having argued in a phenomenological picture, further experimental and theoretical work has to be carried out in order to confirm this assumption. In the near future, we will investigate numerical simulations of the mat growth to verify these ideas.
Furthermore, assumption (4.5) implies the transition from a stochastic description of the mat growth to a deterministic description. This approximation represents the coarse-grained view on the mat growth and greatly simplifies the analysis of the mat model. We have already indicated that the effective mat volume is also treated as a continuous variable, although being defined discretely in the first place. The notion of a time derivative of M in eq. (4.6) reflects this approach.

The parameter $c_1 > 0$ combines the proportionality factor of all three effects mentioned above. We will treat c_1 as a fitting parameter later on, but this constant could be measured in principle. Since the proportionality factor c_1 relates the time scales of the front growth to the interior growth, which will be described in the next section, one can imagine an experimental setup with an optical density measurement to determine the experimental value of c_1. One would have to set up several laser devices at different distances from the attachment point of the cooperators to the glass wall of the pot. By screening the broth pot with the lasers perpendicular to the water surface at these positions over time, one could measure the optical density at different places in the mat over time.
A different setup could consist of only one laser probing different points of the glass vial for the optical density after one another. After having scanned one point in the mat for the optical density, the laser would move to the next point. In this way, both methods

could deliver a spatially resolved density profile of the mat in the pot over time. Moreover, it should be possible to verify the modeled growth of the mat in principle.

4.4.2 Interior growth

As already mentioned, we define the interior growth as the aggregation process of bacteria within the fixed mat skeleton which is build up by cooperators. From the explanations above, it is evident that the more free places are present in the effective mat volume (i.e. the higher $(M - N)$), the faster the growth of the number of individuals N will be. Again, we have to differentiate between cooperators and defectors, since defectors have microscopically an evolutionary advantage over the cooperators as described in chapter 3. This aspect should be reflected in the model of the interior growth.
We follow the spirit of the model of population dynamics (see section 3.4) and separate the growth rate for each trait into a global, trait-independent part for the interior mat growth, $g_{\text{mat}}(x, N, M)$ and the trait-dependent fitness function $f_S(x) = \Phi_S/\Phi_\sim(x)$ for $S \in \{C, D\}$. Following the steps from chapter 3.4, we arrive at the mean-field equation for the interior mat growth:

$$\partial_t \langle N_S \rangle = \langle N_S \rangle \cdot g_{\text{mat}}(\langle x \rangle, \langle N \rangle, M) \cdot f_S(\langle x \rangle) \ , \ S \in \{C, D\} \ . \tag{4.7}$$

Note that we have not included a death rate at this point. The death rate will be formulated as a sinking rate for the sinking of the mat later on.
We choose $g_{\text{mat}}(x, N, M)$ proportional to the number of free places in the mat as motivated above. The global mat growth rate will be normalized to the total number of possible sites M as follows,

$$g_{\text{mat}}(x, N, M) = \frac{M - N}{M} = 1 - \frac{N}{M} = 1 - \frac{\gamma}{z_\sim(x)} =: g_{\text{mat}}(x, N, \gamma) \ . \tag{4.8}$$

We will apply this global growth rate to the stochastic population model later on (see section 4.6).

If we look at the isolated interior growth, that is neglecting all other mechanisms of the mat dynamics for a moment, we obtain the mean-field equation for the total number of individuals (cf. chapter 3) for the interior growth,

$$\partial_t \langle N \rangle = \langle N \rangle \cdot g_{\text{mat}}(\langle x \rangle, \langle N \rangle, M) = \langle N \rangle \cdot (1 - \frac{\langle N \rangle}{M}) \ .$$

The outcome of this calculation is basically that at each point in time the dynamics of the total number of bacteria in the mat follows a logistic growth with a time-dependent carrying capacity $M(t)$ (cf. section 3.3). The dynamics of the carrying capacity is determined by the front growth as described in the last section.
Note that the last equation for the total number of bacteria does not depend on the trait-dependent rates f_S. The reason for this simplification lies in the definition of f_S as relative growth advantages, that is $f_S = \Phi_S/\Phi_\sim$ as pointed out in section 3.4.

4.5 Impact of the mat density on population dynamics

Before we can formulate the full stochastic mat model, let us summarize and specify the impact of the mat volume and the related mat density on the population dynamics, that is on the number of defectors and cooperators. Up to now, we dealt with the consequences of the population dynamics on the mat growth in terms of its effective volume. We have also discussed the influences of the mat structure on the interior growth which resulted in the formulation of the global growth rate of the mat.

4.5.1 Growth of the mat

The growth rate for the bacteria in the mat was already motivated and applied in section 4.4.2. We separate the total growth rate into a global, trait-independent mat growth rate $g_{\text{mat}}(x, N, \gamma) = 1-\gamma/z_{\sim}(x)$, and a microscopic, trait-dependent part $f_S(x) = \Phi_S/\Phi_{\sim}(x)$ for $S \in \{C, D\}$.
If it was possible to hold the density fixed at value γ^*, we would infer that a mat with a higher fraction of cooperators would grow more slowly than a mat with a lower fraction of cooperators since $z_{\sim}(x) = z_C x + z_D(1-x)$ and $z_C < z_D$, that is $g_{\text{mat}}(x_1; \gamma^*) < g_{\text{mat}}(x_2; \gamma^*)$ for $x_1 > x_2$. This would be in contradiction to our phenomenological picture of the mat growth process. The density is not fixed, however, but influenced by the number of cooperators and defectors in the mat, as $\gamma = N/M \cdot z_{\sim}(x)$. This feedback causes the growth advantage of cooperative groups since more cooperative groups can grow larger due to the front growth process. Microscopically, defectors remain to be always better off than cooperators which is implemented by the trait-dependent part of the growth rate. In total, the mat growth process is modeled by a consistent description.

4.5.2 Sinking of the mat

If the average density of a mat reaches the value of the density of water, the mat will sink. Therefore, we introduce a sinking rate at $\gamma = 1$, which reduces the number of bacteria at the water surface. In the experiment, the mat will tilt first such that a certain amount of bacteria in the mat remains close to the liquid-air interface. Bacteria which are sunk are not counted by the experimentalists in the experiment. For our purpose, these bacteria can be regarded as dormant or dead. Hence, the sinking rate can be interpreted as a death rate of the bacteria at the water surface.
From the experiment we obtain that a mat with a high fraction of defectors will sink much faster than a mat with a low fraction of defectors since the density profile of the mat is much more heterogeneous when defectors are present. In other words, the stability of the mat is weakened by the presence of defectors. These considerations lead to the sinking rate $d(x, N, \gamma) = c_2 \cdot (c_3 - x) \cdot \Theta(\gamma - 1)$. The sinking process starts when the mat density

reaches the density of water which is reflected by the Heaviside function. The sinking rate is a linearly decreasing function of the fraction of cooperators: the higher the fraction of cooperators, the lower the sinking rate. One can assume that the sinking of the mat is, in general, a highly non-linear process. It depends on microscopic details and on the detailed structure of the mat. Nevertheless, we want to model the qualitative behaviour of the mat system and do not aim at fitting the observations from the experiment. In this sense, the linear approximation of the sinking rate should be a suitable approach.
The positive constants c_2 and c_3 have to be chosen such that the sinking rate dominates the growth rate for $\gamma > 1$ since the growth of the bacteria will be dominated by the sinking process. Furthermore, c_3 should be greater, but close to 1 in order to account for the observation that mats with a higher fraction of cooperators sink more slowly than mats with a lower fraction of cooperators.

4.6 Formulation of the stochastic mat model

In this section, we extend the deterministic description of the mat growth, which we have obtained so far, to the stochastic mat model. In general, this extension would involve the derivation of the master equation for the probability distribution $P(N_C, N_D, M)$ depending on all three independent variables N_C, N_D, and M. The key idea is to simplify the dynamics of the stochastic mat model, but still include stochastic fluctuations into the analysis. This can be achieved by treating the mat volume M as a deterministic variable, which is reflected by eq. (4.6) and basically follows from the scaling hypothesis (4.5) for the front growth. The number of cooperators and defectors will be treated stochastically by making use of the ideas of the coupled cooperator-defector model presented in chapter 3. Cooperative groups can grow larger and will sink later than non-cooperative groups, and microscopically defectors are always better off than cooperators. The effective volume of the mat could then be regarded as an additional structural element of the cooperator-defector model, together with the notion of the normalized mat density. This additional structure to the population dynamics translates into the growth and survival advantage of cooperative mats.

Speaking in mathematical terms, we couple the normalized density γ to the growth and sinking rate of the stochastic dynamics of N and x, and describe the temporal evolution of the mat volume with the ODE (4.6), which depends on x and M. Let us define the full stochastic model in the following. An illustrated summary of this model is depicted in figure 4.8 at the end of this section.

- We define two stochastic variables, the number of cooperators N_C and the number of defectors N_D which can be transformed to the total number of individuals N and the percentage of cooperators x through,

$$N = N_C + N_D \ , \qquad x = \frac{N_C}{N} \ .$$

In addition to the model of Melbinger et al., we introduce one additional stochastic variable M, the effective mat volume, which is the volume of the smallest cuboid comprising the mat. The normalized mat density is computed via,

$$\gamma = \frac{N}{M} \cdot z_{\sim}(x) = \frac{N}{M} \cdot (z_C \cdot x + z_D \cdot (1-x)) \ ,$$

whereas z_C and z_D denote the structure factor of a cooperating cell and a defecting cell, respectively.

- The temporal evolution of the number of cooperators and defectors in this stochastic model is determined by the master equation for the probability distribution $P(N_C, N_D, t)$,

$$\partial_t P(N_C, N_D, t) = \sum_{S=C,D} \left((\mathbb{E}_S^- - 1)\Gamma_{S\to 2S} + (\mathbb{E}_S^+ - 1)\Gamma_{S\to\emptyset} \right) P(N_C, N_D, t) \ .$$

This model is specified by growth and sinking rates for the cooperating and defecting trait, implemented as birth and sink events via $\Gamma_{S\to 2S}$ and $\Gamma_{S\to\emptyset}$ for $S \in \{C, D\}$. These rates can be decomposed into a global part, which is trait-independent, and a relative part, which is trait-dependent,

$$\begin{aligned} \Gamma_{S\to 2S}(N_C, N_D, \gamma) &= \Gamma_{S\to 2S}(N, x, \gamma) = g(x, N, \gamma) \cdot f_S(x) \cdot N_S \ , \ S \in \{C, D\} \ , \\ \Gamma_{S\to\emptyset}(N_C, N_D, \gamma) &= \Gamma_{S\to\emptyset}(N, x, \gamma) = d(x, N, \gamma) \cdot N_S \ , \ S \in \{C, D\}. \end{aligned}$$

The density of the mat couples with the population dynamics through the global growth and sinking rate; the relative parts remain as in the formulation of Melbinger et al. [2],

$$\begin{aligned} g(x, N, \gamma) &= 1 - \frac{\gamma}{z_{\sim}(x)} \ , \\ d(x, N, \gamma) &= c_2 \cdot (c_3 - x) \cdot \Theta(\gamma - 1) \ ; \ c_2, c_3 > 1 \ , \\ f_S(x) &= \frac{\Phi_S(x)}{\Phi_{\sim}(x)} \ , \Phi_C = 1 - s, \Phi_D = 1, \end{aligned}$$

Cooperative groups grow larger and survive longer due to the better stability of cooperative mats, but within mats defectors are better off than cooperators. The evolutionary advantage of defectors over cooperators is tuned by the value of the selection strength s.

- Although the effective mat volume is defined as a stochastic variable, we will prescribe its temporal evolution to follow the deterministic equation,

$$\partial_t M = c_1 \cdot x(t) \cdot M(t)^{\frac{1}{2}} \cdot \left(1 - \frac{M(t)}{K}\right) \cdot \Theta(\gamma - 1) \quad \text{with } c_1, K > 0 \ . \tag{4.9}$$

The reason for this simplification lies in the ignorance about the microscopic details of the mat growth process as pointed out in detail in the last sections. We introduced an additional factor of $\Theta(1-\gamma)$ by hand in comparison to eq. (4.6) to stop the dynamics of the mat volume during the sinking process. It is assumed that the effective volume and the density of the mat will only change slightly during the sinking, and hence this approximation should be appropriate.

Figure 4.8 summarizes and depicts the mat model together with the phenomenological picture of the growth and the sinking of the mat.

4.7 Parameters of the mat model

What are the parameters of the mat model?

- c_1. This parameter relates the timescale of the front growth process to the timescale at which the interior growth acts. We regard c_1 as a fitting parameter, but it may be measured in an experiment as already proposed. c_1 reflects the growth advantage of mats with a higher percentage of cooperators. In this way, it may be compared to the parameter p in the model of Melbinger et al. (cf. chapter 3) since the constant p was introduced in the growth rate $g = 1+px$ to model the growth advantage of cooperative groups over non-cooperative groups. The parameter c_1 can be interpreted in the same way.

- s. The selection strength s prescribes the microscopic evolutionary advantage of defectors over cooperators. We set $s = 0.15$.

- z_C, z_D. These two constants mainly have an impact on the difference between a purely cooperative mat and a mat with both cooperators and defectors. The qualitative behaviour does not depend on the explicit choice of the values, but it is important to choose $1 < z_C < z_D$. In our simulations, we set $z_C = 2$ and $z_D = 6$. Recall that z_C, z_D are the structure factors and responsible for the different contributions of a cooperator and a defector to the effective density.

- $\gamma(0)$. This parameter prescribes the initial density of the mat. The explicit value does not change the qualitative behavior of the outcome of the computations. For our simulations, we set $\gamma_0 = 0.2$. This value is motivated by the model for the mat and typical initial population sizes applied in simulations. Consider, for example, a cube that is divided into $3^3 = 27$ or $4^3 = 64$ subcubes and an initial population size of 5 individuals, that is 5 sites in this initial mat are occupied, and an initially high percentage of cooperators. The initial density would be $\gamma_0 \simeq N_0/M_0 \cdot z_C$ which lies between 0.37 and 0.16 for our chosen examples.

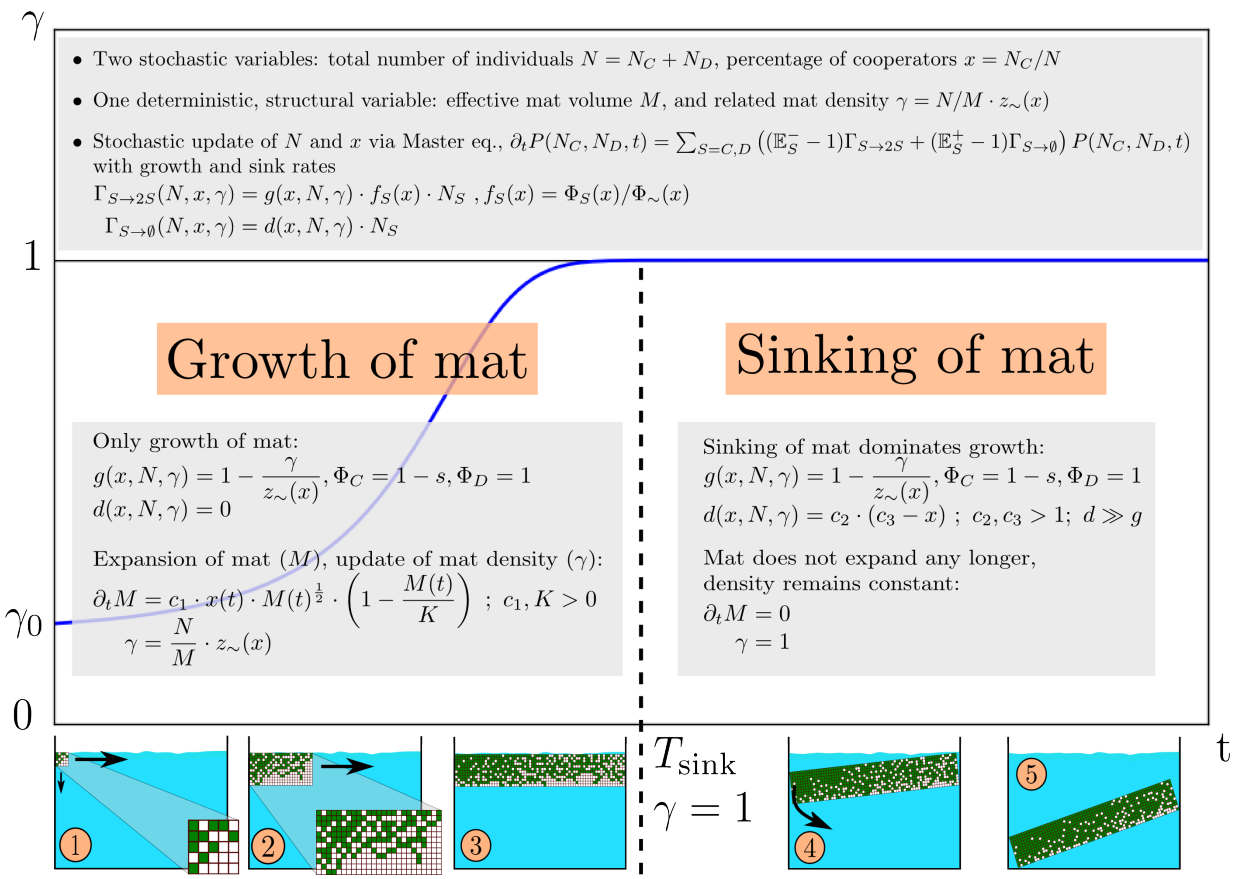

Figure 4.8: Summary and sketch of the mat model. We describe the population dynamics in an evolutionary cooperator-defector setup by taking into account the additional structural of the mat. The model introduces the three variables N, x (both stochastic) and M (defined stochastically, but treated deterministically) from which the mat density γ can be computed. A mat will sink if its effective density reaches the density of water, that is if $\gamma = 1$. This condition divides the evolution of the mat into two regimes: the growth and the sinking of the mat. During the growth phase, defectors are better off than cooperators (parameter s), but cooperative mats grow larger in size and sink at a later point in time. The mat growth is characterized by the parameters c_1, z_C, z_D and K, and the initial conditions N_0, x_0 and γ_0. During the sinking process, the mat does not expand any longer and the growth rate may be neglected. The sinking of the mat is characterized by the parameters c_2 and c_3. Compare also figure 4.4 for the phenomenological picture of the growth and sinking of the mat.

– K. The carrying capacity of the broth pot, K, is determined by the experimental setup. For a closed boundary of the pot, K is finite. The value of K in our analysis is mainly determined by the compromise between computational feasibility and adequate qualitative results. This aspect will be discussed later on. In our simulations, K is specified to 1000.

– c_2, c_3. These fitting parameters define the sinking process of the mat. The higher c_2 and c_3 are, the faster the mat will sink. They also determine the influence of defectors on the sinking process. A higher fraction of defectors leads to a faster sinking of the mat. The two constants should be accessible in an experiment. One has to thoroughly investigate the sinking process, and determine the speed of sinking dependent on the percentage of cooperators in that mat.

4.8 Aside: dynamics of the mat density

Although we do not need the explicit formulation of the temporal evolution of the normalized mat density γ, the result will be instructive in order to compare the phenomenological picture of the mat density, which we have given in the beginning of this chapter, with the mat model. The following calculation can be regarded as a consistency check for the adequate mapping between the observed phenomena and the mat model. The result of the analysis will be an autonomous ODE of first order for the normalized mat density γ which depends on the current density, the total number of individuals N, and the percentage of cooperators x,

$$\partial_t \gamma(t) = h(\gamma, N, x) \ , \tag{4.10}$$

which will be discussed later on.
We have inferred the normalized mat density as (cf. eq. (4.3)),

$$\gamma = \frac{N}{M} \cdot z_\sim(x) = \frac{N}{M} \cdot (z_C \cdot x + z_D \cdot (1-x)) \ .$$

The time derivative of the normalized mat density, γ, reads as,

$$\begin{aligned}
\partial_t \gamma &= \partial_t \left(\frac{1}{M(t)} \cdot (N_C(t) \cdot z_C + N_D(t) \cdot z_D) \right) \ , \\
&\approx \partial_t \left(\frac{1}{M(t)} \cdot (\langle N_C \rangle (t) \cdot z_C + \langle N_D \rangle (t) \cdot z_D) \right) \ , \\
&= \underbrace{-\frac{\partial_t M(t)}{M(t)^2} \cdot (\langle N_C \rangle (t) \cdot z_C + \langle N_D \rangle (t) \cdot z_D)}_{\text{effect of front growth}} + \underbrace{\frac{1}{M(t)} \cdot (\partial_t \langle N_C \rangle (t) \cdot z_C + \partial_t \langle N_D \rangle (t) \cdot z_D)}_{\text{effect of interior growth}} \ .
\end{aligned} \tag{4.11}$$

In the second line, we replaced the discrete quantities N_C and N_D by their mean values $\langle N_C \rangle$ and $\langle N_D \rangle$ to simplify the dynamics of the mat density and treat the mat density deterministically. It is important to note that the stochastic nature of N_C and N_D are retained, only the dynamics of the mat density is formulated from a deterministic point of view (see section 4.6).

The ODE in the last line for the normalized mat density reflects mathematically the two effects explained above. The first term involves the dynamics of the number of possible sites in the mat, $M(t)$, which corresponds to the front growth. The second term involves the change of the bacteria numbers for a mat volume M at time t. This feature was exactly introduced as the interior growth.
From the last equation, it can also be recognized that the front growth reduces the mat density since $\partial_t M$ is positive for all times t (see next section, eq. (4.6)). This property is also clear from its physical meaning: The number of possible sites in the mat, M, can only increase. As long as the number of cooperators and defectors, N_S, rises, the interior growth increases the density of the mat.
In this way, the phenomenological picture of the mat growth is qualitatively represented by the mat growth model.

Let us now combine the two effects, the front growth of the mat and the interior growth, in order to formulate the time evolution of the mat density (see eq. (4.11)). Rewriting the result from the front growth effect (cf. eq. (4.6)) in terms of γ, x, N reveals,

$$\begin{aligned}\frac{\partial_t M(t)}{M(t)} &= c_1 \cdot x(t) \cdot \left(\frac{\gamma}{N \cdot z_\sim(x)}\right)^{\frac{1}{2}} \cdot \left(1 - \frac{N \cdot z_\sim(x)}{\gamma \cdot K}\right) \ , \\ &\approx c_1 \cdot \langle x \rangle (t) \cdot \left(\frac{\gamma}{\langle N \rangle \cdot z_\sim(\langle x \rangle)}\right)^{\frac{1}{2}} \cdot \left(1 - \frac{\langle N \rangle \cdot z_\sim(\langle x \rangle)}{\gamma \cdot K}\right) =: l(\langle N \rangle, \langle x \rangle, \gamma) \ ,\end{aligned} \tag{4.12}$$

where eqs. (4.3), (4.6) have been applied and $l(\langle N \rangle, \langle x \rangle, \gamma)$ was defined for short notation. If only the cooperating trait is present in the mat, the dynamics will simplify through $z_\sim(\langle x \rangle) = z = z_C$.
The term corresponding to the interior growth effect can be converted as follows,

$$\begin{aligned}&\frac{1}{M(t)} \cdot (\partial_t \langle N_C \rangle (t) \cdot z_C + \partial_t \langle N_D \rangle (t) \cdot z_D) \ , \\ &\quad = \frac{\langle N \rangle \cdot g(\langle N \rangle, \langle x \rangle, \gamma)}{M(t)} \cdot (z_C \cdot \langle x \rangle \cdot f_C(\langle x \rangle) + z_D \cdot (1 - \langle x \rangle) \cdot f_D(\langle x \rangle)) \ , \\ &\quad = \gamma \cdot g(\langle N \rangle, \langle x \rangle, \gamma) \cdot \frac{z_C \cdot \langle x \rangle \cdot f_C(\langle x \rangle) + z_D \cdot (1 - \langle x \rangle) \cdot f_D(\langle x \rangle)}{z_\sim(\langle x \rangle)} \ , \\ &\quad = \gamma \cdot g(\langle N \rangle, \langle x \rangle, \gamma) \cdot \frac{(z \cdot f)_\sim(\langle x \rangle)}{z_\sim(\langle x \rangle)} \ , \\ &\quad = \gamma \cdot \left(1 - \frac{\gamma}{z_\sim(\langle x \rangle)}\right) \cdot \frac{(z \cdot f)_\sim(\langle x \rangle)}{z_\sim(\langle x \rangle)} \ .\end{aligned}$$

Thus, we end up with an autonomous ODE of first order as indicated in eq. (4.10),

$$\begin{aligned}\partial_t\gamma &= \gamma\cdot\left(g(\langle N\rangle,\langle x\rangle,\gamma)\cdot\frac{(z\cdot f)_\sim(\langle x\rangle)}{z_\sim(\langle x\rangle)} - l(\langle N\rangle,\langle x\rangle,\gamma)\right)\cdot\Theta(1-\gamma)\ ,\\ &\approx \gamma\cdot\left(\underbrace{\left(1-\frac{\gamma}{z_\sim(x)}\right)\cdot\frac{(z\cdot f)_\sim(x)}{z_\sim(x)}}_{\text{interior growth}} - \underbrace{l(N,x,\gamma)}_{\text{front growth}}\right)\cdot\Theta(1-\gamma)\ ,\\ &= h(N,x,\gamma)\ .\end{aligned} \tag{4.13}$$

We introduced an additional factor of $\Theta(1-\gamma)$ by hand to stop the dynamics of the mat density during the sinking process in the same way as it was done for the dynamics of the effective mat volume M. The dynamics of the individual numbers N_C and N_D, however, will not be stopped when the mat sinks. The sinking rate is greater than the growth rate of the mat and reduces the individual number of the mat at the water surface.
Note that we switched from the deterministic to the stochastic picture for the variables x and N in the second line. The aim was to establish the dynamics of the density. We applied the ideas developed in section 4.4.1 and 4.4.2 and switched back to the stochastic formulation. The result of this simplification is given in eq. (4.13), which reveals again the two antagonizing effects contributing to the dynamics of the density.
The first part can be identified with the interior growth and is basically a logistic growth towards the carrying capacity $z_\sim(x) = z_C x + z_D(1-x) > 1$ on a slightly changed timescale of $z_\sim(x)/(z\cdot f)_\sim(x)$. If only cooperators are present in the mat, that is $x = 1$, we will have $z_\sim(1) = z_C$ and $(z\cdot f)_\sim(1)/z_\sim(1) = f_\sim(1) = 1$. In this case, the timescale of the logistic growth is solely defined by the birth rate of the cooperators (see section 4.6), and the normalized density of the mat grows towards $z_C > 1$. Nevertheless, the dynamics of the mat density is stopped when $\gamma = 1$ is reached.
The second term in eq. (4.13) refers to the front growth of the mat and lowers the speed at which the density of the mat grows. This term represents the observation that mats with a higher fraction of cooperators can grow larger and sink at a later point in time than groups with a lower fraction of cooperators.

All in all, the dynamics of the normalized mat density confirms our phenomenological picture of the growth and sinking of the mat and support the derivation and the definition of the mat model.

5 Analysis of the Mat Model

Let us now have a look at the solutions of the mat model as formulated in the last chapter. We are especially interested in the behaviour of the number of cooperators and defectors since these are the quantities which are experimentally accessible. As already shown in chapter 2, Rainey & Rainey have measured the number of cooperators in presence and absence of defectors. The data is shown again in figure 5.1. We will compare our results to this data from the experiment [1].

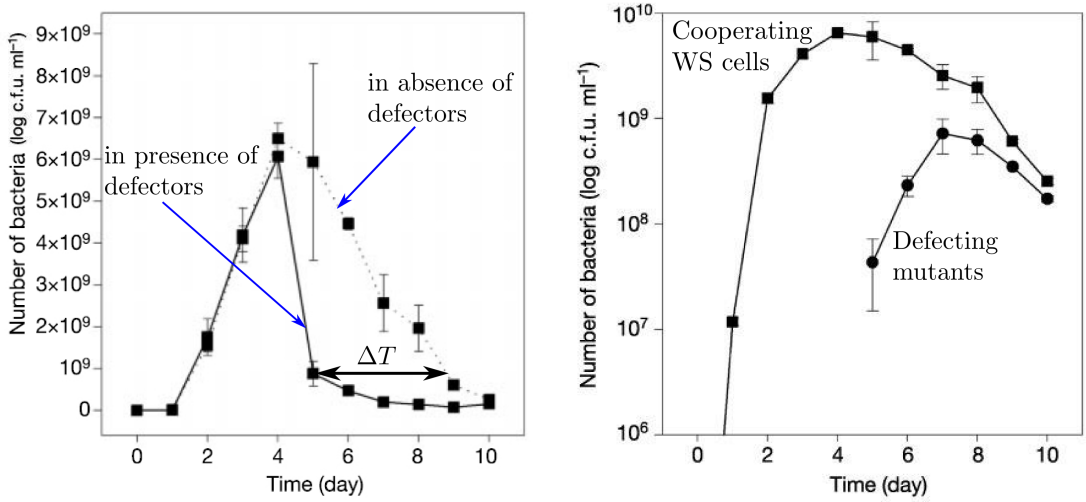

Figure 5.1: Summary of the experimental data of the Rainey & Rainey experiment already presented in figure 2.4 and 2.5.
Left: Emergence of defecting cells in the mat [1]. circles: number of defectors, squares: number of cooperators.
Right: Number of cooperating wrinkly spreader cells in the mat [1]. Dashed line: number of cooperators (wrinkly spreader in the experiment) without defectors. This measurement refers to the case where only cooperators are present in the mat. Solid line: number of WS in the mat in presence of defectors.

5.1 Mean-field analysis

In order to evaluate the influence of stochastic demographic fluctuations, it is instructive to look at the mean-field equations first. This analysis also helps us to specify and narrow down the range of the fitting parameters of the stochastic cooperator-defector model. For the stochastic system described above, the mean-field equations are analogous to eqs. (3.19), (3.20) from chapter (3). The only difference is that the growth and sinking rate now also depend on the normalized density γ,

$$\begin{aligned}\partial_t \langle N\rangle &= \langle N\rangle \cdot (g(\langle x\rangle, \langle N\rangle, \gamma) - d(\langle x\rangle, \langle N\rangle, \langle\gamma\rangle)) \ , \\ \partial_t \langle x\rangle &= \langle x\rangle \cdot (1-\langle x\rangle) \cdot g(\langle x\rangle, \langle N\rangle, \langle\gamma\rangle) \cdot (f_C(\langle x\rangle) - f_D(\langle x\rangle)) \ .\end{aligned}$$

The full mean-field system for the mat model then reads as follows,

$$\begin{aligned}\partial_t \langle N\rangle &= \langle N\rangle \cdot \left(1 - \frac{\gamma}{z_\sim(\langle x\rangle)} - c_2 \cdot (c_3 - \langle x\rangle) \cdot \Theta(\langle\gamma\rangle - 1)\right) \ , \\ \partial_t \langle x\rangle &= -\frac{s}{1 - s\langle x\rangle} \cdot \langle x\rangle \cdot (1-\langle x\rangle) \cdot \left(1 - \frac{\langle\gamma\rangle}{z_\sim(\langle x\rangle)}\right) \ , \\ \partial_t \langle M\rangle &= c_1 \cdot \langle x\rangle \cdot \langle M\rangle^{\frac{1}{2}} \cdot \left(1 - \frac{\langle M\rangle}{K}\right) \ , \\ \langle\gamma\rangle &= \frac{\langle N\rangle}{\langle M\rangle} \cdot z_\sim(\langle x\rangle) \ ,\end{aligned} \tag{5.1}$$

with initial conditions $\langle N\rangle(0) = N_0, \langle x\rangle(0) = x_0$ and $\langle\gamma\rangle(0) = \gamma_0$.
Recall that,

$$\begin{aligned}z_\sim(\langle x\rangle) &= z_C \cdot \langle x\rangle + z_D \cdot (1-\langle x\rangle) \ , \\ (z\cdot f)_\sim(\langle x\rangle) &= z_C \cdot \langle x\rangle \cdot \frac{1-s}{1-s\langle x\rangle} + z_D \cdot (1-\langle x\rangle) \cdot \frac{1}{1-s\langle x\rangle} \ .\end{aligned}$$

Results of mean-field analysis

Figure 5.2 shows the solution of the mean-field equations (5.1) for a specific set of parameters and initial conditions.

In the left part of figure 5.2, the numbers of cooperators and defectors are depicted. The graph shows a qualitatively satisfactory agreement with the experimental data in figure 5.1. The number of cooperators raises approximately exponentially after the dynamics is started (note the logarithmic scale for the number of individuals) and reaches its maximum at about $t \simeq 4.3$. Thenceforth, the number of cooperators decreases steadily, and the speed of decrease is less than the speed of increase has been before. For the number of defectors, we gain a similar picture. N_D increases with a similar speed as the number of cooperators

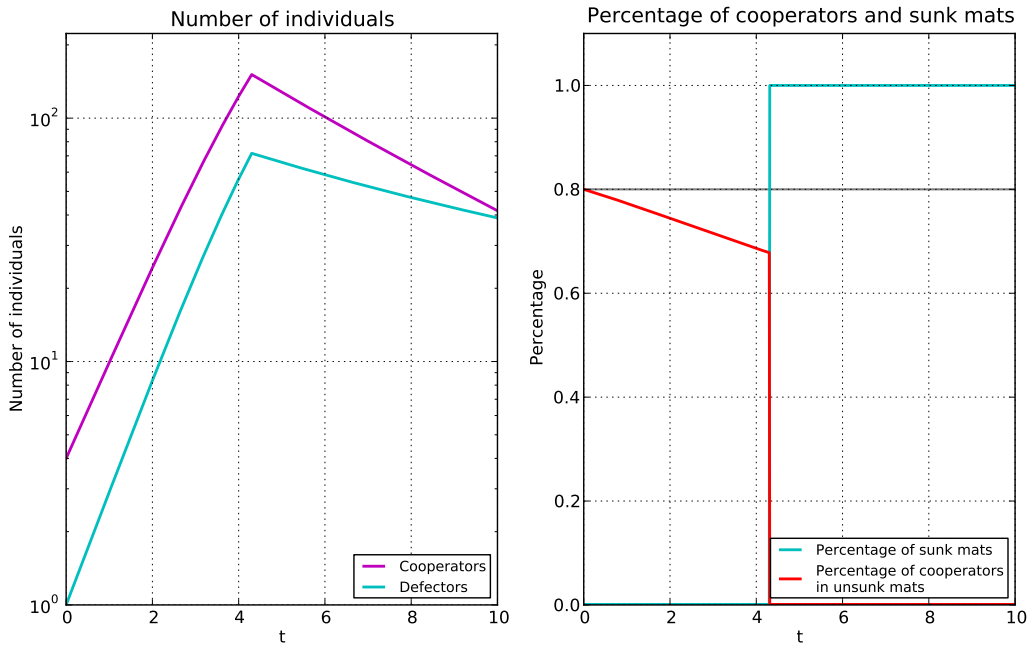

Figure 5.2: Left: Number of cooperating and defecting bacteria as obtained from the mean-field system (5.1). The kink in the number of individuals refers to the sinking of the mat. Right: Percentage of cooperators in the mats obtained from the mean-field system (5.1). The x-average declines for all times and drops to 0 when all mats are sunk. The blue curve shows the fraction of mats which are sunk up to time t.
Chosen parameters: $s = 0.15, c_1 = 20, z_C = 2, z_D = 6, c_2 = 9, c_3 = 1.1$.
Initial values: $N_0 = 5, x_0 = 0.8, \gamma_0 = 0.2$.

in the beginning. The maximum of the number of defectors is reached at the same time as for N_C at about half of the maximal number of cooperators. The speed of decrease of the number of defectors is less than for cooperators such that both individual numbers converge to each other.
The same qualitative behaviour can be found in the data of Rainey & Rainey (cf. figure 5.1) but on a different time scale and a different scale in the number of individuals, which is due to the chosen set of parameters.
Time is measured in dimensionless units of the doubling time in our simulations, that is $\Delta t = 1$ refers approximately to the time in which a population doubles its size. In the experiment, the doubling rate can be assumed to lie between 30 and 60 minutes for bacteria; hence, one day refers to roughly $t = 20$ to 50 doubling times in our simulations. Especially the carrying capacity of the mat, K, plays a crucial role for the outcome in the context of scaling the number of individuals. To gain realistic results for the bacteria number of order 10^9 as observed in the Rainey & Rainey experiment, one has to set K to a value in that range, too. Assigning $K \simeq 10^9$ would lead, however, to very large groups and very

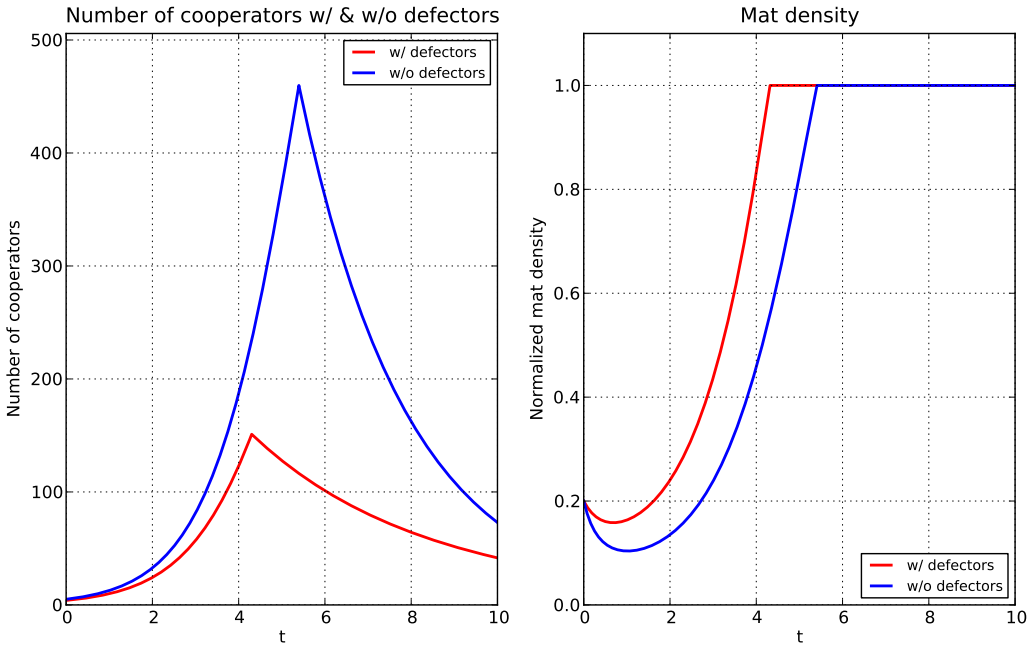

Figure 5.3: Left: Evolution of the number of cooperators in presence and absence of defecting bacteria as obtained from the mean-field system (5.1). The peak refers to the sinking of the according mat.
Right: Density of the mat in presence and absence of defectors. Note the transient decline of the mat density in both cases due to the front growth mechanisms which is more pronounced if defectors are absent. The increase of the density is caused by the interior growth. If the density of the mat reaches the value 1, the mat sinks.
Chosen parameters: $s = 0.15, c_1 = 20, z_C = 2, z_D = 6, c_2 = 9, c_3 = 1.1$.
Initial values: $N_0 = 5, x_0 = 0.8, \gamma_0 = 0.2$.

high birth and sinking rates which are not tractable in stochastic numerical simulations. Hence, we choose the compromise between numerical practicability and adequate qualitative results, and set $K = 1000$.
Furthermore, the number of defectors reaches its maximum with a temporal delay of 3 days in the experiment compared to the maximal value of the number of cooperators. This experimental result is not covered by the mat model since we do not distinguish explicitly between defectors and cooperators during the sinking process (the trait-dependent sinking rate is set to 1).

To understand the mean-field solutions more easily, the right part of figure 5.2 shows the percentage of cooperators in those mats which are not sunk up to that time. This observable makes sense from a biological point of view since these groups can actually reproduce actively. When all mats start to sink at $t = T_{\text{sink}}$, this average, which we will refer to as $\langle x \rangle_{\text{mat}}$ in the following, drops to zero. The fraction of cooperators is decreasing

for all times. This behaviour can also be induced from eqs. (5.1). One recognizes that always $\partial_t \langle x \rangle < 0$ holds true since $\langle \gamma \rangle \leq 1 < z_{\sim}(\langle x \rangle)$.

In figure 5.3, the number of cooperators is plotted for two cases, in presence and in absence of defectors in the mat. The plot of the cooperators without defectors in the mat corresponds to the so called null model as we have referred to it in section 4.1.1. The important point to notice is that the number of cooperators is decreasing after $t \gtrsim 5.4$ (see left part of figure 5.3). This result would be different if we had applied the model of Melbinger et al. naively in the very beginning. Then, for the case of cooperators only ($x = 1$), the graph would show a logistic growth.
On the right-hand side of figure 5.3, the temporal evolution of the according normalized mat density is shown. As one can see from the graph, the density of the whole mat decreases slightly in the beginning. This decline is due to the front growth process which results in a rapid growth of the mat skeleton and lowers the mat density. However, the front growth will be balanced with the interior growth. The relation between front growth and interior growth is mainly influenced by the parameter c_1 as indicated earlier. The mat density passes its minimal value and starts growing at about $t \simeq 0.8$. At $\gamma = 1$, the average mat density of the whole mat equals the density of water. Therefore, the mat sinks and the mat density stays unchanged henceforward. Moreover, this sinking of the mat results in the decrease of the number of individuals as mentioned above.

As one can infer from the right plot in figure 5.3, the density increase is slower when only cooperators are present in the mat, which is clear from a physical point of view. This feature was explicitly implemented in the model and is now reflected by the outcome of the computation. As a consequence, the number of cooperators reaches a higher maximum in the mat without defectors, and the drop of the number of cooperators appears at a later time.
The decline in the number of cooperators in the case without defectors, however, is steeper than in presence of defectors. This outcome is different from the observation in the experiment, where the mat sinks rapidly if it is infiltrated with defectors, whereas a mat consisting solely of cooperators sinks on a much larger time scale (cf. figure 5.1, right picture). On the one hand, the sinking rate and growth rate are proportional to the number of individuals in the mat. Since groups with a higher fraction of cooperators can grow larger than groups with a lower fraction, cooperative mats would sink faster. On the other hand, the sinking rate was introduced to favor cooperative groups. The higher the percentage of cooperators in a mat is, the smaller is the sinking rate. The detailed sinking of a mat, however, is a highly non-linear process. In the our linear approximation with the chosen parameters c_2 and c_3, cooperative mats decline faster than mats with a lower fraction of cooperators in the mean-field case.
Nevertheless, the time at which a purely cooperative mat will be completely sunk is greater than for a mat with defectors since the sinking of the mat starts at a later point in time. This effect is one of the important conclusions of the experiment. The exact relation between these two different effects, the point in time at which the sinking process starts and

the speed of decrease of the individual number, depends on the values of the parameters c_1, c_2, and c_3.
We conclude that the numerical results are in adequately qualitative accordance with the observations of Rainey & Rainey given in figure 5.1. In order to point out the influence of stochastic fluctuations on the dynamics of the mat growth, we will now analyze the outcome of the full stochastic model. For example, one would expect the peaked number of cooperators to smooth out if we included stochastic fluctuations to our analysis. Especially, we will draw attention to the behaviour of the percentage of cooperators since this quantity has shown a qualitative change in the model of Melbinger et al. when we discussed stochastic fluctuations (cf. chapter 3).

5.2 Stochastic simulations of the mat model

Let us examine the results of the full stochastic simulations according to section 4.6. The numerical simulations are executed by employing the Gillespie algorithm which will be described below.

5.2.1 Algorithm for the mat model

We treat the number of cooperators and the number of defectors as stochastic variables, and update their values with the Gillespie algorithm reflecting the stochastic dynamics according to section 4.6. The update of the effective mat volume M and the normalized density γ follows the deterministic ODE given by eq. (4.9). We have introduced the effective mat volume as a discrete stochastic variable, but nevertheless describe its dynamics deterministically due to our ignorance of microscopic details of the mat growth. This averaged view is represented by the assumed scaling law in eq. (4.5) and translates into the ODE for M in eq. (4.9).
A flowchart of the algorithm is depicted in figure 5.4. It shows an adjusted form of the algorithm for the stochastic cooperator-defector model from chapter 3 to account for the structural changes in the mat model.

5.2.2 Results of stochastic simulations of the mat model

In this section, we present the results of the stochastic simulations for the mat model from section 4.6 obtained by executing the algorithm described above.

Figure 5.5 shows the evolution of 1000 mats at four different points in time for one chosen set of parameters and initial values. Each of the four scatter plots depicts the distribution of

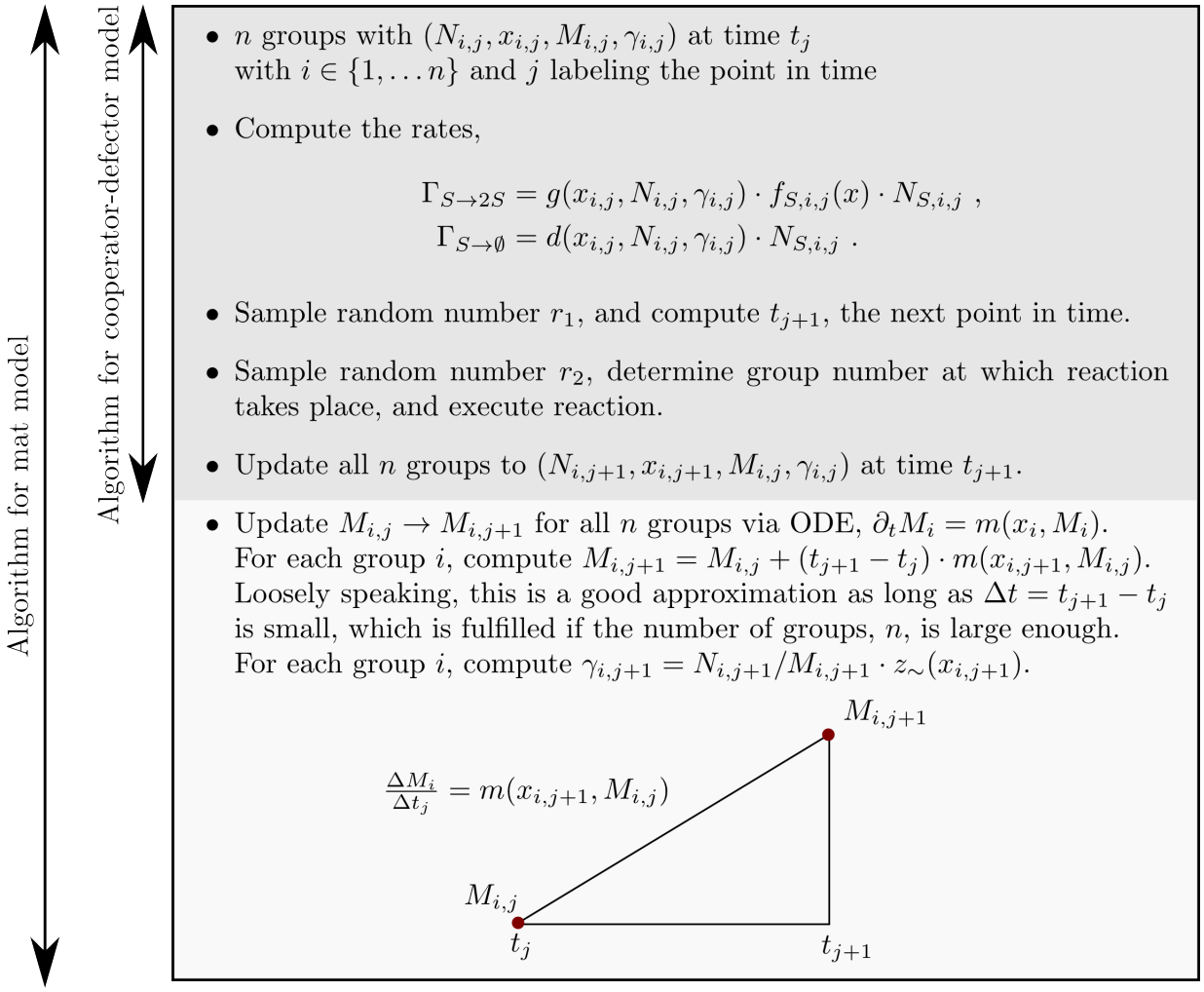

Figure 5.4: The algorithm for the update of the variables N, x, M, and γ in the mat model is an extension of the algorithm for the cooperator-defector model. Whereas the update of the individual numbers N_C and N_D, or equivalently N and x, follows the stochastic Gillespie algorithm, the effective mat volume is updated deterministically. Then, the mat density is computed.

all 1000 mats with respect to their number of individuals, their percentage of cooperators, and their normalized mat density, which is color-coded. The black cross indicates the average over the number of individuals in all groups on the vertical axis, and the averaged percentage of cooperators in all mats that are not sunk up to that point in time. The color-code marks the normalized density of the mat. The deeper the blue of a circle is, the lower the density of the mat will be. In contrast, a red circle refers to a mat with normalized density $\gamma = 1$, that is a mat which is sinking. A sinking mat does not contribute any longer to the average of the fraction of cooperators, $\langle x \rangle_{\text{mat}}$.

The stochastic dynamics is started with all groups containing exactly four cooperators and

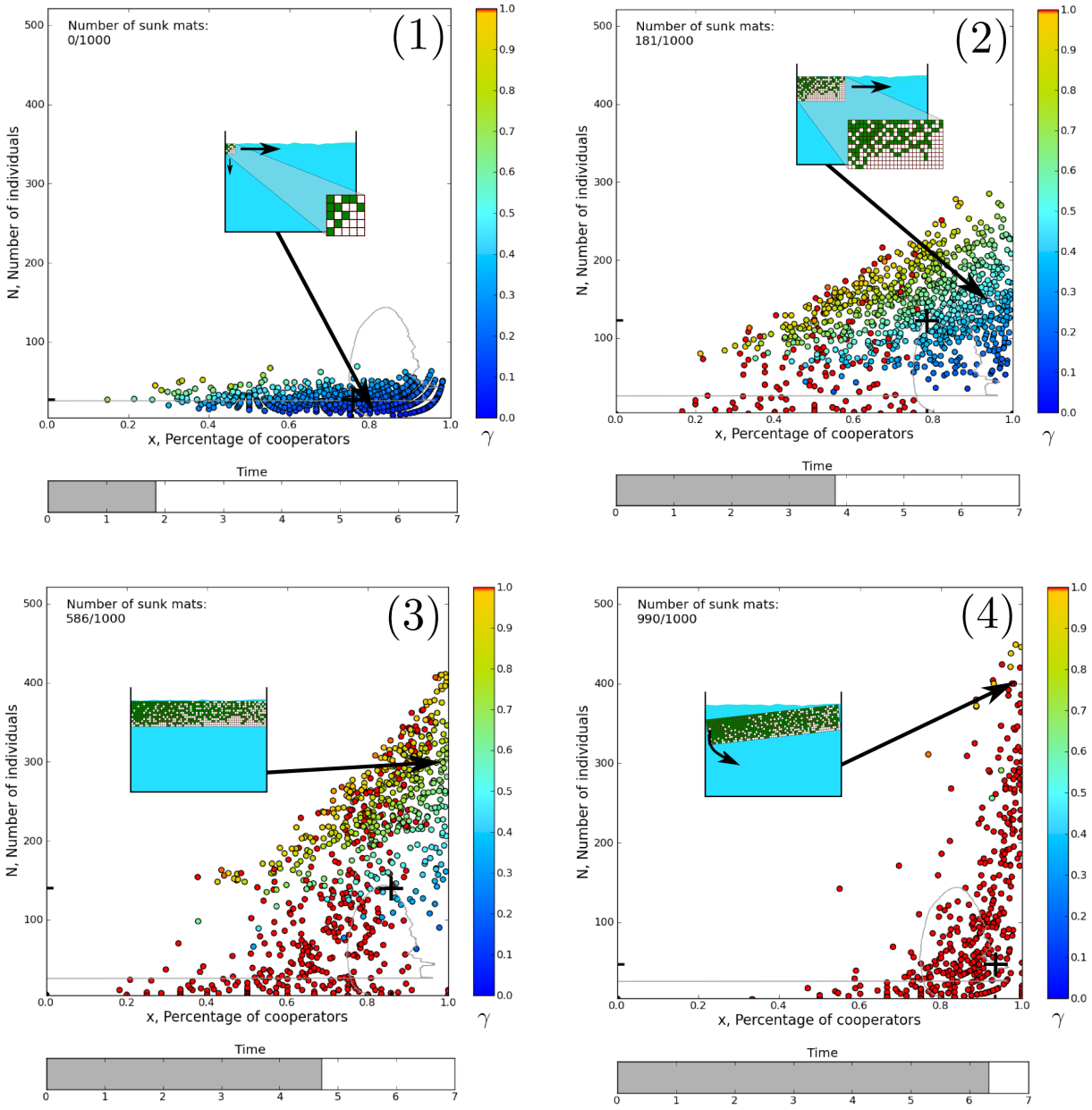

Figure 5.5: Stochastic dynamics of the mat ensemble (1000 groups). The mat density γ is color-coded; red circles represent sinking mats. All groups are equally initialized, but the distribution in x rapidly broadens due to stochastic demographic fluctuations (1). The higher the fraction of cooperators in a mat is after the initial dynamics, the larger the group can grow, and the slower the density of the mat will increase (2), (3). Ultimately, the mat density reaches the density of water and the mat sinks (4).
Chosen parameters: $s = 0.15, c_1 = 20, z_C = 2, z_D = 6, c_2 = 9, c_3 = 1.1$.
Initial values: $N_0 = 5, x_0 = 0.8, \gamma_0 = 0.2$.

one defector; the initial density is set to $\gamma_0 = 0.2$. The peaked density distribution for the fraction of cooperators rapidly spreads which is due to stochastic fluctuations influencing the population dynamics significantly for a low number of individuals in the mats (cf. chapter 3). Figure 5.5 (1) shows this broadening of the x-distribution shortly after the dynamics has been started. All mats started from the same position in the N-x-diagram at $N_0 = 5, x_0 = 0.8$, but at $t \simeq 1.8$ this distribution has spread dramatically in the x-range. One recognizes that the higher the fraction of defectors in a mat is, the higher the density of that mat will be on average for the same number of individuals. In other words, the density of a mat will increase more slowly if the percentage of cooperators is higher, which is due to the front growth mechanism of the spreading mat. Defectors do not contribute to the stability of the mat and weaken the structure of the mat. Therefore, the effective density contribution to the mat density for a defector is higher ($z_D = 6$ here) than for a cooperator ($z_C = 2$ here), and the density at which the mat sinks is reached more quickly with a higher percentage of defectors. This is the reason why the first mats sink in the left part of the mat bulk ensemble in the scatter plot. Figure 5.5 (2) represents this property at $t \simeq 3.8$. One the one hand, one can see that a mat with a low percentage of cooperators ($0.2 \lesssim x \lesssim 0.3$) grows only up to a maximal size of 100 to 200 individuals. After having reached the sinking condition $\gamma = 1$, the mat sinks and the number of bacteria at the liquid-air interface decreases quickly. In the diagram, the red circle then drops along the vertical direction as a mat would sink in the glass vial, metaphorically speaking. On the other hand, mats with a high fraction of cooperators ($x \gtrsim 0.8$) can grow much larger (up to 450 individuals) and will survive longer.
In figure 5.5 (2) and (3), we observe at later times that for a constant fraction of cooperators, mats that are larger and that are composed of more individuals have a higher density than mats with only a small number of constituents. This attribute is caused by the interior growth mechanism which results in an increase of the density. At $t \simeq 4.8$ (third picture in the figure), more than half of all mats are sunk. On average, only those mats which have a high percentage of cooperators have survived up to then.
This is also the reason, why the average fraction of cooperators over all mats which are not sunk up to that time, $\langle x \rangle_{\text{mat}}$, increases again and even exceeds the initial value x_0. First, the average over x decreases when the evolution of the mats is started because of the selective advantage of defectors. Due to stochastic fluctuations in the beginning, however, the distribution in x broadens dramatically. For later times the mats with a low fraction of cooperators will then be sunk and do not contribute to the average $\langle x \rangle_{\text{mat}}$ any longer. Only the mats with a high percentage of cooperators and an accordingly high individual number will contribute. As a result, $\langle x \rangle_{\text{mat}}$ will raise again.
Ultimately, all mats will be sunk. Figure 5.5 (4) shows a situation, just before all mats have arrived at the density of water $\gamma = 1$. When all mats are sinking or are already sunk, we set the fraction of cooperators to zero.

Up to now, we have gained a qualitative understanding of how the ideas that led to the mat model affect the qualitative behaviour of the dynamics of the mat ensemble in the stochastic simulations. The average population size, $\langle N \rangle$, and the average fraction of

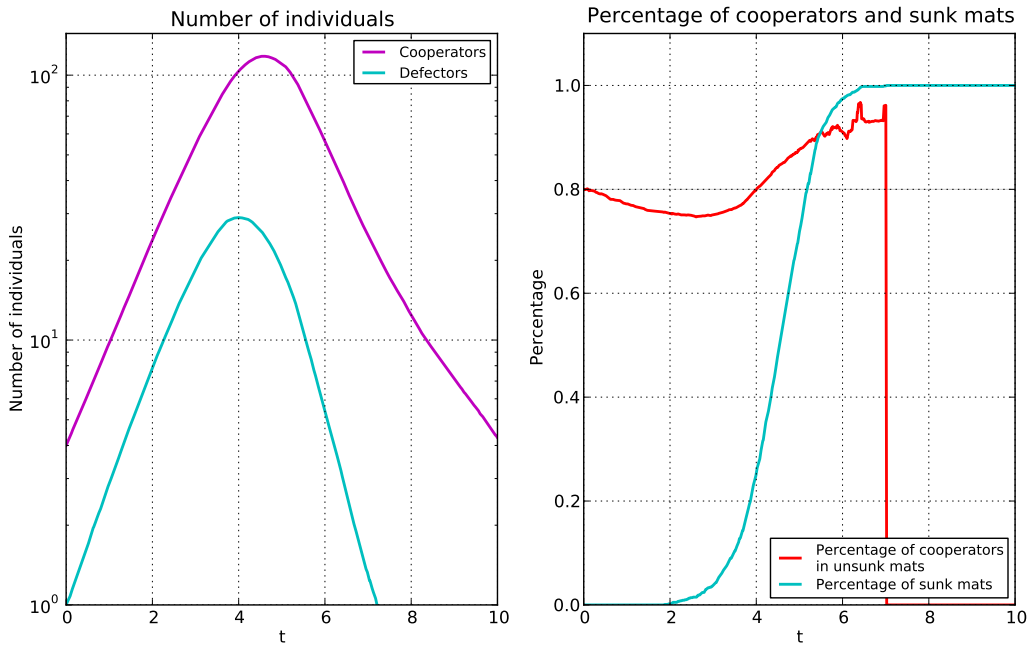

Figure 5.6: Left: Average number of cooperating and defecting bacteria as obtained from the stochastic mat model 4.6. The graph represents the ensemble average over 1000 groups. For details, see text.
Right: Percentage of cooperators in the mat obtained from the stochastic mat model 4.6. After a transient period of steady decline, the x-average increases again due to stochastic fluctuations in the beginning of the temporal evolution. The blue curve shows the cumulated distribution of the sinking times for the ensemble of 1000 mats.
Chosen parameters: $s = 0.15, c_1 = 20, z_C = 2, z_D = 6, c_2 = 9, c_3 = 1.1$.
Initial values: $N_0 = 5, x_0 = 0.8, \gamma_0 = 0.2$.

cooperators over all mats at the surface, $\langle x \rangle_{\text{mat}}$, have already been introduced and will be discussed in more detail in the following. In order to compare the outcome of the simulations with the data from the Rainey & Rainey experiment, we will now have a closer look at these time-dependent averages.

Figure 5.6 and 5.7 are the corresponding graphs of the stochastic simulations as figures 5.2 and 5.3 are for the mean-field analysis of the mat model from section 4.6. Both figures are obtained from the same data presented in figure 5.5. They reduce the full information about all mats to the dynamics of the time-dependent ensemble average of different observables. The left subfigures can again be compared to the data from Rainey & Rainey depicted in figure 5.1. In our description, we want to focus on the differences between the outcome of the stochastic simulations and the mean-field solution of the mat model.
The main difference lies in the influence of stochastic fluctuations which scale as $\sim 1/\sqrt{N}$

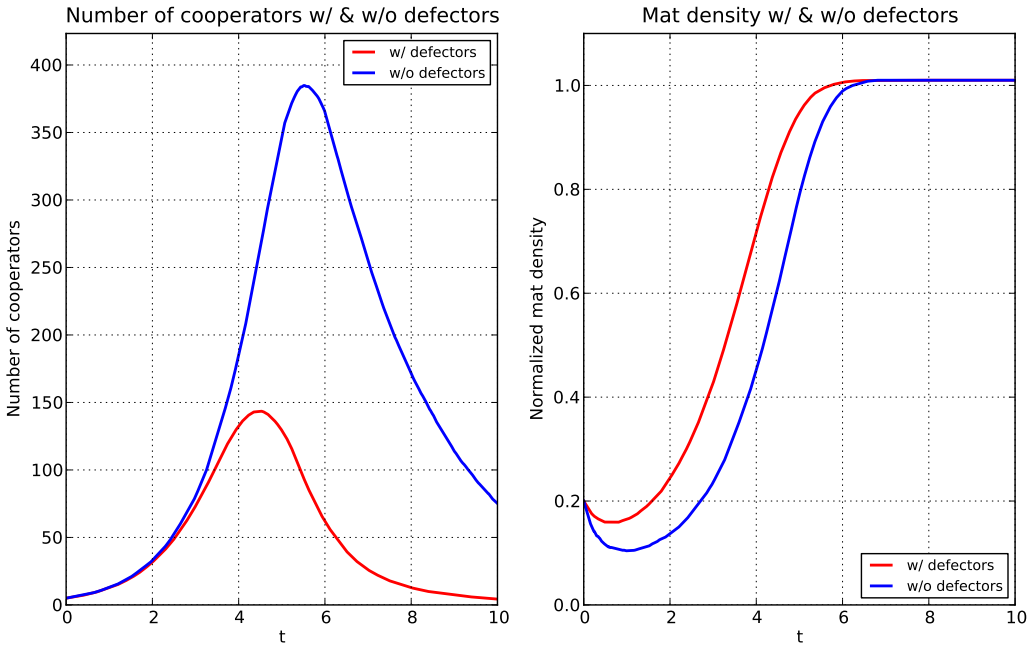

Figure 5.7: Left: Evolution of the number of cooperators in presence and absence of defecting bacteria as obtained from the stochastic mat model 4.6. The graph is in qualitative good agreement with the according data from Rainey & Rainey depicted in figure 5.1. Right: Density of the mat in presence and absence of defectors.
Chosen parameters: $s = 0.15, c_1 = 20, z_C = 2, z_D = 6, c_2 = 9, c_3 = 1.1$.
Initial values: $N_0 = 5, x_0 = 0.8, \gamma_0 = 0.2$.

and are especially important in the beginning of the temporal evolution when the population size is small (see chapter 3). These stochastic demographic fluctuations cause the spreading of the x-distribution initially peaked around x_0. From the discussion of figure 5.5, we already know that this broadening has an impact on the time at which a mat sinks. In contrast to the mean-field case, where all mats sink at the same time because of the absence of stochastic fluctuations, we obtain a distribution over the sinking times in the stochastic case. The blue curve on the right in figure 5.6 depicts the cumulated distribution of sunk mats. The time at which the sinking process starts is smeared out. For the mean-field solution, this graph is a step-function having the step at $t \simeq 4.3$ (cf. figure 5.2).
Moreover, the spread in x at the beginning of the evolution also affects the average number of individuals. For the same reason, the peak in the number of cooperators and defectors in figure 5.2 is smoothed out in case of stochastic simulations (see left part of figure 5.6). The decline in the number of defectors, however, is steeper than the decrease in the number of cooperators, and both individual numbers decrease much faster than in the mean-field model. Compared to the data from Rainey & Rainey these results remain in qualitatively

good accordance.
The most dramatic change in the results from the mean-field solution to the stochastic simulation can be observed in the x-average over all mats which are not sunk, $\langle x \rangle_{\text{mat}}$. While the mean-field behaviour of this quantity shows a steady decrease, the outcome of the stochastic simulations reveals a different behaviour. In the beginning, $\langle x \rangle_{\text{mat}}$ declines in the same way as for the mean-field case. From the point, where the first mats sink (at $t \simeq 2.0$), we notice a turnaround from a decrease to an increase of this observable. The percentage of cooperators over all unsunk mats, $\langle x \rangle_{\text{mat}}$, averages only over the mats at the surface. This average is taken over less and less mats before all mats are sunk. That is also the reason, why $\langle x \rangle_{\text{mat}}$ becomes more choppy before dropping to zero. Since more cooperative mats can survive longer than less cooperative groups, the x-averages increases again.
We can conclude that the fraction of cooperators in the whole mat ensemble can increase due to stochastic fluctuations in contrast to the mean-field solution, where this quantity decreases for all times. Note that the stochastic fluctuations are crucial for the dynamics of the mat ensemble. We have expected this dependency since the mat model can be understood as an extension of the cooperator-defector model of Melbinger et al.
The result in the mat model, however, is a transient increase of cooperation *after* some time and not a transient increase *in the beginning* as in the cooperator-defector model from chapter 3. This transient increase of cooperation in the mat model is determined by the time at which the first groups sink and the time at which all mats are sunk.

Comparing figure 5.7 with the deterministic analogue in figure 5.3, we can confirm the results from above, namely the smearing out of the peaky curves in the mean-field picture caused by the stochastic broadening of the x-distribution. As a consequence, the shapes of the curves for the number of cooperators with and without defectors are in better qualitative agreement with the experimental data (figure 5.1) than the mean-field results.

5.2.3 Parameter study

In section 4.6, we have already interpreted the role of different parameters for the dynamics of the mat model. Let us now quantify the influence of biologically relevant parameters in a systematic way.
The most important parameters for the qualitative behavior of the stochastic mat model are the selection strength s, that is the evolutionary advantage of defectors over cooperators, and the growth advantage c_1 of cooperative groups. These two quantities reflect the two antagonizing principles: cooperative groups grow to a larger size, but defectors are better off microscopically.
In addition, we also discuss the initial percentage of cooperators x_0 to highlight the importance of the presence of cooperators in the beginning, and the initial population size N_0 scaling the impact of demographic fluctuations.
In order to quantify the impact of a chosen parameter or initial condition on the level

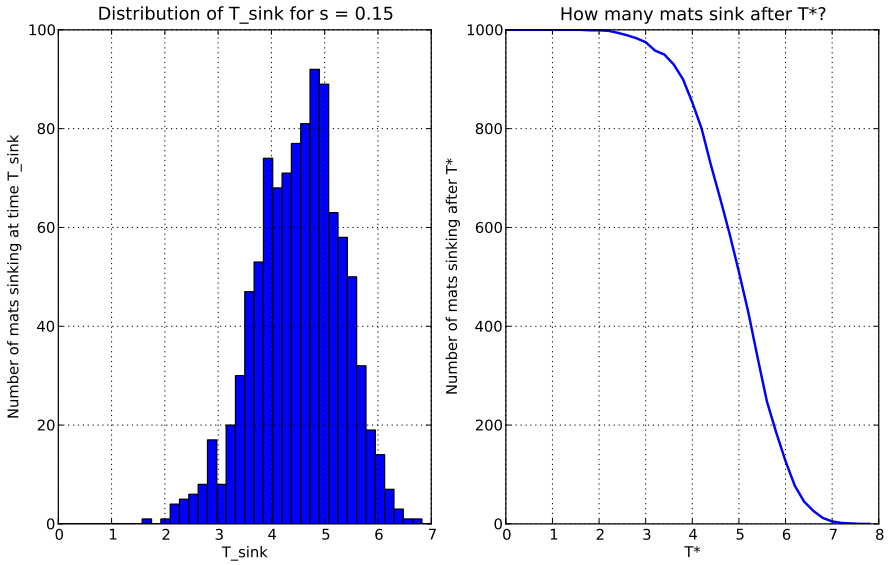

Figure 5.8: Distribution of the sinking time T_{sink} for a mat ensemble of 1000 mats. The left diagram shows the histogram for the number of mats sinking at time T_{sink}. The distribution of the sinking time shows a pronounced peak around which the sinking times are symmetrically distributed. This distribution decays rapidly for smaller and larger times. Thus, one could approximate the distribution of sinking times by a Gaussian. The mean sinking time $\langle T_{\text{sink}} \rangle$ will be used as an observable to characterize the mat ensemble for a given set of parameters. On the right, the number of mats that sink after time T^* is depicted. This curve shows a cumulated version of the left distribution of sinking times which will be applied later on.
Chosen parameters: $s = 0.15, c_1 = 20, z_C = 2, z_D = 6, c_2 = 9, c_3 = 1.1$.
Initial values: $N_0 = 5, x_0 = 0.8, \gamma_0 = 0.2$.

of cooperation, we define suitable observables with which we can compare the outcome of the stochastic mat model for different sets of parameters. These observables should be biologically relevant and should discriminate between cooperative and non-cooperative groups.

The crucial property of the mats in the stochastic mat model is that they sink after a specific time T_{sink} (see figure 5.5 and 5.6). In our model, the sinking time of a mat is defined as the time until the normalized mat density reaches the value $\gamma = 1$ since a mat cannot reproduce, from a biological point of view, after it is sunk (cf. chapter 6). This property is important for the next section, where we consider regrouping steps with mats that are not sunk. For this reason, a suitable observable of the mat ensemble is the mean sinking time $\langle T_{\text{sink}} \rangle$. We assume from our phenomenological picture of the mat growth that the sinking time should increase if cooperative groups are favored.

Another reasonable observable with which to characterize a mat and with which to dis-

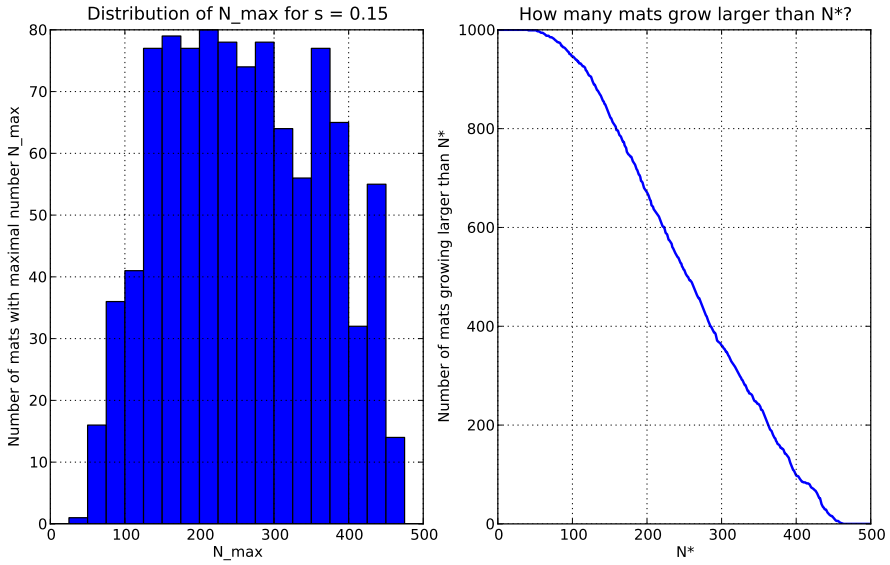

Figure 5.9: Distribution of the maximal number of individuals $N_{\max}$ for a mat ensemble of 1000 mats. The left diagram is a histogram for the maximal number of individuals, $N_{\max}$, comprised by a mat. The distribution of the maximal number of individuals shows a broad maximum between $N_{\max} \simeq 150 \ldots 400$. A Gaussian approximation would not lead to an optimal fit of this distribution. The mean maximal number of individuals $\langle N_{\max} \rangle$ will be used as an observable to characterize the mat ensemble for a given set of parameters. On the right, the number of mats that grow larger than N^* are depicted. This curve shows a cumulated version of the left distribution of $N_{\max}$ which will be applied later on.
Chosen parameters: $s = 0.15, c_1 = 20, z_C = 2, z_D = 6, c_2 = 9, c_3 = 1.1$.
Initial values: $N_0 = 5, x_0 = 0.8, \gamma_0 = 0.2$.

criminate the level of cooperation is the maximal number of individuals $N_{\max}$ the mat comprises. Again, more cooperative groups should be able to incorporate more individuals than non-cooperative groups since only cooperators build up the mat skeleton. Therefore, we will also compute the mean maximal number of bacteria $\langle N_{\max} \rangle$ of a mat ensemble.

Figure 5.8 and 5.9 show the distribution of the sinking time T_{sink} and the maximal number of individuals $N_{\max}$ within a mat ensemble of 1000 groups for the set of parameters we have already analyzed before (see figures 5.5, 5.6, 5.7).
The distribution of sinking times reflects once more the influence of stochastic fluctuations. All groups start with the same initial conditions, but the sinking times show a symmetric smearing out around the maximum. If stochastic effects were absent, only one peak with the same sinking time for all mats would show up in this diagram. The same holds true for the distribution of the maximal number of individuals, where the broadening of the distribution is even more dramatic.
From the analysis of figure 5.5, we concluded that the larger a group grows, the longer

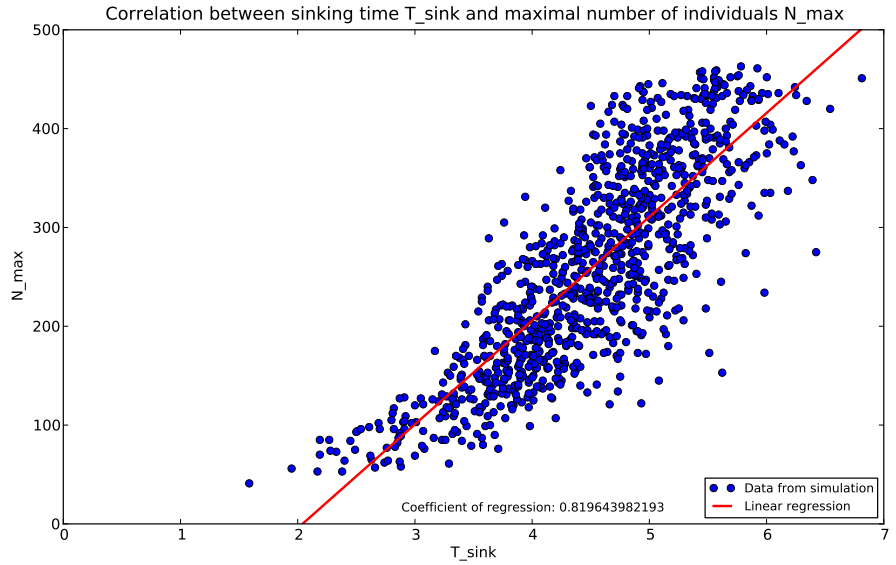

Figure 5.10: Scatter plot of the maximal number of individuals $N_{\max}$ versus the sinking time T_{sink} for the mat ensemble containing 1000 groups. A linear regression analysis supports the phenomenological picture that groups growing large in size will also sink at a later point in time. The linear correlation between the two observables is backed up by the regression coefficient $r = 0.81$, which is nearly 1.
Chosen parameters: $s = 0.15, c_1 = 20, z_C = 2, z_D = 6, c_2 = 9, c_3 = 1.1$.
Initial values: $N_0 = 5, x_0 = 0.8, \gamma_0 = 0.2$.

the mat will survive before it sinks. Hence, one might raise the question in which sense the distributions of $N_{\max}$ and T_{sink} reflect the same information about the mat ensemble. The answer to this question can be inferred from figure 5.10, where the maximal number of individuals in the mat, $N_{\max}$, is plotted versus the sinking time of the mat, T_{sink}. The scatter plot shows the distribution for the whole mat ensemble of 1000 groups. From a linear regression analysis we can support the earlier observation, that the observables $N_{\max}$ and T_{sink} are highly correlated for this set of parameters, and in this sense just reflect two sides of the same coin. The detailed analysis of different parameter sets reveals that the approximately linear correlation holds also true in general. Nevertheless, we want to quantify the effect of a change in the parameters for both observables.

Selection pressure s and growth advantage of cooperative groups c_1

The selection strength s quantifies the evolutionary advantage of defectors over cooperators. The quantitative impact of the variation of this parameter on the mean sinking time and the mean maximal population size is shown in figure 5.11. One recognizes that both observables decrease with an increase of the selection strength s. Hence, the more

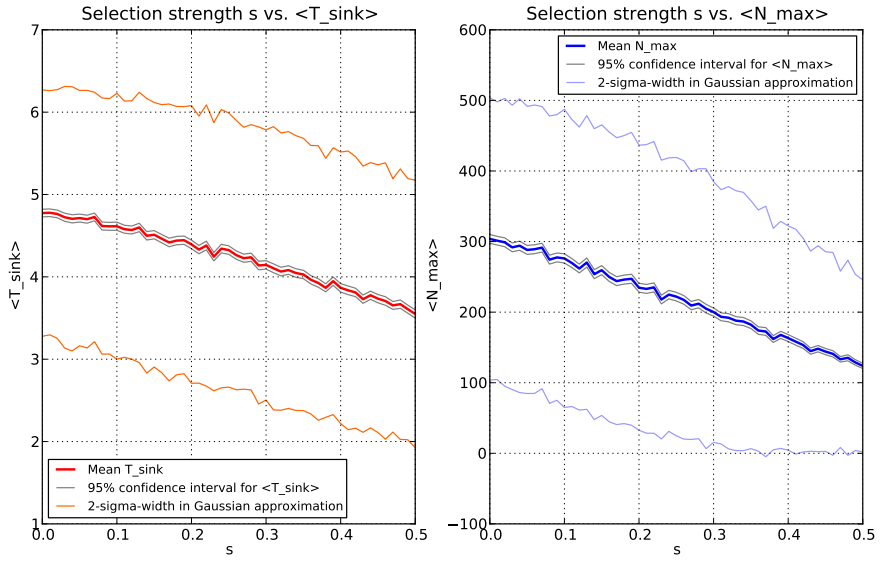

Figure 5.11: Influence of the selection pressure s on $\langle T_{\text{sink}} \rangle$ (left) and $\langle N_{\text{max}} \rangle$ (right). The higher the selection strength is, the higher the microscopic evolutionary advantage of defectors over cooperators will be. Therefore, the average sinking time (left plot) and the average maximal population size decrease with an increase of s. Chosen parameters: $c_1 = 20, z_C = 2, z_D = 6, c_2 = 9, c_3 = 1.1$.
Initial values: $N_0 = 5, x_0 = 0.8, \gamma_0 = 0.2$.

defectors are favored, the faster the mat will sink, and the smaller the population grows in size. These results confirm our phenomenological picture of the mat growth. Figure 5.12 depicts the influence of the variation of c_1, the growth advantage of cooperative groups. The greater the parameter c_1, the higher the mean sinking time and the bigger the maximal population size. In this way, the term 'growth advantage of cooperative groups' for c_1 is justified. Note, however, that both the sinking time and the maximal population number level off for high values of c_1. One can assign this effect to the finite value of K, the carrying capacity of the mat. For large values of c_1, the mat skeleton can be thought of as being build up immediately after the mat dynamics is started. Hence, a further increase of the parameter c_1 does not increase the advantage of cooperators any more.
As a summary, figure 5.13 shows a color plot of $\langle T_{\text{sink}} \rangle$ and $\langle N_{\text{max}} \rangle$, whereas both the selection strength s and the cooperative advantage c_1 are varied simultaneously. The plot combines the two antagonizing driving forces for the stochastic mat model. A higher selection strength s results in shorter sinking times, whereas a bigger cooperator's advantage c_1 enlarges the time at which the mat sinks. Mats are successful (large sinking time and large maximal population size) when cooperators are favored (small s and large c_1).

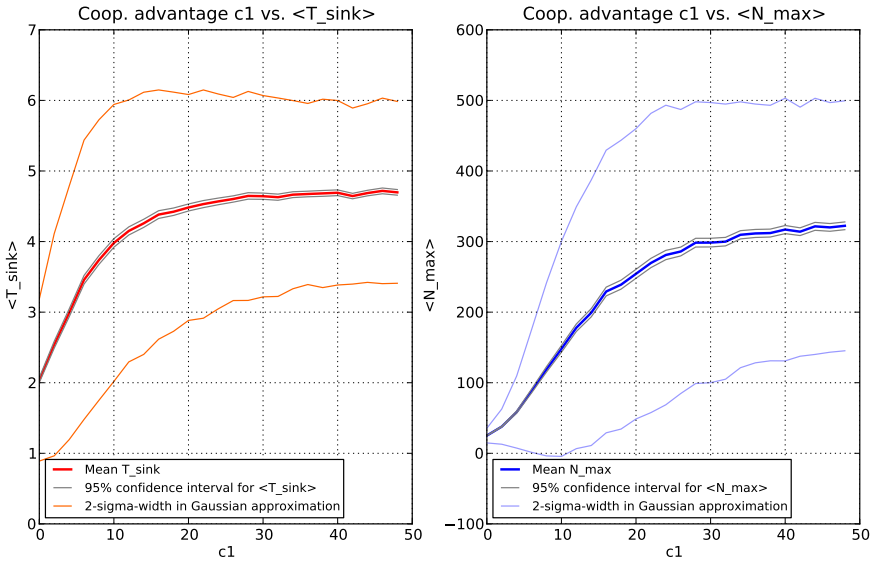

Figure 5.12: Influence of the advantage of cooperative groups c_1 on $\langle T_{\text{sink}} \rangle$ (left) and $\langle N_{\text{max}} \rangle$ (right). The higher c_1 is, the more cooperative mats are favored. Therefore, the average sinking time and the average maximal population size increase with an increase of c_1. Both curves, however, level off for $c_1 \gtrsim 25$. For large values of c_1, the mat skeleton can be thought of as being build up immediately after the mat dynamics is started. Hence, a further increase of the parameter c_1 does not increase the advantage of cooperators any more.
Chosen parameters: $s = 0.15, z_C = 2, z_D = 6, c_2 = 9, c_3 = 1.1$.
Initial values: $N_0 = 5, x_0 = 0.8, \gamma_0 = 0.2$.

Initial percentage of cooperators x_0 and initial population size N_0

To complete the analysis of the stochastic mat model, we investigate the influence of the relevant initial conditions on the mat dynamics. In non-equilibrium statistical mechanics, initial conditions often play a crucial role for the outcome and the behavior of the system. It can be recognized from figure 5.14 that a higher initial fraction of cooperators increases the sinking time and the maximal population size. The microscopic picture behind the mat growth supports this observation since cooperators build up the mat framework which is essential for the maximal size and for the stability of the mat. We have already argued that a high initial fraction of cooperators would represent the biological situation of the mat growth best within our model.
Figure 5.15 represents the influence of the initial mat size N_0 on the evolutionary dynamics of the mat ensemble. The lower N_0, the bigger is the impact of stochastic fluctuations on the population size, and the broader the distribution in the percentage of cooperators will spread in the beginning (see also figure 5.5). Thus, for a small initial population size, mats with a high fraction of cooperators can form, which enlarges their mean sinking time.

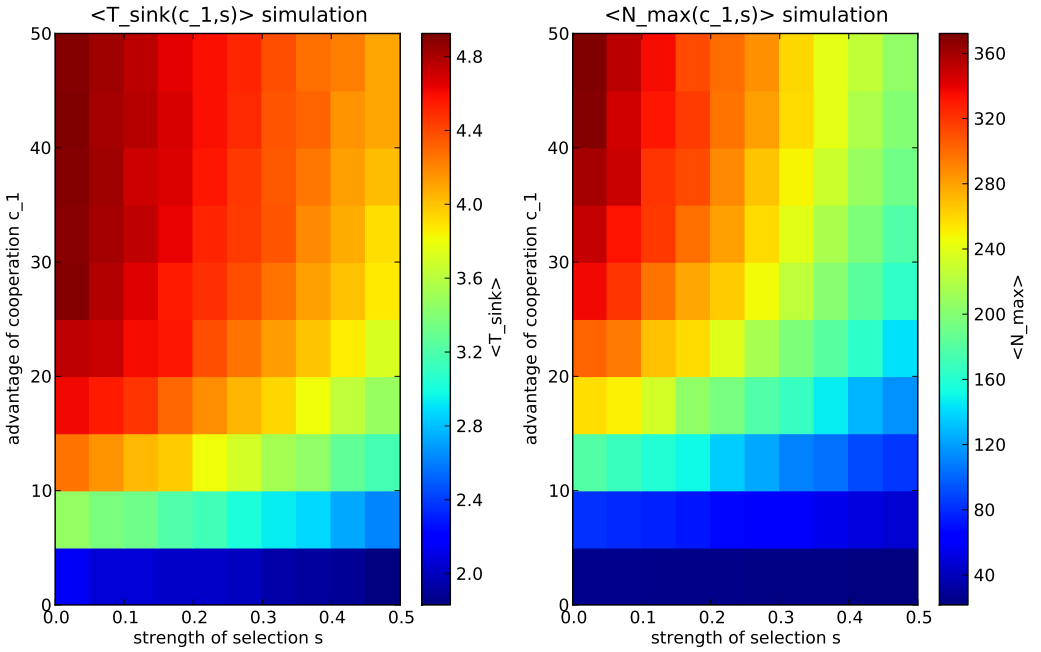

Figure 5.13: Impact of selection strength and cooperator's advantage on mat dynamics. The sinking time (left) and the maximal population size (right) are color-coded and plotted as a function of the two most relevant parameters of the mat model, the selection strength s and the growth advantage of cooperative groups c_1. These two parameters represent the antagonizing principle that defectors are microscopically better off but cooperative groups grow larger. Both plots confirm that the lower s and the higher c_1, the higher $\langle T_{\text{sink}} \rangle$ and $\langle N_{\max} \rangle$ are. We can conclude that the sinking time of a mat decreases when the selection pressure is increased or the growth advantage of cooperative groups is lowered.
Chosen parameters: $z_C = 2, z_D = 6, c_2 = 9, c_3 = 1.1$.
Initial values: $N_0 = 5, x_0 = 0.8, \gamma_0 = 0.2$.

5.3 Stochastic mat model in a nutshell

Let us briefly summarize the mat model and the results obtained from the numerical simulations so far.
Our goal is to investigate the interplay between the biologically relevant timescales leading to cooperation in the mat experiment (chapter 2, figure 4.4). We have defined a stochastic model for the growth and sinking of bacterial mats (section 4.6, figure 4.8). A mat is characterized by the number of cooperating and defecting cells (N_C and N_D or equivalently N and x), and by the effective mat volume M. The number of cooperators and defectors follows a stochastic update [2]. Microscopically, defectors are always better off, but cooperative groups can grow larger in size. Within an effective coarse-grained description, the growth

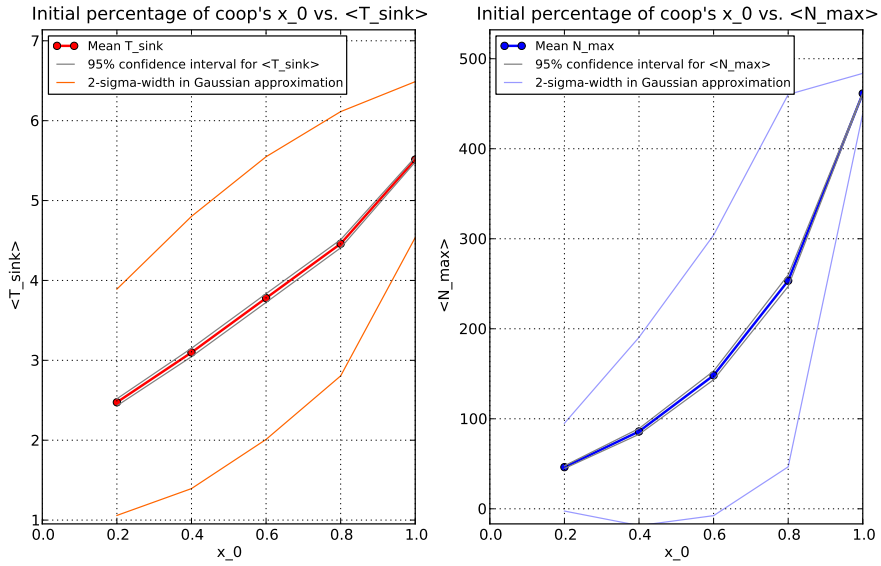

Figure 5.14: Influence of the initial fraction of cooperators x_0 on T_{sink} (left) and $N_{\max}$ (right). An increased percentage of cooperators results in a later sinking of the mats and a bigger population size.
Chosen parameters: $s = 0.15, c_1 = 20, z_C = 2, z_D = 6, c_2 = 9, c_3 = 1.1$.
Initial values: $N_0 = 5, \gamma_0 = 0.2$

of the mat is abstracted in a deterministic, non-spatial picture (section 4.4, eq. (4.6)). In this averaged view, we assume that the mat only grows at its surface. Hereby, we effectively introduce a scaling hypothesis for the dynamics of the mat volume: the growth rate of the mat volume is proportional to its square root. Moreover, the mat expansion is mediated by the presence of cooperating cells. Without cooperators, the mat would not grow in size. The mat density is then computed via the microscopic occupation of the mat volume (eq. (4.3)). Thereby, defectors contribute to the mat density with a larger weight than cooperators since they do not overproduce the sticky polymer ($1 < z_C < z_D$). The mat starts to sink, when its density reaches the density of water ($\gamma = 1$).

This mat model combines population dynamics with its internal evolution for mat populations. The average percentage of cooperators $\langle x \rangle_{\text{mat}}$ reveals a transient increase of cooperation after some time due to demographic fluctuations in the beginning of the growth dynamics (figure 5.5). Cooperative groups grow larger in size and sink later in time, and thus have a higher probability to survive. The sinking time $\langle T \rangle_{\text{sink}}$ increases if the mat expansion is accelerated via c_1, and if the selection pressure s is lowered (figure 5.13). The lower the initial size of the mat N_0, the higher is the impact of stochastic fluctuations ($\propto 1/\sqrt{N_0}$) on the population size and the sinking time (figure 5.15).
In the next chapter, we will apply repeated population bottlenecks to the mat dynamics, which may pave the way for the maintenance of cooperation in structured populations.

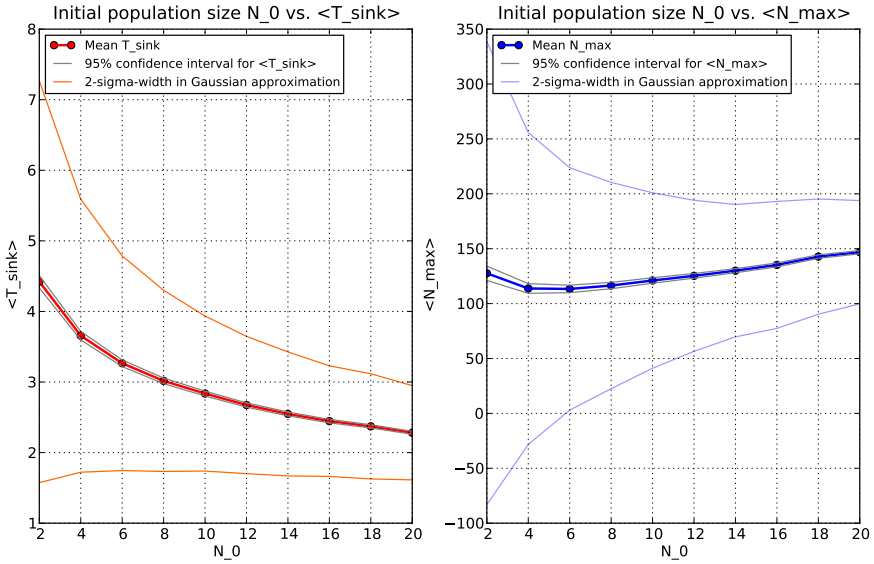

Figure 5.15: Influence of the initial population size N_0 on T_{sink} (left) and $N_{\max}$ (right). The mean sinking time decreases with an increase of the initial population size N_0. This effect crucially depends on demographic fluctuations scaling as $1/\sqrt{N}$. One can infer the importance of stochastic fluctuations from the 2σ-lines in both plots indicating the high variance of the sinking time for small N_0. Since the distribution of the sinking times can be approximated to be Gaussian, 95% of all sinking times lie in the regime comprised by the 2σ-lines. This approximation does not hold for the distribution of $N_{\max}$, but still the 2σ-lines indicate the strong impact of stochastic fluctuations for small N_0. Note, however, that the average maximal population size is hardly affected by N_0.
Chosen parameters: $s = 0.15, c_1 = 20, z_C = 2, z_D = 6, c_2 = 9, c_3 = 1.1$.
Initial values: $x_0 = 0.5, \gamma_0 = 0.2$.

6 Outlook: structured mat populations

During the last three chapters, we have introduced the mat experiment of Rainey & Rainey (chapter 2), and we have developed and analyzed the mat model (chapter 4 and 5). It was shown that the qualitative outcome of the mat model is in good agreement with the experimental results. Let us now turn to the maintenance of cooperation using the example of the mat experiment and the according mat model. This chapter can be understood as an outlook to the maintenance of cooperation and reflects work which is still in progress.

6.1 Structured populations and regrouping steps

Recall that we have already discussed the maintenance of cooperation in a general context in chapter 1. The main motivation to study this issue was to gain insights into the transition from single-celled organisms to multicellularity. We have argued that in the simplest case, structured populations might pave the way to sustain cooperative behavior. In other words, the division of the whole population into sub-populations could be one possibility of how cooperation might have advanced in the course of evolution [90, 65].
Speaking more specifically, we would like to reveal scenarios within the mat model giving rise to an increase of cooperation. We have already seen in figure 5.6 that the average fraction of cooperators shows a time window in which the initial fraction of cooperators is exceeded. From a multi-level perspective, the time window of the transient increase of cooperation is determined by the interplay of the already introduced intra-group evolution and inter-group evolution (cf. chapter 1). The intra-group evolution reflects the evolutionary advantage of defectors over cooperators within one subpopulation, whereas inter-group evolution favors cooperative mats over non-cooperative mats.
As we have found out in the previous chapter, the intra-mat evolution is mainly determined by the selection pressure s. The growth advantage of cooperative groups is mediated by the parameter c_1 and the initial conditions x_0 and N_0. It is important to note that the parameters s and c_1 are determined by the structure, the metabolic properties, and other microscopic details of the bacteria and their growth. It might be possible to determine the value of both parameters from the experiment. In contrast to the values of x_0 and N_0, however, s and c_1 are not directly adjustable in an experimental setup.

Consider, for example, the setup in figure 6.1 in which a population is repeatedly dispersed into subpopulations after a specific time period, and as a consequence a population

structure is explicitly imposed.

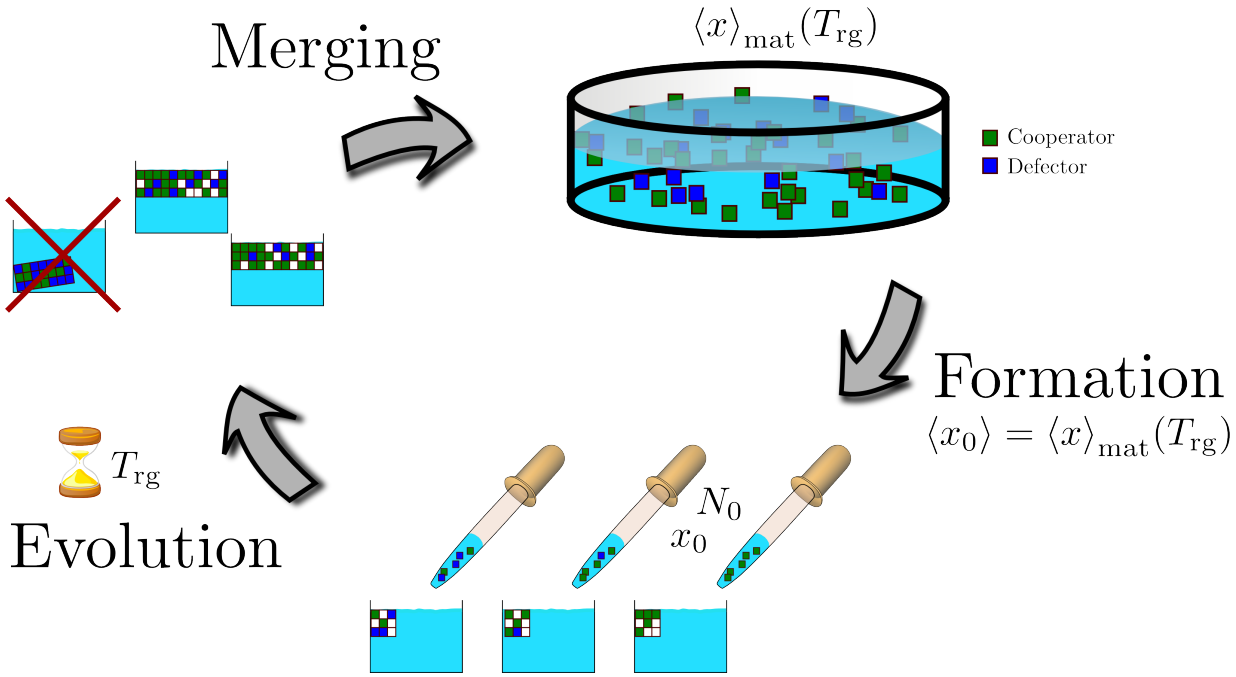

Figure 6.1: Repetitive life cycle as a generic setup to establish maintenance of cooperation in the mat experiment. The formation step leads to the division of the whole population into sub-populations. Each subpopulation evolves separately following the stochastic dynamics of the mat model up to a predefined regrouping time T_{rg}. Then, all mats (or parts of them) which are not sunk up to that time are merged into one big population. The fraction of cooperators in this well-mixed population is given by $\langle x \rangle_{\mathrm{mat}}$, that is the fraction of cooperators over all sub-populations. The repeated application of this regrouping scheme leads to three different scenarios which depend on the value of the regrouping time T_{rg}: stable coexistence of defectors and cooperators, a pure cooperation scenario, and a regime in which cooperation ceases. Future work will quantify this phenomenological picture.

This repetitive cycle consists of three steps:

1. Formation. This process refers to the division of a well-mixed population into several sub-populations. We start from the whole population which has a specific fraction of cooperators $\langle x \rangle_{\mathrm{mat}}$ and from which the sub-populations are founded. Thereby, each sub-population has N_0 bacteria with a fraction of cooperators x_0 in the beginning. In other words, the initial number of cooperators is initialized stochastically, whereas the initial total group size N_0 is fixed. Note that $\langle x_0 \rangle = \langle x \rangle_{\mathrm{mat}}$ since the sub-populations are founded from the "ancestral" population.

2. Evolution. The temporal evolution for all mats lasts for a predefined time T_{rg}, the regrouping time. During this time, there is no interaction between the different mats.

All mats evolve separately following the stochastic dynamics described in chapter 4.

3. Merging. After the regrouping time T_{rg}, all mats (or parts of them) which are not sunk up to that time are merged into one big population. The fraction of cooperators in this well-mixed population is then given by $\langle x \rangle_{\mathrm{mat}}$.

Note that the division of a whole population into several sub-populations seems artificial at first glance. Nevertheless, many biological scenarios are known in which a "regrouping" step is an adequate description. For example, population bottlenecks justify the application of regrouping steps. These situations can be caused by environmental or other external factors with the consequence that large parts of a population suddenly die out or parts of the whole population are separated from the rest.
The consideration of a repetitive life cycle as proposed in 6.1, however, should be regarded as a simplified, but generic approach to more detailed scenarios. The key point is that we show that cooperation can be maintained in principle by combining mat dynamics with this regrouping step in a general setup.

The concept of a regrouping step is adapted from [90] to the mat experiment. Cremer et al. could show in [90] that such a setup with a repetitive cycle for the cooperator-defector model presented in section 3.4.1 leads to regimes in which cooperation can emerge and evolve. Moreover, stable coexistence between cooperators and defectors can be achieved. These regimes crucially depend on the regrouping time T_{rg}.
The same idea seems promising for the scheme presented in figure 6.1 for the mat sub-populations. In figure 5.6, we investigated a mat ensemble with a fixed initial percentage of cooperators x_0 for all mats. In the repetitive cycle, however, the number of cooperators is sampled from a binomial distribution with parameters N_0 and probability $\langle x_0 \rangle$ in order to generalize the dynamics to arbitrary $\langle x_0 \rangle$. Figure 6.2 shows the analogue of figure 5.6 for a mat population for different $\langle x_0 \rangle$ that is the evolution of one single step of the repetitive circle.

From figure 6.2, we can recognize the impact of the average initial fraction of cooperators $\langle x_0 \rangle$ and the initial average mat size N_0 on the time window in which the percentage of cooperators exceeds its initial value. Note that the distribution of sinking times is crucial to the dynamics of the sub-populations. Non-cooperative mats will sink faster, whereas cooperative mats grow larger in size and sink at a later point in time.
In particular, we can distinguish between three regimes for each set of parameters (figure 6.2, right). The first regime shows a transient decrease of cooperation. Here, the evolution of many groups is dominated by the selection pressure leading to groups in which the x-average drops. Some groups, however, show an increase of cooperation due to a high fraction of cooperators in the beginning since bigger mats have a larger weight to the average fraction of cooperators. Therefore, the fraction of cooperators increases again after some time and ultimately exceeds the initial level of cooperation. In addition to stochastic demographic fluctuations in the beginning of the mat dynamics which have been discussed in the last chapter, another effect enforces the formation of highly cooperative groups. We

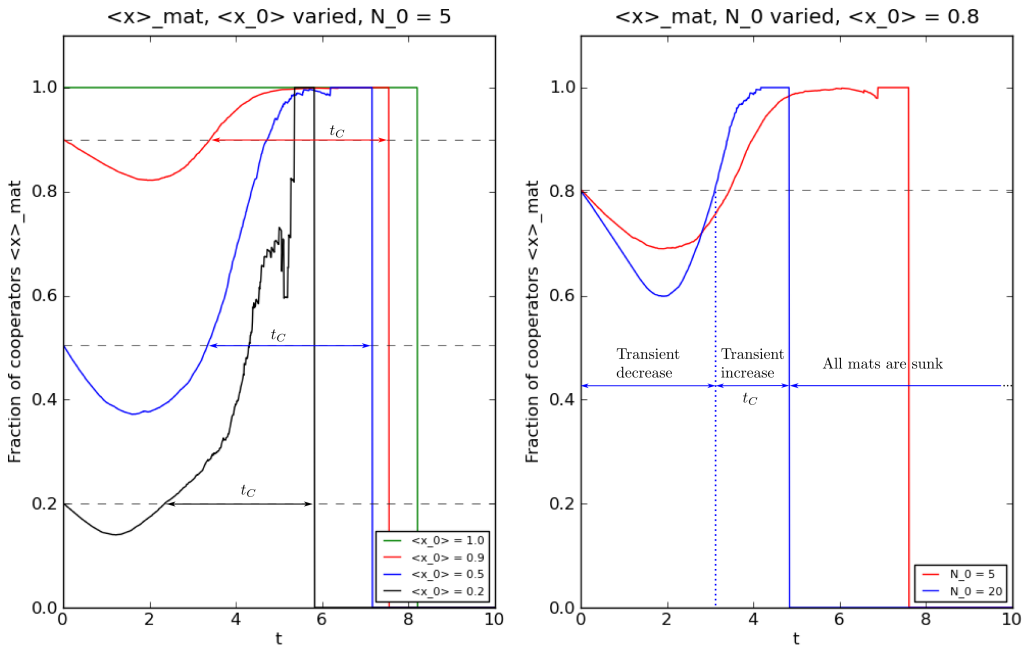

Figure 6.2: Fraction of cooperators for several combinations of initial conditions: one regrouping step. The left plot shows $\langle x \rangle_{\text{mat}}$ for three different values of $\langle x_0 \rangle$ and fixed initial group size $N_0 = 5$; the right plot depicts $\langle x \rangle_{\text{mat}}$ for two different values of $\langle N_0 \rangle$ and fixed initial fraction of cooperators $x_0 = 0.8$. For each set of parameters, we can distinguish three different regimes for the fraction of cooperators over all sub-populations. In the beginning, we observe a transient decrease which is followed by a transient increase in the percentage of cooperators for the time period t_C. When all mats are sunk, $\langle x \rangle_{\text{mat}}$ drops to zero. By repeatedly applying a regrouping step at time T_{rg}, one can infer on the regimes in which cooperation becomes stable.
Chosen parameters: $s = 0.5, c_1 = 20, z_C = 2, z_D = 6, c_2 = 9, c_3 = 1.1$.
Initial values: $\gamma_0 = 0.2$; Number of groups = 5000.

impose additional stochasticity to the dynamics of the mat sub-populations by initializing the mats from a binomial distribution. For example, this sampling gives rise to initialized groups that are purely cooperative even for values of x_0 which are less than 1. Therefore, a population whose sub-populations are initialized with a large mat size $N_0 = 20$ (figure 6.2, right plot) will also contain mats which are purely cooperative if x_0 and the number of groups are sufficiently high. This effect causes a regime in which only purely cooperative mats remain unsunk, that is the average fraction of cooperators is 1, whereas all other mats are already sunk.
The regime in which the fraction of cooperators exceeds its initial level is characterized by the time window t_C. This period ends with the sinking of the last mat. From figure 6.2, we can infer that the length of the time window t_C increases with a higher value of $\langle x_0 \rangle$ since more cooperative mats can survive longer. Moreover, it can be recognized that the

time, at which the period of the transient increase begins, shifts to shorter times for lower values of $\langle x_0 \rangle$.
One could also think of randomizing initial conditions for the group size N_0 [90, 65] for the single regrouping step. We do not follow this way here since an increased variance in N_0 would lead to even more solely cooperative groups in the beginning and hence ease the way to an increase of cooperation.
Now, we can consider repeated regrouping steps with a fixed regrouping time T_{rg} as shown in figure 6.1. Numerical simulations are work in progress, but qualitatively, one can already infer some basic features of this regrouping scenario from figure 6.2. For every initial fraction of cooperators $\langle x_0 \rangle$, there will always be a time regime in which cooperation can increase since stochastic fluctuations lead to groups in which the x-average exceeds the initial average level. These groups gain significance for the overall average in the percentage of cooperation since their size is much larger than for non-cooperative groups which also sink at a much shorter time. If the regrouping time is chosen large enough, all mats will be sunk, and in this way the next regrouping step would not be executable. This scenario would lead to an extinction of cooperators.
Therefore, we expect three different regimes for the regrouping: stable coexistence of defectors and cooperators, a pure cooperation scenario, and a regime in which cooperation ceases. Future work will quantify this phenomenological picture.

6.2 Outlook

As already mentioned, we will examine the repeated life cycle by means of numerical simulations in the near future. Moreover, it is interesting to refine the regrouping step to more realistic scenarios in such a way that it might be tested by biologists. First discussions in this direction have already been conducted with Prof. Jung from the microbiology department of the Ludwig-Maximilians University Munich.
One possible setup could involve the consideration of geometric boundary conditions. One could imagine a situation in nature in which the reproduction would be triggered by the breaking away of small parts of the ancestral mat at shores, at leaves of water plants, or at stone edges as described above. Then, we only regroup with those mats that are not sunk and that have reached a particular threshold in size. The latter condition translates into a condition on the mat volume M and can be investigated from a theoretical point of view by applying the mat model. All mats enclosing too less volume do not arrive at the next 'shore'. Only those groups arriving at the next shore can form new mats (as propagules).
To conclude this theoretical picture, the variation on the mat level could be mediated by the variation of the percentage of cooperators in the mat propagule. In this way, selection pressure could act on the level of mats and a possible way to the higher level selection might be paved. This transition might be considered as a kick-start towards the evolution of multicellularity, where mats could reproduce as a whole.
In summary, it will be a long road to finally reveal the transition from single-celled or-

ganisms to multicellularity. It surely needs some more scientific creativity to uncover this secret of nature. In this thesis we have shown, however, that the interplay between the dynamics of mat formation and the evolution within the mats is a promising starting point.

A Contents of the enclosed CD

The CD enclosed with this thesis contains the following data:

- This document as pdf-file.
- The C++ source code which has been used for numerical simulations.
- Many tools in Python for the analysis of the data obtained from simulations.

Bibliography

[1] P B Rainey and K Rainey. Evolution of cooperation and conflict in experimental bacterial populations. *Nature*, 425:72, 2003.

[2] A. Melbinger, J. Cremer, and E. Frey. Evolutionary dynamics in growing populations. *Phys. Rev. Lett.*, 105:178101, 2010.

[3] Charles Darwin. *Origin Of Species*. John Murray, 1859.

[4] MJ Russell, AJ Hall, AG Cairns-Smith, and PS Braterman. Submarine hot springs and the origin of life. *Nature*, 336(6195):117–117, 1988.

[5] Cairns-Smith. *Seven Clues to the Origin of Life*. Cambridge University Press, 1985.

[6] Masatoshi Nei. Analysis of Gene Diversity in Subdivided Populations. *Proceedings of the National Academy of Sciences of the United States of America*, 70(12):3321–3323, December 1973.

[7] Catherine A. Lozupone and Rob Knight. Species divergence and the measurement of microbial diversity. *FEMS Microbiology Reviews*, 32(4):557–578, July 2008.

[8] Peter Chesson. Mechanisms of maintenance of species diversity. *Annual Review of Ecology and Systematics*, 31(1):343–366, 2000.

[9] J. Maynard-Smith and E. Szathmary. *The Major Transitions in Evolution*. Oxford University Press, Oxford, 1995.

[10] S. Okasha. *Evolution and the Levels of Selection*. Oxford University Press, Oxford, 2006.

[11] Paul B. Eckburg, Elisabeth M. Bik, Charles N. Bernstein, Elizabeth Purdom, Les Dethlefsen, Michael Sargent, Steven R. Gill, Karen E. Nelson, and David A. Relman. Diversity of the Human Intestinal Microbial Flora. *Science*, 308(5728):1635–1638, June 2005.

[12] J. Maynard Smith. *Evolution and the Theory of Games*. Cambridge University Press, Cambridge, 1982.

[13] Wallace. On the Tendency of Species to form Varieties, and on the Perpetuation of Varieties and Species by Natural Means of Selection,. *Jour. of the Proc. of the Linnean Society*, 1(3):53–62, 1858.

[14] U. Kutschera. A comparative analysis of the darwin-wallace papers and the development of the concept of natural selection. *Theory in Biosciences*, 122(4):343–359, 2003. 10.1007/s12064-003-0063-6.

[15] Godfrey-Smith. *Darwinian Populations and Natural Selection*. Oxford University Press, 2009.

[16] R. C. Lewontin. The units of selection. *Annual Review of Ecology and Systematics*, 1(1):1–18, 1970.

[17] Qiong Gan, Tadashi Yoshida, Oliver G. McDonald, and Gary K. Owens. Concise review: Epigenetic mechanisms contribute to pluripotency and cell lineage determination of embryonic stem cells. *STEM CELLS*, 25(1):2–9, 2007.

[18] S. M. Gasser, R. Paro, F. Stewart, and R. Aasland. Multi-author review 'epigenetic control of transcription'. introduction: the genetics of epigenetics. *Cellular and Molecular Life Sciences*, 54(1):1–5, 1998. 10.1007/s000180050120.

[19] Richard E Michod, Yannick Viossat, Cristian A Solari, Mathilde Hurand, and Aurora M Nedelcu. Life-history evolution and the origin of multicellularity. *Journal of Theoretical Biology*, 239(2):257–72, Mar 2006.

[20] Joel L Sachs. Resolving the first steps to multicellularity. *Trends Ecol Evol (Amst)*, 23(5):245–8, May 2008.

[21] Bonner. *First Signals - the evolution of multicellular development*. Princeton University Press, Princeton, 2001.

[22] L W Buss. Evolution, development, and the units of selection. *Proceedings of the National Academy of Sciences*, 80(5):1387–1391, 1983.

[23] George C. Williams. Pleiotropy, natural selection, and the evolution of senescence. *Evolution*, 11(4):pp. 398–411, 1957.

[24] Rainey Paul B. Unity from conflict. *Nature*, 446(7136):616–616, apr 2007. 10.1038/446616a.

[25] M L Guerinot. Microbial iron transport. *Annual Review of Microbiology*, 48(1):743–772, 1994.

[26] A S Griffin, S A West, and A Buckling. Cooperation and competition in pathogenic bacteria. *Nature*, 430:1024, 2004.

[27] Angus Buckling, Freya Harrison, Michiel Vos, Michael A Brockhurst, Andy Gardner, Stuart A West, and Ashleigh Griffin. Siderophore-mediated cooperation and virulence in pseudomonas aeruginosa. *FEMS Microbiol. Ecol.*, 62(2):135, 2007.

[28] P B Rainey and M Travisano. Adaptive radiation in a heterogeneous environment. *Nature*, 394:69–72, 1998.

[29] GENE E. ROBINSON, ROBERT E. PAGE, COLETTE STRAMBI, and ALAIN STRAMBI. Hormonal and genetic control of behavioral integration in honey bee colonies. *Science*, 246(4926):109–112, 1989.

[30] P. Kirk Visscher. A quantitative study of worker reproduction in honey bee colonies. *Behavioral Ecology and Sociobiology*, 25(4):247–254, 1989. 10.1007/BF00300050.

[31] William Morton Wheeler. The ant-colony as an organism. *Journal of Morphology*, 22(2):307–325, 1911.

[32] R Axelrod and WD Hamilton. The evolution of cooperation. *Science*, 211(4489):1390–1396, 1981.

[33] Nathan J. Mlot, Craig A. Tovey, and David L. Hu. Fire ants self-assemble into waterproof rafts to survive floods. *Proceedings of the National Academy of Sciences*, 108(19):7669–7673, 2011.

[34] M. A. Nowak. Five rules for the evolution of cooperation. *Science*, 314:1560, 2006.

[35] S A West, A S Griffin, and A Gardner. Social semantics: altruism, cooperation, mutualism, strong reciprocity and group selection. *J Evol Biol*, 20(2):415–32, Mar 2007.

[36] R L Trivers. The evolution of reciprocal altruism. *Quart. Rev. Biol.*, 46:35, 1971.

[37] M. A. Nowak and K. Sigmund. Tit for tat in heterogeneous populations. *Nature*, 335:250–253, 1992.

[38] B. Rockenbach and M. Milinski. The efficient interaction of indirect reciprocity and costly punishment. *Nature*, 444:718–723, 2006.

[39] C. Hauert, A. Traulsen, H. Brandt, M A Nowak, and K. Sigmund. Via freedom to coercion: The emergence of costly punishment. *Science*, 316:1905–1907, 2007.

[40] SMITH J. MAYNARD. Group selection and kin selection. *Nature*, 201(4924):1145–1147, mar 1964. 10.1038/2011145a0.

[41] Hamilton W. D. The evolution of altruistic behavior. *The American Naturalist*, 97(896):354–356, sep 1963.

[42] W. D. Hamilton. The genetical evolution of social behaviour. I+II. *J.Theor. Biol.*, 7:1, 1964.

[43] Haldane. Population genetics. *New Biology*, 18(34), 1995.

[44] J Cremer. *Evolutionary principles promoting cooperation.* PhD thesis, LMU Munich, 2011.

[45] A Melbinger. *On the Role of Fluctuations in Evolutionary Dynamics and Transport on Microtubules.* PhD thesis, LMU Munich, 2011.

[46] Oren Harman. The price of altruism, and the limits of scientific inquiry. *BMC Proceedings*, 5(Suppl 1):L11, 2011.

[47] David Sloan Wilson and Edward O Wilson. Rethinking the theoretical foundation of sociobiology. *Quart. Rev. Soc. Biol.*, 82(4):327, 2007.

[48] Stuart A West, Ashleigh S Griffin, Andy Gardner, and Stephen P Diggle. Social evolution theory for microorganisms. *Nat. Rev. Microbiol.*, 4(8):597, 2006.

[49] George R. Price. Selection and covariance. *Nature*, 227:520, 1970.

[50] http://www.buzzle.com/articles/pseudomonas-fluorescens.html, 2011.

[51] N.J. Palleroni. *Pseudomonadaceae. Bergey's Manual of Systematic Bacteriology.* The Williams and Wilkins Co., 1984.

[52] Joao B. Xavier and Kevin R. Foster. Cooperation and conflict in microbial biofilms. *Proceedings of the National Academy of Sciences*, 104(3):876–881, 2007.

[53] Erik Alpkvist, Cristian Picioreanu, Mark C.M. van Loosdrecht, and Anders Heyden. Three-dimensional biofilm model with individual cells and continuum eps matrix. *Biotechnology and Bioengineering*, 94(5):961–979, 2006.

[54] Paul B. Rainey and Benjamin Kerr. Cheats as first propagules: A new hypothesis for the evolution of individuality during the transition from single cells to multicellularity. *BioEssays*, 32(10):872–880, 2010.

[55] Andrew J. Spiers, Sophie G. Kahn, John Bohannon, Michael Travisano, and Paul B. Rainey. Adaptive divergence in experimental populations of pseudomonas fluorescens. i. genetic and phenotypic bases of wrinkly spreader fitness. *Genetics*, 161(1):33–46, 2002.

[56] Patrick Goymer, Sophie G. Kahn, Jacob G. Malone, Stefanie M. Gehrig, Andrew J. Spiers, and Paul B. Rainey. Adaptive divergence in experimental populations of pseudomonas fluorescens. ii. role of the ggdef regulator wspr in evolution and development of the wrinkly spreader phenotype. *Genetics*, 173(2):515–526, June 2006.

[57] Eleni Bantinaki, Rees Kassen, Christopher G. Knight, Zena Robinson, Andrew J. Spiers, and Paul B. Rainey. Adaptive divergence in experimental populations of pseudomonas fluorescens. iii. mutational origins of wrinkly spreader diversity. *Genetics*, 176(1):441–453, May 2007.

[58] Michael J. McDonald, Stefanie M. Gehrig, Peter L. Meintjes, Xue-Xian Zhang, and Paul B. Rainey. Adaptive divergence in experimental populations of pseudomonas fluorescens. iv. genetic constraints guide evolutionary trajectories in a parallel adaptive radiation. *Genetics*, 183(3):1041–1053, November 2009.

[59] Andrew J. Spiers, John Bohannon, Stefanie M. Gehrig, and Paul B. Rainey. Biofilm formation at the air–liquid interface by the pseudomonas fluorescens sbw25 wrinkly spreader requires an acetylated form of cellulose. *Molecular Microbiology*, 50(1):15–27, 2003.

[60] Libby, Hammerschmidt, and Rose. Radio interview on the evolution of individuality with radio nz national, 2011.

[61] Michael J. McDonald, Tim F. Cooper, Hubertus J. E. Beaumont, and Paul B. Rainey. The distribution of fitness effects of new beneficial mutations in pseudomonas fluorescens. *Biology Letters*, 7(1):98–100, 2011.

[62] R. Craig MacLean, Graham Bell, and Paul B. Rainey. The evolution of a pleiotropic fitness tradeoff in pseudomonas fluorescens. *Proceedings of the National Academy of Sciences of the United States of America*, 101(21):8072–8077, 2004.

[63] Robinson Terence J. Review: Species evolution: The role of chromosome change. *Systematic Biology*, 44(4):578–580, dec 1995.

[64] Beaumont Hubertus J. E., Gallie Jenna, Kost Christian, Ferguson Gayle C., and Rainey Paul B. Experimental evolution of bet hedging. *Nature*, 462(7269):90–93, nov 2009. 10.1038/nature08504.

[65] M Lechner. On mutation and migration in structured populations. master thesis., 2011.

[66] E Frey. Evolutionary game theory: Theoretical concepts and applications to microbial communities. *Physica A: Statistical Mechanics and its Applications*, 389(20):4265–4298, 2010.

[67] Josef Hofbauer and Karl Sigmund. *Evolutionary Games and Population Dynamics*. Cambridge University Press, 1998.

[68] Peter D. Taylor and Leo B. Jonker. Evolutionary stable strategies and game dynamics. *Mathematical Biosciences*, 40(1-2):145–156, 1978.

[69] J. Maynard Smith and G. R. Price. The Logic of Animal Conflict. *Nature*, 246(5427):15–18, November 1973.

[70] J Gore, H Youk, and A van Oudenaarden. Snowdrift game dynamics and facultative cheating in yeast. *Nature*, 459:253, 2009.

[71] J F Nash. *Non-cooperative games*. PhD thesis, Princeton university, 1950.

[72] R M Dawes. Social dilemmas. *Annual Review of Psychology*, 31(1):169–193, 1980. doi: 10.1146/annurev.ps.31.020180.001125.

[73] T R Malthus. *An Essay on the Principle of Population, as it affects the Future Improvement of Society with remarks on the Speculations of Mr. Godwin, M. Condorcet, and Other Writers*. J. Johnson, London, 1798.

[74] J Monod. The growth of bacterial cultures. *Annual Review of Microbiology*, 3(1):371–394, 1949.

[75] P. F. Verhulst. Notice sur la loi que la population pursuit dans son accroissement. *Corresp. Math. Phys.*, 10:113–121, 1838.

[76] C J Krebs. *Ecology: The Experimental Analysis of Distribution and Abundance*. Cambridge University Press, 1972.

[77] Alfred J. Lotka. Undamped oscillations derived from the law of mass action. *Journal of the American Chemical Society*, 42:1595, 1920. →WWW.

[78] Vito Volterra. Variazioni e fluttuazioni del numero d'individui in specie animali conviventi. *Mem. R. Acca. Naz. dei Lincei*, 2, 1926.

[79] S. Wright. Evolution in mendelian populations. *Genetics*, 16:97–159, 1931.

[80] C. W. Gardiner. *Handbook of Stochastic Methods*. Springer, Berlin, 2007.

[81] N.G. Van Kampen. *Stochastic Processes in Physics and Chetry (North-Holland Personal Library)*. North Holland, 2nd edition, 2001.

[82] R. A. Fisher. *The Genetical Theory of Natural Selection*. Oxford University Press, Oxford, 1930.

[83] Francesca Di Patti, Sandro Azaele, Jayanth R. Banavar, and Amos Maritan. System size expansion for systems with an absorbing state. *Phys. Rev. E*, 83(1):010102, Jan 2011.

[84] P Stephani. Stochastic effects in evolutionary and population dynamics. master thesis., 2011.

[85] Daniel Gillespie. A general method for numerically simulating the stochastic time evolution of coupled chemical reactions. *Journal of Computational Physics*, 22(4):403–434, 1976.

[86] John S Chuang, Olivier Rivoire, and Stanislas Leibler. Simpson's paradox in a synthetic microbial system. *Science*, 323(5911):272, 2009.

[87] Buckling Angus, Kassen Rees, Bell Graham, and Rainey Paul B. Disturbance and diversity in experimental microcosms. *Nature*, 408(6815):961–964, dec 2000. 10.1038/35050080.

[88] Michael A Brockhurst. Population bottlenecks promote cooperation in bacterial biofilms. *PLoS ONE*, 2(7):e634, Jan 2007.

[89] Susanne Ude, Dawn L. Arnold, Christina D. Moon, Tracey Timms-Wilson, and Andrew J. Spiers. Biofilm formation and cellulose expression among diverse environmental pseudomonas isolates. *Environmental Microbiology*, 8(11):1997–2011, 2006.

[90] J Cremer, A Melbinger, and E Frey. Minimal premises for the evolution and maintenance of cooperation. to be published, 2011.

[91] John W. Drake, Brian Charlesworth, Deborah Charlesworth, and James F. Crow. Rates of spontaneous mutation.

[92] A Johnson, J Lewis, M Raff, K Roberts, P Walter, and B Alberts. *Molecular biology of the cell*. Garland Science, 4 edition, 2002.

[93] D. E. O. Juanico. Self-organized pattern formation in a diverse attractive-repulsive swarm. *EPL (Europhysics Letters)*, 86(4):48004, 2009.

[94] Diffusion-limited aggregation, a kinetic critical phenomenon. *Phys. Rev. Lett.*, 47(19):1400–1403, Nov 1981.

[95] M Eden. Fourth berkeley symp. on mathematical statistics and probability. 4:233, 1961.

[96] Collins Joseph B. and Levine Herbert. Diffuse interface model of diffusion-limited crystal growth. *Phys. Rev. B*, 31(9):6119, may 1985.

[97] J T Kuhr, M Leisner, and E Frey. Range expansion with mutation and selection: Dynamical phase transition in a two-species eden model. 2011.

[98] R Jullien and R Botet. Scaling properties of the surface of the eden model in d=2, 3, 4. *Journal of Physics A: Mathematical and General*, 18(12):2279, 1985.

[99] Nadell Carey D. and Bassler Bonnie L. A fitness trade-off between local competition and dispersal in vibrio cholerae biofilms. *Proceedings of the National Academy of Sciences*, aug 2011. 10.1073/pnas.1111147108.

[100] Eshel Ben-Jacob, Inon Cohen, and Herbert Levine. Cooperative self-organization of microorganisms. *Advances in Physics*, 49(4):395–554, 2000.

List of Figures

Acknowledgement

First of all, I would like to thank my supervisors Professor Erwin Frey, Anna Melbinger, and Jonas Cremer. I am indebted to Erwin Frey for giving me the opportunity to work as a member of the statistical and biological physics group. I would like to thank him for the open and creative conversations we have had, not only about the topics concerning this thesis, but also about different ideas in the field of evolutionary and statistical physics that arouse my curiosity.
I wish to express my gratitude to Anna Melbinger and Jonas Cremer for their constant support and our constructive discussions. They introduced me to the scientific field of evolutionary physics and shared their scientific knowledge with me. I deeply appreciate their handling of open-mindedness, critical questioning, and goal-oriented thinking. Anna's and Jonas' advice has always been fruitful and inspiring to me. After every meeting, I felt to have taken one step forward with a deeper understanding of evolutionary physics.
My thanks also go to Jan-Timm Kuhr with whom I had interesting discussions and consultations on the growth of bacterial biofilms and colonies.
Furthermore, I wish to thank my roommates in the "Kinderzimmer" for the open and pleasant atmosphere. Thomas Fehm, Alessio Boschini, Markus Weber, Philipp Stephani and Matthias Lechner accompanied me in the course of the last year and enriched my everyday life as a physicist with discussions on physics and beyond to a large extent. I would like to point out Matthias' help, support, and consulting with all the technical problems I have had, especially in the beginning of my work. I called for his assistance much too often, but nevertheless he always helped me out. By now, basically everything that runs on my laptop stems from his and also Philipp's advice. I also appreciate the critical and detailed remarks of Matthias on the mat model. Moreover, I am grateful to Markus for the interesting and challenging discussions on the rock-paper-scissors dynamics. It has always been, and still is, a welcome variety to my project. More generally, I am also thankful to all members of the whole statistical physics group. It is fun to work in such a friendly and productive atmosphere.

I would also like to thank Falk Toeppel and Christian Foth for their thorough proofreading and their critical comments on this work.
In addition, I am indebted to my parents and grand-parents, for giving me constant financial and moral support throughout my studies.
Last, but not least, I want to thank my girlfriend Anja. Not only does she take my mind off physics, it is also a pleasure to test and try out various cooperator and defector strategies without her knowledge in our common household.

Ich versichere, die Arbeit selbstständig angefertigt und dazu nur die im Literaturverzeichnis angegebenen Quellen benutzt zu haben.

München, den 27. September 2011